

Membranes as separators of dispersed emulsion phases

Promotoren: dr. ir. K. van 't Riet
hoogleraar in de levensmiddelenproceskunde
dr. M.A. Cohen Stuart
hoogleraar in de fysische chemie (kolloïdchemie)

Co-promotor : dr. ir. A. van der Padt
universitair docent bij de vakgroep levensmiddelentechnologie,
sectie proceskunde

N1102201, 2255

Ageeth G. Lefferts

Membranes as separators of dispersed emulsion phases

Proefschrift

ter verkrijging van de graad van doctor

op gezag van de rector magnificus,

dr. C.M. Karssen,

in het openbaar te verdedigen

op woensdag 14 mei 1997

des namiddags te 4 uur in de Aula

van de Landbouwniversiteit Wageningen

wn 941207

This project was funded by the Foundation for Chemical Research in the Netherlands, projectnumber 700-43-022.

ISBN 90-5485-709-9

BIBLIOTHEEK
LANDBOUWUNIVERSITEIT
WAGENINGEN

Stellingen

- 1 Membranen kunnen worden toegepast om stabiele olie-in-water emulsies te destabiliseren; het aanleggen van een elektrisch veld werkt daarbij zeer bevorderend.

Dit proefschrift, Hoofdstuk 5.

- 2 Het is opmerkelijk dat Daiminger et al. opmerken dat het opmerkelijk is dat de scheidingsefficiëntie in hun systeem onafhankelijk is van de grootte van het membraanoppervlak.

U. Daiminger, W. Nitsch, P. Plucinski and S. Hofmann, Novel techniques for oil/water separation, 1995, *Journal of Membrane Science*, vol.99, p.197-203.

- 3 Gezien het grote aantal (empirisch georiënteerde) publicaties dat er niet in slaagt om een antwoord te geven op de vraag welke materiaaleigenschappen van coalescentie-filters het coalescentiegedrag van druppels bepalen, is het noodzakelijk dat hiernaar meer fundamenteel onderzoek verricht wordt.

O.a. E. J. Clayfield, A.G. Dixon, A.W. Foulds and R.J.L. Miller, The coalescence of secondary dispersions, 1985, *Journal of Colloid and Interface Science*, vol.104, no.2, p.500-519.

G.K. Anderson and C.B. Saw, Oil/water separation with surface modified membranes, 1987, *Environmental Technology Letters*, vol 8, p.121-132

- 4 Voortbordurend op stelling 3 biedt reflectometrie mogelijkheden om op een snelle en eenvoudige manier inzicht te verkrijgen in de coalescentie-bevorderende eigenschappen van oppervlakken.

Dit proefschrift, Hoofdstuk 6.

- 5 AIO's doen er verstandig aan een aanzienlijk deel van hun tijd en energie te steken in het ontwikkelen van hun leidinggevende vaardigheden door het begeleiden van studenten, gezien de nadruk die hierop wordt gelegd tijdens sollicitatieprocedures.
- 6 Om de slagingskans van samenwerkingsverbanden tussen universiteiten en industrie te vergroten, verdient het aanbeveling dat beide partijen zich op de hoogte stellen van onderhandelings technieken, zoals bijvoorbeeld beschreven in het Harvard-Onderhandelingsproject.

R. Fisher and W. Ury, *Getting to yes: negotiation agreement without giving in*, Boston: Houghton Mifflin, 1981.
- 7 In de industrie bestaat dringend behoefte aan praktisch toepasbare kennis ten aanzien van kristallisatie.
- 8 Een landrover in 'zijn achteruit' is gelukkig soms sneller dan een olifant in 'zijn vooruit'.
- 9 Pogingen om de sfeer tijdens internationale tennistoernooien te vergroten door het inhuren van brallerige Nederlandse studenten werken averechts.
- 10 Sportieve auto's bestaan niet.

Stellingen behorende bij het proefschrift 'Membranes as separators of dispersed emulsion phases'.

Ageeth Lefferts

Wageningen, 14 mei 1997

Contents

1	Introduction	1
2	Transport mechanisms in dispersed phase separators: oil properties	7
3	Transport mechanisms in dispersed phase separators: hydrodynamics	39
4	Coalescence in a dispersed phase separator	69
5	Performance of a dispersed phase separator enhanced by an electric field	97
6	General Discussion	121
	Summary	147
	Samenvatting	151
	Nawoord	155
	Curriculum Vitae	157

1 Introduction

Large volumes of waste water containing varying amounts of oil are produced in industries such as the edible oil and detergent processing industries, the textile industry (scouring water) and the engineering industry (cutting, lubricating and engine oils)¹. These waste waters can either be reused or discharged into coastal waters or municipal sewage systems. Purification of the industrial waste waters is always necessary in order to meet stringent legislation. For example, discharges into the North Sea are permitted only if the oil content is smaller than 40 ppm².

According to Porter³, aqueous waste streams can be divided into three groups, based on the condition of the oil phase. The first group contains free floating oil. Because the density of oil is often smaller than that of water, gravity separators can be used to separate both phases. In the second group, the primary emulsions, the oil is present in the form of instable emulsion droplets. Generally, the droplet diameters vary between 10 and 50 μm . These instable droplets easily coalesce after collision, forming large droplets that can be removed using gravity settlers, sometimes combined with a chemical or mechanical treatment. However, large problems are encountered with the third group, so called secondary emulsions. In this case, the dispersed phase consists of very stable droplets, with a diameter smaller than 10 μm . Because these oil droplets do not coalesce easily, methods used to separate instable emulsions are not adequate. Often, expensive

ultracentrifuges must be used, combined with flotation, coalescers and fibrous or granular bed filtration.

Conventional coalescers

A detailed overview of the extensive literature about coalescers is given by Sherony et al.⁴. Usually, coalescers are beds or filters, made of some kind of powder or fibrous material (e.g. glass, polypropylene, polyethylene, fluoropolymers, teflon, cellulose, stainless steel, quartz). The separation mechanism is based on the capture of droplets which flow through the pores of the coalescer. Due to this capture, the chance of droplet-droplet collision is enhanced and coalescence will occur. In this way the captured drop grows until it is reentrained into the emulsion again. Next, these large droplets can be separated out of the emulsion using gravity.

Conventional emulsion membrane filtration

In recent years, membrane filtration is applied widely to separate emulsions. Ultrafiltration and reverse osmosis have been found to be very effective for this purpose^{2,5-10}. In case of waste water purification, the continuous, aqueous phase is permeated through a hydrophilic membrane, ending up with an enriched emulsion as the retentate and a pure water phase as the permeate (figure 1a). The concentrated retentate can be burnt afterwards. Low energy costs, possibility for continuous operation and easy handling make membrane filtration an attractive alternative method to separate emulsions^{5,7,11}. However, a disadvantage of the system is the large volume of continuous water phase that has to be removed, especially if the oil concentration is low. If the dispersed phase can permeate efficiently instead of the continuous phase, no such disadvantage exists (figure 1b).

Dispersed Phase Separators

Generally, the removal of a phase out of an emulsion using a membrane requires two processes to be dealt with. Firstly, the phase must contact the membrane. If the

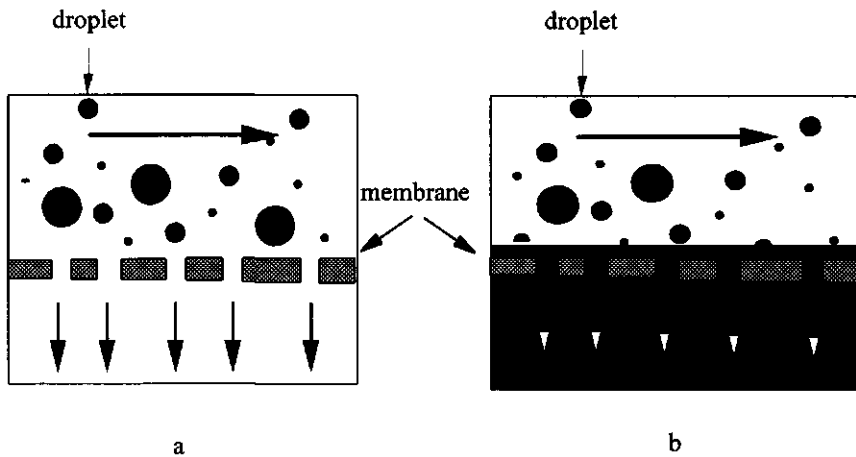


Figure 1, (a) Permeation of the continuous phase using membrane filtration and (b) permeation of the dispersed phase using a dispersed phase separator.

continuous phase has to be removed this condition will always be fulfilled. However, in case of dispersed phase removal the droplets have to be transported out of the bulk in order to reach the membrane. Secondly, the phase must be able to permeate through the membrane. Hence, the phase should have the same polarity as the membrane. If this condition is met for the continuous phase, permeation of this phase will be successful. In contrast, permeation of the dispersed phase is not obvious because the (stable) droplets must coalesce with the membrane before they can permeate. Whether this occurs, is dependent on membrane properties, as well as emulsion properties and process variables. Thus, the dispersed phase separator is in fact a combination of a conventional coalescer and membrane filtration. The membrane surface promotes coalescence (similar to a coalescer) but in the mean time the coalesced phase is separated from the continuous

water phase as well in contrast to conventional coalescers, which need an additional process to separate the coalesced droplets out of the emulsion.

Aim of the thesis

Although some research has been reported concerning dispersed phase separators^{12, 13}, little is known about the mechanisms controlling the efficiency of the separation. The aim of this thesis is to gain knowledge about these mechanisms in order to be able to optimize the process. Experimental results are explained and modeled theoretically, both in case of transport of oil droplets from the bulk to the membrane and in case of coalescence of the droplets against the membrane. In this way, the rate limiting process and its main parameters can be identified and optimized. As a model emulsion a secondary hexadecane-in-water emulsion, stabilized by the nonionic surfactant Tween-40, is chosen. The stable, dispersed phase fraction is smaller than 0.06 (w/w). This model emulsion has been chosen because of the attractiveness of applying dispersed phase separators for the purification of waste waters which contain 5-10% oil. Moreover, we focus on small, stable droplets because of the challenge to separate these emulsions.

Outline of the thesis

In chapter 2 and 3 the transport mechanisms responsible for droplet movement from the bulk towards the membrane surface are discussed both experimentally and theoretically. The most important mechanism is direct interception of the droplets by the membrane. The influence of several parameters (droplet size, density difference between dispersed and continuous phase, module configuration, hydrodynamics) is discussed. It is concluded that the process is transport limited.

Chapter 4 deals with the description of the coalescence mechanism. The theoretical discussion is strengthened by experimental results concerning coalescence of primary emulsions onto liquid interfaces as well as onto membranes. Extrapolation of the theory to secondary droplets confirms the conclusion of chapter 2 and 3 of transport limitation. Only in case of high surfactant concentration the process becomes limited by coalescence.

In chapter 5 the possibilities of using electrophoresis as an additional transport mechanism is discussed. Three systems are compared; all show a significant improvement of the transport.

Finally, in chapter 6 a general discussion is presented in which dispersed phase separators are compared with other separation methods. Problems encountered when applying the system in practice are discussed. Ideas for optimization are given. Some new results concerning the influence of membrane surface roughness on coalescence indicate that coalescence can be improved by choosing an appropriate surface roughness.

References

- 1 **G.K. Anderson, C.B. Saw and M.S. Le**, Oil/water separation with surface modified membranes, 1987, *Environmental Technology Letters*, vol. 8, p.121-132.
- 2 **J. Koning and D.M. Koenhen**, Membranes and their use in the treatment of oily water, *Chemicals in the oil industry: development and applications*, 1990.
- 3 **M.C. Porter**, *Handbook of industrial membrane technology*, Moyes publication, Park Ridge, New Jersey, USA, 1988.
- 4 **D.F. Sherony, R.C. Kintner and D.T. Wasan**, Coalescence of Secondary Emulsions in fibrous beds, 1978, *Surface and Colloid Science*, vol.10, p.99-161.
- 5 **A. Benedek and F.A. Tonelli**, Innovative technologies for treatment of oily waste waters, 1992, *Iron and Steel Engineer*, vol 6, p.44-49.
- 6 **D. Bhattacharyya, A.B. Jumawan and R.B. Grieves**, Ultrafiltration characteristics of oil-detergent-water systems: membrane fouling mechanisms, 1979, *Separation Science and Technology*, vol.14, no.6, p.529-549.

- 7 **R.R. Bhawe and H.L. Fleming**, Removal of oily contaminants in waste water with microporous alumina membranes, 1988, *AIChE Symposium Series: Membrane materials and processes*, vol.84, no.261, p.19-27.
- 8 **K. Scott, J.F. Mc Convey and A. Adhamy**, Application of cross flow microfiltration to emulsion separation in extraction processes, 1992, *Journal of Membrane Science*, vol.72, p.245-257.
- 9 **G.B. Tanny and D. Hauk**, Filtration of particulates and emulsions with a pleated, thin channel cross-flow module, 1980, *Separation Science and Technology*, vol.15, no.3, p.317-337.
- 10 **F. Vigo, C. Uliana and P. Lupino**, The performance of a rotating module in oily emulsions ultrafiltration, 1985, *Separation Science and Technology*, vol.20, no.2/3, p.213-230.
- 11 **L.K. Bansal**, Concentration of oily and latex waste waters using ultrafiltration inorganic membranes, 1976, *Proceedings of the third national Conference on complete water reuse; symbiosis as a means of abatement for multimedia pollution*, June 27-30, Cincinnati, Ohio, p.274-285.
- 12 **H. Unno, H. Saka and T. Akehata**, Oil separation from oil-water mixture by a porous poly(tetrafluoroethylene) (PTFE) membrane, 1986, *Journal of Chemical Engineering of Japan*, vol. 19, no.4, p.281-286.
- 13 **K. Ueyama, K. Fukuura and S. Furusaki**, Oil-phase permeation behavior of O/W emulsion through a porous polytetrafluoroethylene membrane, 1987, *Journal of Chemical Engineering of Japan*, vol.20, no.6, p.619-622.

2 **Transport mechanisms in dispersed phase separators: oil properties**

Summary

The reuse or discharge of industrial waste waters, contaminated with small amounts of dispersed oil, requires a purification treatment for which membranes can be used. If only little oil is present, removal of the dispersed phase might be preferable to the more commonly applied removal of the continuous phase because of a decrease of the required membrane area. In this chapter the rate determining mechanism is examined of the removal of surfactant stabilized oil droplets using a polypropylene membrane (either transport of droplets towards or coalescence with the membrane), without any water permeation. As a model oil (bromo-) hexadecane is used in a concentration of less than 6 weight percent. It is shown that stable oil droplets with different size distributions (d_{12} between 0.5 and 12.4 μm) can be removed from the emulsions in the experimental module. The system has been described by solving the convective diffusion equation assuming that all droplets arriving at the membrane surface are irreversibly consumed by an unspecified, extremely fast absorbence reaction. Theoretically calculated and experimentally determined data of both oil concentration and droplet size during filtration agree qualitatively, indicating that the system is transport limited. Under the experimental conditions, the transport of small droplets is mainly determined by the diffusion mechanism while gravity and interception dominate in case of large droplets. Although the latter mechanism is difficult to model, the theory describes the permeation of the dispersed phase reasonably well. It can be used to optimize the dispersed phase separator so that the system can compete with conventional membrane filtration.

Introduction

The separation of stable, dispersed oil droplets out of waste waters is often troublesome. As mentioned in chapter 1, several separation methods with or without chemical additions can be used, such as gravity settlers, flotation, fibrous bed coalescers and membrane filtration. The latter permeates the continuous, aqueous phase, while a concentrated emulsion is retained. Low energy costs, possibility for continuous operation and easy handling make membrane filtration an attractive emulsion separation method. However, large volumes of the continuous phase have to permeate, especially if the oil concentration is low. In case of efficient permeation of the dispersed phase no such disadvantage exists. For this purpose a dispersed phase separator can be used: the dispersed phase on the feed side of the membrane is transferred into a continuous phase at the permeate side of the membrane.

It can be deduced that if both systems have the same membrane area and if they comprise identical emulsions, the minimum value of the dispersed phase flux, $J_{d,min}$ [$\text{m}\cdot\text{s}^{-1}$], must equal:

$$J_{d,min} = J_c \cdot \frac{V_d}{V_c} \quad (1)$$

in order to have the same filtration time and hence to be competitive to the continuous phase permeation system. Here, J_c [$\text{m}\cdot\text{s}^{-1}$] is the flux of the continuous phase in the continuous phase permeation system, V_d [m^3] is the volume of the dispersed phase and V_c [m^3] is the volume of the continuous phase. Equation (1) can be used as a tool to roughly compare the two systems although other factors such as the desired composition of the end products should also be taken into account.

A dispersed phase separator can be partly compared with a conventional coalescer. A coalescer through which an emulsion is pumped catches droplets, thus enlarging the chance of droplet-droplet collision and coalescence. The captured droplets will grow and

eventually they can be separated using gravitational methods. In the dispersed phase separator presented in the present research, the emulsion is pumped alongside the membrane and droplets can be captured when near to the membrane. Once the droplet coalesces with the membrane it can be removed simply by permeation. Growth of the droplets is not necessary, neither is the use of gravity settlers.

In the past some research has been performed on the possibilities of a membrane to act as a coalescer¹. The total emulsion is permeated through a polypropylene hollow fiber membrane resulting in a destabilization of the emulsion. However, oil and water phase still have to be separated after the filtration process. Thus, the membrane acts as a conventional coalescer. Others investigated a dispersed phase separator system similar to ours. For example, the permeation of large ($10\text{ }\mu\text{m} < d_{32} < 150\text{ }\mu\text{m}$) oil droplets without the presence of a surfactant through a polytetrafluorethylene (PTFE) dead end membrane is studied by Unno et al.². Ueyama et al.³ studied the permeation of small ($d_{32} < 10\text{ }\mu\text{m}$), SDS-stabilized oil droplets with a total volume of 50% in the emulsion through a PTFE membrane. These publications are strongly descriptive and do not provide a satisfactory theoretical explanation of the experimental observations.

In the present thesis permeation of oil droplets without any water permeation is studied. In this chapter the theory behind the dispersed phase separator is explored with emphasis on the transport mechanisms of small ($d_{32} < 12\text{ }\mu\text{m}$), surfactant stabilized droplets from the bulk towards a flat sheet membrane. The weight fraction of the oil in the emulsion is smaller than 0.06. The effect of both droplet size distribution and density difference between continuous and dispersed phase is investigated.

Theory

Originally, the capture mechanisms described for coalescers involve capture of solid particles out of gases but they also have been used in case of capture of those particles out of fluids^{4, 5, 6}. In this chapter these mechanisms will be applied to predict the capture

of dispersed oil droplets out of emulsions in membrane systems. It is assumed that these small liquid droplets, which are rigid⁷, behave as solid particles as will be discussed later in this paper. In figure 1, 5 types of capture mechanisms are presented that are relevant for the permeation of the dispersed phase when using a flat sheet, cross flow membrane module. *Inertial impaction* occurs when droplets deviate from curved fluid streamlines whereas droplets will be removed by *interception* if the location of the streamlines and the droplet size results in contact between the membrane and the droplet. This occurs when the minimum distance between the streamline and the membrane is less than or equal to the droplet radius. *Diffusive capture* results from the Brownian motion of very small droplets caused by collision of the droplets with fluidum molecules. Consequently, the droplets follow a zigzag path as they pass through the channel, thus increasing the probability of droplet capture. *Gravitational settling* is the removal of droplets from the flow stream because of the density difference between droplet and fluidum. *Electrostatic*

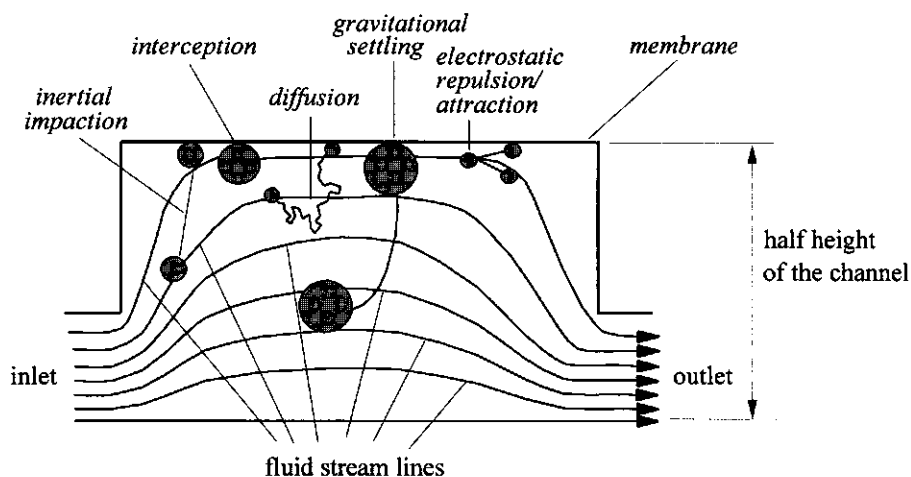


Figure 1, Particle capture mechanisms (not to scale).

deposition results from attractive forces between charged droplets and an oppositely charged membrane.

Convective diffusion equation

Based on the mechanisms discussed above, several theories for predicting deposition rates of flowing colloidal particles onto various collector surfaces have been developed. A review of these models has been given by Adamczyk et al.⁸. For particle-collector systems subjected to both flow and Brownian motion a mass balance can be expressed by the convective diffusion equation:

$$\frac{\partial n}{\partial t} + \nabla \cdot \vec{j} = Q \quad (2)$$

with \vec{j} [$\text{m}^2 \cdot \text{s}^{-1}$] is the particle flux vector, n [m^{-3}] is the particle concentration, t [s] is the time and Q [$\text{m}^{-3} \cdot \text{s}^{-1}$] is a source term. Here, the particle flux vector consists of a diffusion term and a convective term:

$$\vec{j} = -\bar{D} \nabla n + \vec{v} n \quad (3)$$

with \bar{D} [$\text{m}^2 \cdot \text{s}^{-1}$] is the diffusion dyadic and \vec{v} [$\text{m} \cdot \text{s}^{-1}$] is the velocity vector of the particles. The latter is determined by hydrodynamic forces and external and colloidal force fields. The deposition rate of particles on a given collector can be calculated by solving the convective diffusion equation. However, problems are encountered when doing so because of changes of hydrodynamic forces in the vicinity of solid surfaces. Moreover, the description of the colloidal droplet-wall interactions often breaks down at very short distances⁹. Consequently, simplifying assumptions regarding particle-collector interactions are often made.

Perfect sink model

A frequently used simplified approach to solve the convective diffusion equation is the 'perfect sink' model. In this model it is assumed that all particles arriving at a distance sufficiently close to the collector surface, are irreversibly consumed by an unspecified, extremely fast absorbance reaction. This approach proved to be useful for performing numerical calculations of the amount of particles that are captured in time. However, it must be kept in mind that a disadvantage of the model is that it does not take into account the possibility of a finite rate of the absorbance reaction.

The boundary conditions of the perfect sink model are that the source term Q is zero and that at $t = t_0$, the particle concentration n is equal to the initial concentration of the particles n_0 . Also, for $t > t_0$, $n = 0$ at $h \leq \delta$ and $n = n_\infty$ at $h = b$. Here, n_∞ is the bulk concentration of the particles, h [m] is the distance between particle and collector, δ [m] is the primary minimum distance between the particle and the wall (i.e. the distance between particle and wall at which the total colloidal repulsion energy is minimal, this distance is sometimes assumed to be zero) and b [m] is the half height of the channel. Even with these simple boundary conditions, the convective diffusion equation can not be solved analytically when the hydrodynamic corrections and colloidal forces are taken into account. Hence, numerical and approximate analytical methods which use dimensionless parameters have been derived to solve the equation⁸.

The magnitude of hydrodynamic, colloidal (also called specific) and external forces relative to the diffusional forces can be expressed by a variety of dimensionless parameters. In this paper we consider 4 dimensionless numbers to be important. Firstly, the relative magnitude of hydrodynamic and diffusional effects can be denoted by the Peclet number, Pe [-], which for parallel plates is equal to $3\bar{v} \cdot a^3 / (2b^2 \cdot D_\infty)$. Here, a [m] is the particle radius and \bar{v} [m·s⁻¹] the average velocity of the fluid. D_∞ [m²·s⁻¹], the diffusion coefficient of the particles in the bulk, is given by the Stokes-Einstein equation $kT / (6\pi\eta a)$ with k [J·K⁻¹] being the constant of Boltzmann, T [K] the absolute temperature and η [N·s·m⁻²] the dynamic viscosity. Secondly, the adhesion number Ad accounts for the dispersion interactions between particle and wall. It is defined by $Ad = A_{123} / (6kT)$, where

A_{123} [J] is the Hamaker constant for the dispersion interaction of particle 1 with wall 2 through medium 3. Thirdly, the double layer number DL regards the electrostatic interactions between particle and wall. It is equal to $4\pi\epsilon\epsilon_0\zeta_1\zeta_2a/(kT)$, where ϵ [-] is the dielectric constant of the medium, ϵ_0 [C·V⁻¹·m⁻¹] is the permittivity of the vacuum and ζ_1 and ζ_2 [V] are the zeta-potentials of the particle and wall respectively. Finally, the gravity number Gr which takes the gravity force into account is described by $4\pi(\rho_1-\rho_3)ga^4/(3kT)$, with ρ_1 and ρ_3 [kg·m⁻³] being the densities of the particle and the medium respectively and g [m·s⁻²] the gravity acceleration.

Dependent on the magnitudes of these numbers, several approximate solutions of the perfect sink model are known for parallel plate systems. The results are often expressed in terms of the dimensionless local mass transfer Sherwood number:

$$Sh_l = \frac{j_l \cdot a}{D_\infty \cdot n_\infty} \quad (4)$$

where j_l [m²·s⁻¹] is the local normal component of the particle flux vector at the collector surface. Because j_l depends on the position of the particle on the collector surface, Sh_l is a local quantity. A global measure of the deposition rate can be obtained by averaging Sh_l over the entire collector surface (Sh).

Approximate solutions of the perfect sink model for parallel plates

It is assumed that electrostatic forces are negligible and that the only external force field is the gravity force field which is responsible for the mechanism of gravitational settling. Inertial impaction does not occur because in the present research the density of the droplets is always smaller than the density of the water phase. Taking this into account, the approximate solutions relevant for this paper can be divided into three groups.

The first solution is called the Smoluchowski-Levich approximation and is valid if $DL \ll Pe$ and if no external force field is present ($Gr = 0$). Above that it is assumed that the increase of van der Waals attraction a particle experiences while approaching a

solid wall is balanced by the increase of hydrodynamic drag away from the wall. The latter can be a result of lateral migration induced by an inertial lift force¹⁰. Therefor, both hydrodynamic drag and van der Waals attraction are ignored (Ad is assumed to be 0). In the discussion of this chapter it is shown that this assumption is valid, because both the lift force and the van der Waals force are negligible compared to the permeation velocity. In case of laminar flow in a parallel plate channel with $Pe < 10^2$ it can be derived that¹¹

$$Sh_{Pe} = \frac{1.017}{\left(\frac{L}{b}\right)^{\frac{1}{3}}} \cdot Pe^{\frac{1}{3}} \quad (5)$$

Here, L is the length of the plate [m] and the subscript ' Pe ' denotes that Pe dominates Gr .

The second approach, for which the subscript ' Gr ' is used, is applicable if deposition is mainly caused by the gravity force field, thus if $DL \ll Gr$ and $Pe \ll Gr$. It can be deduced that:

$$Sh_{Gr} = Gr \quad (6)$$

The third situation to be considered occurs if $DL \ll (Gr \approx Pe)$. In this case no exact or approximate analytical solutions of the convective diffusion equation are available. The approach often attempted is to assume additivity of the two deposition rates caused by diffusion and gravity forces. The additivity rule can be expressed as:

$$Sh_{tot} = Sh_{Pe} + Sh_{Gr} \quad (7)$$

The flux can be calculated by combining equation 5, 6 or 7 with equation 4. Also, it is possible to add Sh_i , the Sherwood number which accounts for interception, to equation 7. This will be discussed later.

The perfect sink model as described above is used to model the transport of the dispersed phase of oil-in-water emulsions from the bulk towards the membrane in a flat sheet membrane module. Originally, the perfect sink model has been developed for solid

particles. As stated before, the small droplets used in this project can be considered to be rigid spheres as far as transport is concerned. Furthermore, the main difference between deposition of solid and liquid particles is due to differences in physical-chemical conditions. These conditions are related to different colloidal interactions, which are not considered in the perfect sink model as described above. Also, droplet-droplet interaction is assumed to be absent; this condition will be met because the oil concentration is always low.

Materials and Methods

The membrane module

A hydrophobic polypropylene membrane (Enka, Accurel) with an average pore size of $0.1\ \mu\text{m}$ is placed in a flat sheet, cross flow module, made of perspex. A teflon spacer is placed at the permeate side. The length of the module is $0.12\ \text{m}$, the channel height is $3\ \text{mm}$ and the effective membrane area is $3.24 \cdot 10^{-3}\ \text{m}^2$. The module is placed horizontally using a leveling instrument in such a way that the membrane is situated on the upper side of the channel. The fluid flows parallel to the membrane except at the in- and outlet (figure 2). Care has been taken that the position of the tubes is similar for all experiments although small changes could not be avoided.

Filtering procedure

Before the membrane is placed into the module it is wetted using dodecane (Merck, p.a.) to prevent adsorption of surfactant into the pores of the membrane. The emulsion, which is stirred in a vessel with a magnetic stirrer, is pumped with a flow rate of approximately $4 \cdot 10^{-2}\ \text{m} \cdot \text{s}^{-1}$ through the module using a gear pump. However, during the experiment a change in flow rate of $\pm 10\ \%$ is often detected. A pressure of circa $0.05\ \text{bar}$ is regulated

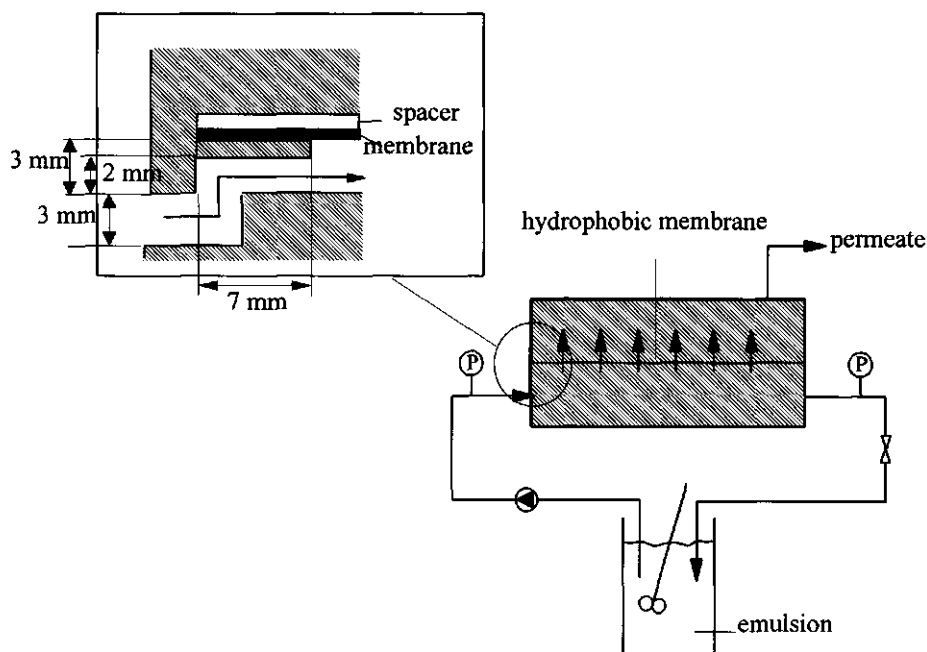


Figure 2, Membrane system

with a pressure valve on the retentate side of the module. The permeate is collected into a beaker, while the retentate is led back to the vessel containing the emulsion. During this batch process, oil concentration and droplet size distribution are determined of samples that are taken from the feed.

Preparation of the emulsions

Emulsions are made by mixing an aqueous solution of $1 \text{ g} \cdot \text{l}^{-1}$ of the nonionic surfactant poly(20)oxyethylene-sorbitan-monopalmitate (Tween-40, Sigma, p.a.) with specified amounts of n-hexadecane (Merck, p.a.) or 1-bromohexadecane (Janssen Chimica). The densities of both oils are 773 and $999 \text{ kg} \cdot \text{m}^{-3}$, respectively. The oil concentration in the emulsions is always smaller than 6 weight percent. Emulsions with different droplet size distributions are prepared by using three different mixing methods. Firstly, 100 ml

emulsion is sonified during 10 minutes at an energy output of 70 Watt using a *Branson sonifier*, type 250. Secondly, 100 ml emulsion is homogenized during 15 minutes using a *Condi Labhomogenizer*. The pressure, which can not be adjusted, is circa 100 bar. The third method to prepare emulsions employs a *Silverson mixer*, type L4R. In this apparatus, a 4-bladed turbine stirrer presses liquid through a perforated stator. A volume of 100 ml emulsion is mixed during 2 minutes at 1200 rpm. To assure maximal dispersion of the oil, the oil phase is always added gradually to the solution during the mixing process. Care has been taken to prepare identical emulsions in case of multiple experiments. However, variations of $\pm 5\%$ both in the initial oil concentration as in the d_{32} have been observed.

Measurement of the oil concentration in the emulsion

Ten μl of sample is diluted with 990 μl ethanol (Merck, p.a.) and 1 μl of this dilution is injected in a Carlo Erba gas chromatograph (GC 6000, vega series) with a 10 m CP-Sil 5 CB capillar column (Chrompack, The Netherlands) and a cold on-column injection system. At the moment of injection the oven temperature is 80 °C. After one minute, the temperature is increased at 15 °C·min⁻¹ up to 250 °C. The F.I.D detection of hexadecane and bromohexadecane occurs at 370 °C. To calculate the concentration, a calibration curve is used.

Measurement of droplet size distributions

Because generally determination of droplet size distributions is quite inaccurate, especially in case of small droplets ($<0.2\ \mu\text{m}$), several methods have been used and compared. Firstly, with an Axiomat (Zeiss) *microscope* a qualitative impression of the size distribution is obtained. Secondly, *spectroturbidimetry* as described by Walstra¹² is used. In this method, the optical density of the emulsion is measured at several wave lengths and, with other data such as concentration and refractive indices, a specific turbidity spectrum is calculated and compared with theoretical spectra. Subsequently,

the average volume/surface droplet diameter, d_{32} , can be deduced from the theoretical spectrum that matches best. Accurate results can be obtained for droplets with a d_{32} between 0.2 and 15 μm . Also, the *dynamic light scattering* method is applied. The variation of intensity of scattered light in time is measured so the diffusion coefficient can be calculated. With the Stokes-Einstein relation the volume averaged diameter, d_{30} , can be derived, which is usually somewhat smaller than the average volume/surface droplet diameter. This method can be used for droplets with a diameter smaller than 0.2 μm . Finally, measurements have been performed with the *Coulter Laser LS 130* with a Polarization Intensity Differential Scattering unit. This apparatus uses polarized, monochromatic light at three wavelengths. The difference in scattering of horizontally and vertically polarized light is measured at five different scattering angles. These measurements form a pattern that varies sensitively with droplet size. This method can be used for droplets with a diameter as small as 0.1 μm .

Characteristics of the various emulsions

All homogenized and sonified emulsions are stable. The average droplet size does not increase during several days of storage, so droplet-droplet coalescence is negligible. A cream layer of stable oil droplets is formed only after several weeks. An exception are emulsions with hexadecane when prepared with the Silverson mixer. Then, such a cream layer can already be detected after 24 hours. The droplet size distributions of the

Table 1. Average diameters (d_{32} 's [μm] for static and polarized scattering and d_{30} for dynamic scattering) as determined by various scattering methods.

scattering	bromohexadecane			hexadecane		
	homogenized	sonified	Silverson	homogenized	sonified	Silverson
static				0.50	0.44	
dynamic	0.48	0.73		0.49	0.77	
polarized	0.55	0.94	8.45	0.63	0.82	12.4

emulsions with bromohexadecane as measured with the Coulter Laser are shown in figure 3. Similar distributions have been observed for emulsions with hexadecane as the oil phase. Table 1 shows the results of the different methods. The values differ substantially, probably because not a single method is suitable to measure the whole range of droplet sizes within one distribution. However, it still can be seen that the average droplet sizes of emulsions prepared with the Silverson mixer are larger than those of the two other emulsions. The most important difference between the distributions of the homogenized and the sonified emulsions is their width; the distribution of the sonified emulsion is broader. It is known from literature that droplet size distributions of sonified emulsions often have two peaks. It is possible that in the

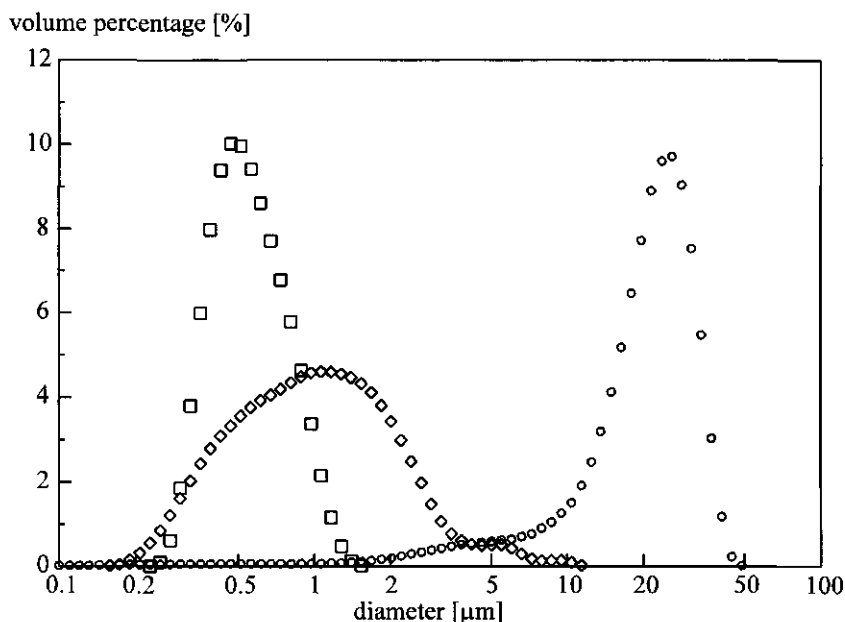


Figure 3. Droplet size distributions of bromohexadecane emulsions ($0.05 \text{ g}\cdot\text{g}^{-1}$) as measured with the Coulter Laser. Squares denote the homogenized emulsion, diamonds the sonified and circles the Silverson mixed emulsion.

present investigation the two peaks could not be distinguished by the methods used, resulting in a single peak and a broader distribution.

Procedure to fit the experimental flux data

The experimental data can be fitted by a formula based on mass balances over the membrane module and over the vessel containing the emulsion. By fitting the data, the apparent deposition velocity of the oil droplets on the membrane, v' [$\text{m}\cdot\text{s}^{-1}$], is determined. It's value is an indication for the efficiency of oil droplet separation; an increase of v' means an increase of the velocity at which oil droplets permeate through the membrane. Thus, v' can be used to compare different experiments. The derivation of the fit formula is given in the appendix.

Transport Model

The calculations using the perfect sink model start by determining the four dimensionless numbers for each droplet size group z . Then, the appropriate solution of the perfect sink model is determined (equation 5, 6 or 7). If Pe and Gr do not differ by more than a factor 100 the additivity rule is applied. Next, the theoretical flux j_z is calculated as a function of time. The interception deposition mechanism can be incorporated in equation 7 by defining a supplementary deposition flux, denoted by the subscript i .

$$j_{z,i} = \frac{a_z}{b} \cdot \frac{\phi \cdot n_z}{O} \quad (8)$$

Here, O [m^2] is the membrane surface. The underlying thought is that per volume unity that flows in the module a droplet fraction of a_z/b permeates through the membrane because it is in contact with the membrane. It must be kept in mind that this relationship is a straightforward approach to calculate the fraction of oil which is present at the membrane at the inlet of the module and therefore should permeate. This assumption is in line with the perfect sink assumption.

Finally, it is necessary to calculate the 'overall' deposition velocity v'' [$\text{m}\cdot\text{s}^{-1}$] which can be compared to the experimentally fitted v' . Therefor, the procedure to determine v'' is similar to the one determining v' .

Results and Discussion

Experimental results

During a filtration experiment the oil flux decreases in time because oil permeates out of the emulsion. No water can be detected in the permeate (measured by Karl Fisher titration). The reproducibility between the apparent deposition velocities of two similar experiments is $\pm 30\%$. Severe fouling of the membrane by the surfactant is not the cause for this inaccuracy; no systematically flux decreases are detected when several experiments with identical emulsions are performed without renewing the membrane. On the other hand, changes in pump delivery during the experiments might contribute partly to the low reproducibility as will deviations in the initial oil concentration and droplet size distribution. Moreover, small variations in the flow pattern due to changes in the position of both the inlet tube and the module, as well as due to changes of flow velocity might effect the interception mechanism, thus influencing the total flux.

To discuss the validity of formula 1, the filtration of a homogenized bromohexadecane-in-water emulsion is taken as an example. The oil concentration in the emulsion decreases from $0.055 \text{ g}\cdot\text{g}^{-1}$ at the beginning of the experiment to $0.01 \text{ g}\cdot\text{g}^{-1}$ after 150 hours. The related flux values are 0.17 and $0.0015 \text{ l}\cdot\text{hr}^{-1}\cdot\text{m}^{-2}$ respectively. The magnitude of the initial flux might fulfill the criterion of formula 1 because usually the value of J_c ranges between 1 and $100 \text{ l}\cdot\text{hr}^{-1}\cdot\text{m}^{-2}$ ^{13, 14, 15}. Thus, initially, when $V_d/V_c = 0.05$, $J_{d,\min}$ ranges between 0.05 and $5 \text{ l}\cdot\text{hr}^{-1}\cdot\text{m}^{-2}$. At the end of the experiment V_d/V_c equals 0.008 , resulting in $0.008 \text{ l}\cdot\text{hr}^{-1}\cdot\text{m}^{-2} < J_{d,\min} < 0.8 \text{ l}\cdot\text{hr}^{-1}\cdot\text{m}^{-2}$. Here, the criterion of formula 1 is not met. The initial flux value indicates that permeation of the dispersed phase is a very

promising method and can compete with conventional filtration methods. However, the process should be optimized to increase the flux values at very low oil volumes in the emulsion.

Influence of droplet size distribution and density of the oil phase

Several filtration experiments have been performed with droplet size distribution and density difference as variables. Figure 4a shows the oil concentration in the emulsion during the filtration of bromohexadecane-in-water emulsions with three different droplet size distributions. The difference between the curves of the sonified and the homogenized

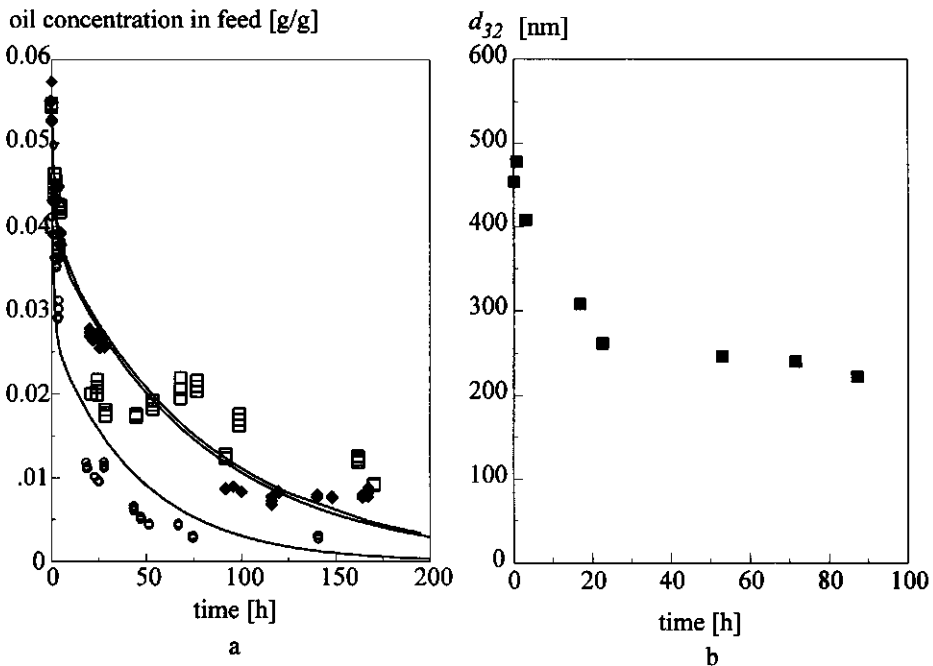


Figure 4. (a) Measured (marks) and fitted (lines) concentration curves during the filtration of three bromohexadecane-in-water emulsions: \blacklozenge homogenized emulsion with $d_{32} = 0.6 \mu\text{m}$, \square sonified emulsion with $d_{32} = 0.9 \mu\text{m}$ and \circ emulsion prepared with the Silverson mixer, $d_{32} = 8.5 \mu\text{m}$. The values for v' are shown in table 2. (b) Average droplet diameter during the filtration of the homogenized emulsion from figure 4a as measured with the dynamic light scattering method.

emulsions (both small d_{32}) is small. However, the oil phase of the Silverson mixed emulsion (large d_{32}) clearly permeates faster. During the filtration experiments the average droplet sizes have also been measured. An example is given in figure 4b; similar droplet size decreases have been detected for all types of emulsions and with all droplet size measurement methods. Combination of figures 4a and 4b indicates that large droplets permeate faster than small ones. A similar result was found by Ueyama et al. during the filtration of droplets stabilized by SDS with a PTFE dead end membrane³.

An example of the influence of the density of the dispersed phase on the filtration behavior is given in figure 5. The concentration of hexadecane in the emulsion ($\rho = 773 \text{ kg}\cdot\text{m}^{-3}$) decreases faster than the bromohexadecane concentration ($\rho = 999 \text{ kg}\cdot\text{m}^{-3}$). This

oil concentration in feed [g/g]

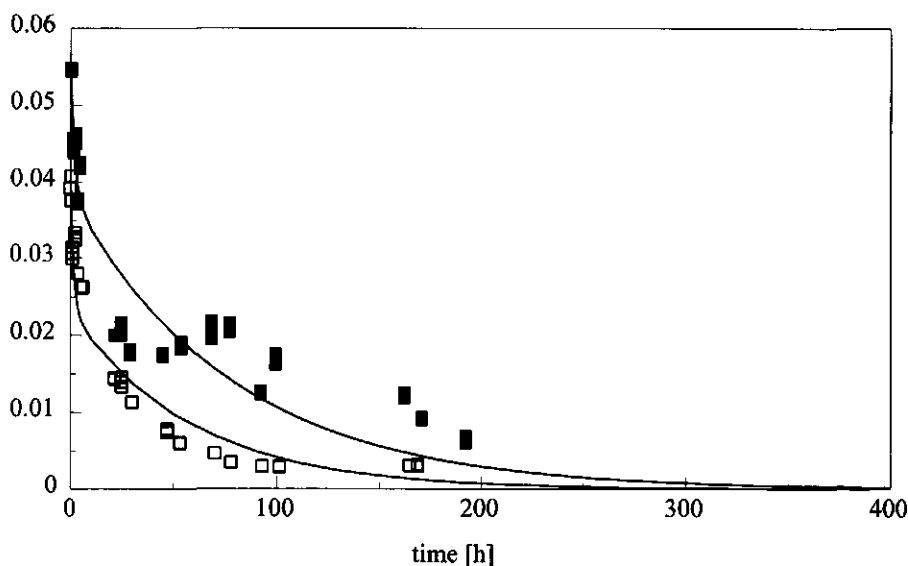


Figure 5. Oil concentration of two sonified emulsions during filtration: ■ bromohexadecane-in-water emulsion and □ hexadecane-in-water emulsion. The values for ν' are shown in table 2.

result has also been found in case of filtration of emulsions with different droplet size distributions.

In table 2 the apparent deposition velocities of the various experiments are summarized. It shows that the difference between the apparent deposition velocities of hexadecane and bromohexadecane is highest for emulsions with a large d_{32} . This indicates the importance of the effect of the gravity force on the deposition velocity in case of hexadecane.

Table 2. Summary of the values of v' [$\mu\text{m}\cdot\text{s}^{-1}$] averaged over two similar experiments, during filtration of several emulsions.

method of mixing	bromohexadecane	hexadecane
homogenized	0.14	0.16
sonified	0.14	0.21
Silverson mixed	0.25	0.49

The perfect sink model

The filtration experiments have been simulated using the perfect sink theory. In figure 6 simulations of the effect of droplet size on the relative contributions of the different transport mechanisms (diffusion, gravity and interception) to the total flux are given. In case of bromohexadecane Pe/Gr , which is independent of droplet size, is equal to 15.1 while for hexadecane this ratio is 0.067. Thus, in both cases the additivity rule has been applied (equation 7 and 8).

It is calculated that both the importance of the interception mechanism as well as that of the gravity mechanism increases with increasing droplet diameter. For small droplets the deposition rate is mainly determined by diffusion. This is consistent with the statement of Rubow¹⁵ that the removal of sub micrometer particles from gases can be predicted accurately when using both the interception and the diffusion mechanism.

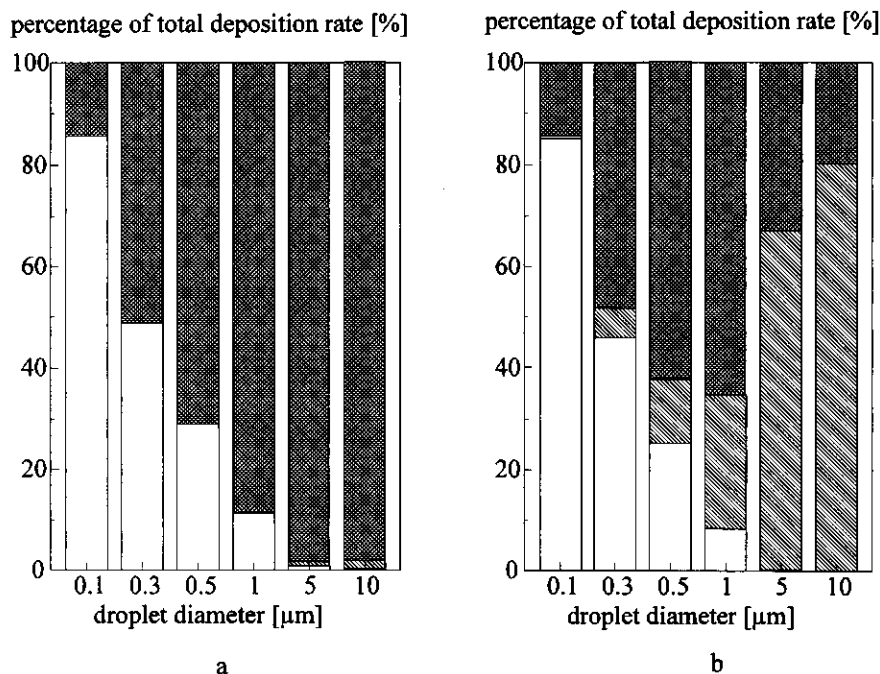


Figure 6. Simulations of the relative contribution of the transport mechanisms to the total flux as function of droplet diameter with an average fluid velocity of $4 \cdot 10^{-2} \text{ m s}^{-1}$ for (a) a homogeneous bromohexadecane-in-water emulsion and (b) a homogeneous hexadecane-in-water emulsion: empty bars denote diffusion mechanism, bars with crossed fill pattern denote interception mechanism and diagonal filled bars denote gravity mechanism.

Also, the *absolute* deposition velocity is a function of droplet size (figure 7). At each flow rate a droplet size with the lowest deposition velocity can be determined. In case of separation of emulsions by flowing through coalescers this is called the most penetrating particle size⁸ although in this work it would be better to call it the least permeating droplet size. In figure 7 a high fraction of permeated oil corresponds with a high apparent deposition velocity. Thus, it can be seen that the difference between the apparent deposition velocities of a sonified ($d_{32} = 0.9 \mu\text{m}$) and a homogenized ($d_{32} = 0.6 \mu\text{m}$)

emulsion is negligible compared to the difference between one of these and the apparent deposition velocity of the Silverson mixed emulsion ($d_{32} = 8.5 \mu\text{m}$). This is coherent with the results from figure 4a.

At a constant flow rate the least permeating droplet size is somewhat smaller for hexadecane than for bromohexadecane. This is due to the large density difference in case of hexadecane, which improves the permeation of large droplets. This is also the reason for the higher total filtration rate of large hexadecane droplets compared to large bromohexadecane droplets. The effect diminishes if the droplet size decreases. This is

permeated oil/oil before filtration [g/g]

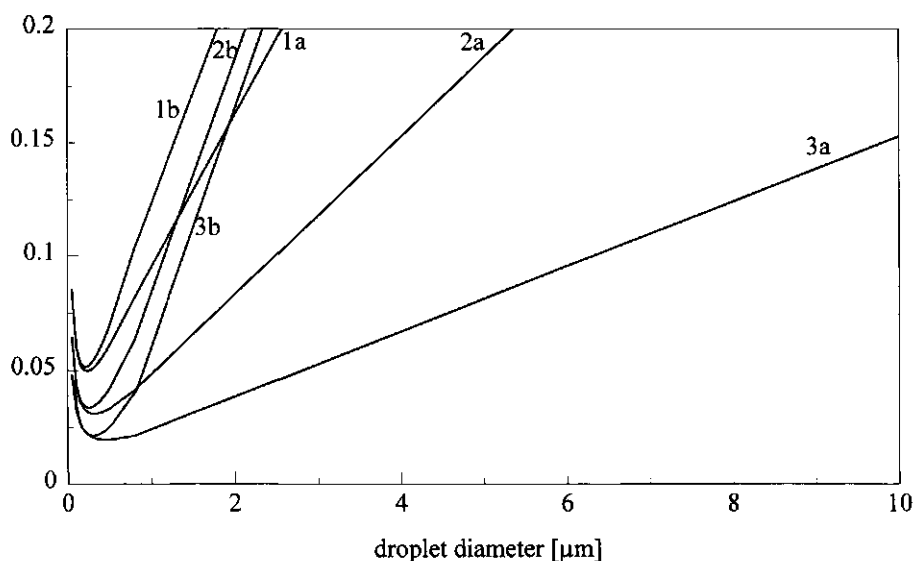


Figure 7, Fraction of oil that permeated after 3 hours filtration, calculated for homogeneous emulsions of bromohexadecane (a) and hexadecane (b) as a function of droplet diameter with different average velocities of the fluid; $37 \cdot 10^{-3} \text{ m} \cdot \text{s}^{-1}$ for line 1, $17 \cdot 10^{-3} \text{ m} \cdot \text{s}^{-1}$ for line 2 and $6.2 \cdot 10^{-3} \text{ m} \cdot \text{s}^{-1}$ for line 3.

consistent with the experimental data of figure 5 and table 2. For all emulsions the apparent deposition velocity of hexadecane is larger than that of bromohexadecane and the difference is highest for the emulsions with large d_{32} .

The total fraction of oil that has permeated after 3 hours filtration increases with increasing flow rate. This is caused by the increased amount of droplets that contacts the membrane due to interception per unit of time. Thus, the relative contributions of both the diffusion and the gravity mechanism decrease while the influence of the interception mechanism increases with increasing flow rate.

Simulations of droplet size distributions after filtration

To determine whether the perfect sink theory can be applied not only qualitatively but also quantitatively, simulations and experimental data have been compared. Firstly, the droplet size distribution after filtration, calculated using the perfect sink theory, has been compared with the experimentally determined droplet size distribution (figure 8). For all emulsions a similar decrease of average droplet size has been both measured and calculated (table 3).

Table 3. Comparison of d_{32} values [μm] before (measured using polarized scattering) and after filtration (measured and calculated, implying that interception occurs).

method of mixing	dispersed phase	measured before filtration	measured after filtration	calculated after filtration
homogenized	bromohexadecane	0.55	0.22	0.45
sonified	bromohexadecane	0.94	0.23	0.44
Silverson	bromohexadecane	8.45	0.25	0.32
homogenized	hexadecane	0.63	0.32	0.34
sonified	hexadecane	0.82	0.22	0.26
Silverson	hexadecane	12.4	0.42	0.19

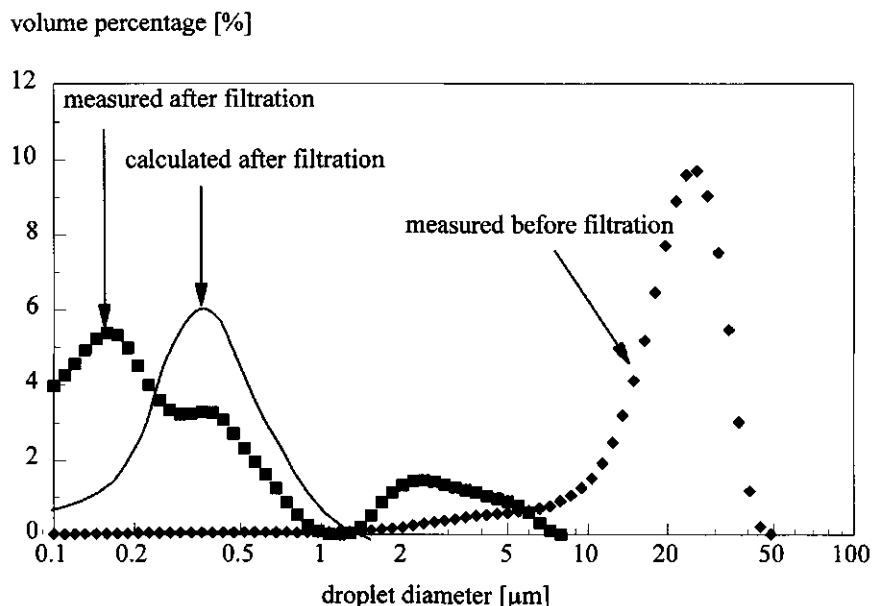


Figure 8, Measured and calculated droplet size distributions before and after the filtration of a Silverson mixed bromohexadecane-in-water emulsion. The calculation includes the interception mechanism.

Experiments and simulations show that during filtration of oil-in-water emulsions all large droplets are removed from the emulsion. Their filtration rate is high due to gravitation and/or interception (figure 6 and 7). Eventually, also smaller droplets permeate, mainly caused by diffusion. For example, for a sonified hexadecane-in-water emulsion the weight fraction of oil has been reduced from 0.038 to 0.00061 after 800 hours of filtration. Thus, 98.4% of the oil has been removed, which should include a large fraction of the small droplets.

Considering figure 7 it is expected that not only large droplets but also droplets smaller than the least permeating droplet size will be removed from the emulsion with a

high filtration rate. Unfortunately, our droplet size measurements are unable to detect a decrease of the volume fraction of these very small droplets.

The deviation between the calculated and measured d_{32} after filtration might be partly due to the inaccuracy of the measurements of the distributions before filtration. These distributions, which are used for the calculations, are quite broad. Hence, the amount of small droplets is probably underestimated. Small changes of the input distributions, such as increasing the fraction of droplets with a diameter smaller than 1 μm , result in a better similarity between the calculated and measured values of d_{32} after filtration.

Simulations of oil concentration during filtration

A second way to validate the model is to compare experimentally determined and predicted oil concentrations in the feed during filtration. Simulations have been carried out with and without interception because this mechanism is expected to be important (figure 6). On the other hand, it is difficult to quantify in the given experimental setup. An experiment with a Silverson mixed emulsion with red colored bromohexadecane as the dispersed phase showed an accumulation of red color at the entrance of the module. This indicates the importance of the interception mechanism at the entrance.

An example of the simulation of the oil concentration during filtration is given in figure 9 and in table 4 the predicted and apparent deposition velocities are compared. As can be seen in table 4, in almost all cases v' is in between v'' without and with interception. Only in case of the Silverson mixed hexadecane-in-water emulsions the modeled values are always too high. This can be caused, among other things, by the inaccuracy of the droplet size measurements as mentioned before. A small overestimation of the amount of large droplets will cause a large overestimation of the calculated deposition velocity due to gravity, which becomes the dominant transport mechanism for large hexadecane droplets (figure 6).

Thus, generally formula (8) overestimates the interception effect. Nevertheless, implementation of the mechanism of interception can be used to improve the predictions

Table 4. Comparison of apparent deposition velocities, v' [$\mu\text{m}\cdot\text{s}^{-1}$] derived from experimental data averaged over two similar experiments and deposition velocities, v'' [$\mu\text{m}\cdot\text{s}^{-1}$], predicted by the perfect sink model.

	bromohexadecane			hexadecane		
	v'	v'' without interception	v'' with interception	v'	v'' without interception	v'' with interception
homogenized	0.14	0.01	0.23	0.16	0.08	0.22
sonified	0.14	0.04	0.28	0.21	0.14	0.31
Silverson	0.25	0.18	5.31	0.49	5.01	10.42

oil concentration in feed [g/g]

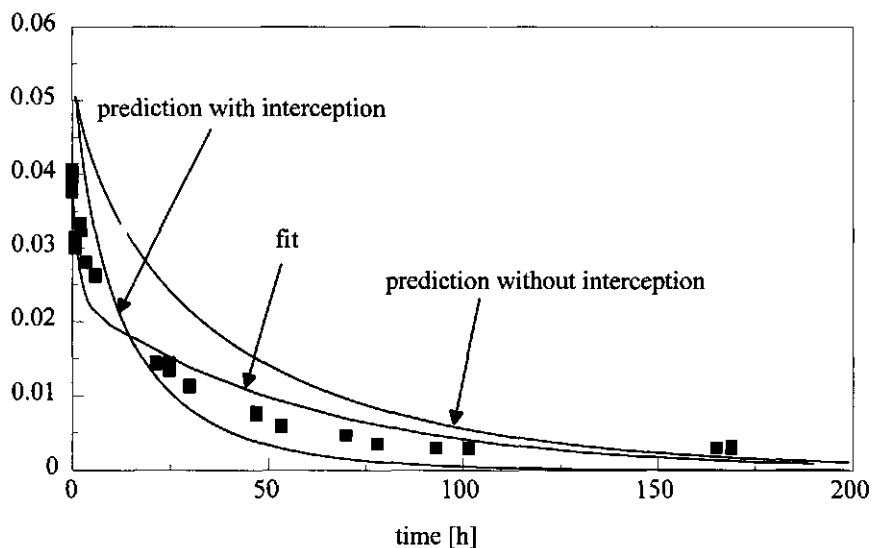


Figure 9. Experimental data and both the fitted and predicted values of the oil concentration during filtration of a sonified hexadecane-in-water emulsion. The deposition velocities are given in table 4.

according to the perfect sink model. This is consistent with the observation of other research groups that interception often is an important transport mechanism^{3,16}.

A final remark concerns the assumption that the hydrodynamic drag and the van der Waals attraction a droplet experiences in the vicinity of the membrane are both negligible. As stated before, the drag is induced by inertial lift forces and is also called the tubular pinch effect. The lift velocity can be calculated as a function of droplet size¹⁰. These calculations show that for small droplets ($a < 2 \mu\text{m}$) close to the membrane the lift velocity varies between $1 \cdot 10^{-12}$ and $1 \cdot 10^{-9} \text{ m}\cdot\text{s}^{-1}$. These values are much smaller than the deposition velocities in table 4, indicating that it is justified to ignore the drag effect in case of small droplets. Moreover, the van der Waals attraction is noticeable at very short distances from the membrane only (nanometers). At larger distances the effect can be neglected too.

Accuracy of the flux predictions

The model assumptions are not always met. For example, the model is valid for $Pe < 10^2$. If this condition is not met, an underestimation of the deposition velocities can be expected¹¹. This is true for $\bar{v} = 4 \cdot 10^{-2} \text{ m}\cdot\text{s}^{-1}$ and $d_{32} > 1.1 \mu\text{m}$. However, this effect is negligible compared to the effect of interception. Moreover, the model assumes laminar flow in the module. The Reynolds number in the channel is 111, fulfilling this condition, yet at the entrance and the exit of the module stable, laminar vortices can occur. However, these will be small compared to the total length of the module. Moreover, the correctness of the assumption of perfect sink is questionable since coalescence costs time (see also chapter 4 of this thesis). Finally, predictions will always deviate from the experimental values because of the $\pm 30\%$ reproducibility of the filtration experiments as discussed earlier. In literature about coalescers⁸, deviations between experimentally determined deposition fluxes and those predicted using the perfect sink theory in the absence of colloidal interactions, range between 10 and 20%. Taking the previous mentioned inaccuracies into account, it can be concluded that this might also be true in the present research.

Conclusions

The dispersed phase of stable oil-in-water emulsions can be separated in a cross flow, flat sheet membrane module with a polypropylene membrane. No additional separation process of the permeate is needed, because the permeated oil phase contains no water. Only little fouling of the membrane by the nonionic surfactant Tween-40 has been detected. The perfect sink theory is successful in modeling the experimental data, assuming that no colloidal interactions occur. This indicates that the transport mechanism is the limiting step in the separation.

If the average flow velocity is $4 \cdot 10^{-2} \text{ m} \cdot \text{s}^{-1}$, the transport of small droplets is mainly determined by the diffusion mechanism while for large droplets gravity (if Δp is large) and interception dominate. Generally, large droplets ($d > 1 \text{ } \mu\text{m}$) have high fluxes. During filtration experiments, the oil concentration of emulsions with a large d_{32} reduces faster than in case of emulsions with a small d_{32} . Also, the average droplet size decreases during the experiments. It is calculated that droplets with a diameter smaller than $0.1 \text{ } \mu\text{m}$ also permeate fast, but this has not been proven experimentally. The relative contributions of all mechanisms to the total flux depend on the flow velocity.

Deviations between predicted and experimental data are caused partly by experimental difficulties related to (measurement of) droplet size distributions and variations in flow pattern and flow velocity. Also, accurate modeling of the interception mechanism is hard. Although all these factors make accurate estimations difficult, the model provides reasonable predictions of the time dependent concentration of oil phase in the emulsion, certainly from a qualitative point of view. The perfect sink model can therefor be used to describe the transport in a dispersed phase separator, thus leading to a better understanding of the mechanisms controlling the system. With the gained knowledge efforts can be made to improve the fluxes so that the system becomes competitive to the continuous phase permeation system.

Acknowledgements

The author wishes to thank the Foundation for Chemical Research in the Netherlands for their financial support and both G.R. Kolenbrander and J.M.S. Renkema for performing parts of the experiments, as well as P.S. Vermeiden for developing the fit procedure. Moreover, the department of Physical and Colloid Chemistry is gratefully acknowledged for assistance with the dynamic light scattering analysis and especially B.H. Bijsterbosch for fruitful discussions.

Appendix

Two mass balances can be defined, one over the membrane module and the other over the vessel containing the emulsion. In an ideally mixed membrane module this balance is:

$$V_{mod} \cdot \frac{dn(t)}{dt} = \phi \cdot n_{in}(t) - \phi \cdot n(t) - v' \cdot O \cdot n(t) \quad (9)$$

with V_{mod} [m^3] being the volume of the module, n the droplet concentration in the module, n_{in} the inlet droplet concentration and ϕ [$m^3 \cdot s^{-1}$] the pump delivery (assuming that the volume of extracted oil is negligible, so $\phi_{in} = \phi_{out} = \phi$). The mass balance over the ideally mixed vessel is:

$$V_{ves} \cdot \frac{dn_{ves}(t)}{dt} = \phi \cdot n_{ves,in}(t) - \phi \cdot n_{ves}(t) \quad (10)$$

where V_{ves} [m^3] is the volume of the vessel, n_{ves} the droplet concentration in the vessel and $n_{ves,in}$ the inlet droplet concentration in the vessel. Because $n_{ves,in} = n$ and $n_{ves} = n_{in}$ equations (9) and (10) can be written as:

$$V_{mod} \cdot \frac{dn(t)}{dt} = -(\phi + v' \cdot O) \cdot n(t) + \phi \cdot n_i(t) \quad (11)$$

$$V_{ves} \cdot \frac{dn_{in}(t)}{dt} = \phi \cdot n(t) - \phi \cdot n_i(t) \quad (12)$$

These equations can be solved using Laplace transformation to give:

$$n(t) = \frac{n(0)}{\lambda'' - \lambda'} \cdot \left[(A - \lambda')e^{-\lambda't} - (A - \lambda'')e^{-\lambda''t} \right] \quad (13)$$

with A , λ' and λ'' [s^{-1}] being:

$$A = \frac{\phi \cdot (V_{mod} + V_{ves})}{V_{mod} \cdot V_{ves}}$$

$$\lambda' = \frac{1}{2} \cdot \left[\left(A + \frac{O}{V_{mod}} \cdot v' \right) - \sqrt{\left(A + \frac{O}{V_{mod}} \cdot v' \right)^2 - \left(\frac{4\phi \cdot O}{V_{mod} \cdot V_{ves}} \cdot v' \right)} \right]$$

$$\lambda'' = \frac{1}{2} \cdot \left[\left(A + \frac{O}{V_{mod}} \cdot v' \right) + \sqrt{\left(A + \frac{O}{V_{mod}} \cdot v' \right)^2 - \left(\frac{4\phi \cdot O}{V_{mod} \cdot V_{ves}} \cdot v' \right)} \right] \quad (14)$$

If the emulsion is heterodisperse the total droplet concentration can be calculated as:

$$n(t) = \sum_{z=1}^Z n_z(t) \quad (15)$$

and

$$n_z(t) = \frac{F_z \cdot n(0)}{\lambda_z'' - \lambda_z'} \cdot \left[(A_z - \lambda_z')e^{-\lambda_z't} - (A_z - \lambda_z'')e^{-\lambda_z''t} \right] \quad (16)$$

Z is the number of droplet size groups, $n_z(t)$ the concentration of droplets of size group z at time t and F_z the fraction of droplets of size group z at $t=0$ $\left(\frac{n_z(0)}{n(0)} \right)$. The experimental

and modeled data can be fitted, by using equation (13) with v' as the fit parameter, by minimizing the residual sum of squares between the experimental or theoretical and the fitted concentration $n(t)$.

Nomenclature

Symbols

a	droplet or particle radius	[m]
A	constant according to formula (14)	[s ⁻¹]
A_{123}	Hamaker constant of droplet or particle 1 with wall 2 through medium 3	[J]
Ad	adhesion number	[-]
b	half height of the channel	[m]
d_{30}	volume averaged droplet diameter	[m]
d_{32}	volume/surface averaged droplet diameter	[m]
D	diffusion coefficient	[m ² ·s ⁻¹]
\bar{D}	diffusion dyadic	[m ² ·s ⁻¹]
DL	double layer number	[-]
F	fraction of droplets with a certain size at $t=0$	[-]
g	gravity acceleration	[m·s ⁻²]
Gr	gravity number	[-]
h	distance between droplet or particle and membrane	[m]
J	volume flux	[m·s ⁻¹] and [l·hr ⁻¹ ·m ⁻²]
j	normal component of droplet or particle flux vector	[m ² ·s ⁻¹]
\vec{j}	droplet or particle flux vector	[m ² ·s ⁻¹]
k	constant of Boltzmann	[J·K ⁻¹]
L	length of membrane	[m]

n	droplet or particle concentration	$[\text{m}^{-3}]$
O	membrane area	$[\text{m}^2]$
Pe	Peclet-number	$[-]$
Q	source term	$[\text{m}^3 \cdot \text{s}^{-1}]$
Sh	Sherwood-number, averaged over the entire collector surface	$[-]$
t	time	$[\text{s}]$
T	absolute temperature	$[\text{K}]$
v	velocity of the fluid	$[\text{m} \cdot \text{s}^{-1}]$
\bar{v}	average velocity	$[\text{m} \cdot \text{s}^{-1}]$
\vec{v}	velocity vector of the droplets or particles	$[\text{m} \cdot \text{s}^{-1}]$
v'	apparent deposition velocity of droplets on membrane, determined by fitting experimental data	$[\text{m} \cdot \text{s}^{-1}]$
v''	deposition velocity of droplets on membrane, determined by perfect sink model	$[\text{m} \cdot \text{s}^{-1}]$
V	volume	$[\text{m}^3]$
Z	total number of droplet size groups	$[-]$
δ	primary minimum distance between droplet/particle and membrane	$[\text{m}]$
ϵ	dielectric constant of the medium	$[-]$
ϵ_0	permittivity of the vacuum	$[\text{C} \cdot \text{V}^{-1} \cdot \text{m}^{-1}]$
η	dynamic viscosity	$[\text{N} \cdot \text{s} \cdot \text{m}^{-2}]$
λ'	constant according to formula (14)	$[\text{s}^{-1}]$
λ''	constant according to formula (14)	$[\text{s}^{-1}]$
ϕ	pump delivery	$[\text{m}^3 \cdot \text{s}^{-1}]$
ρ	density	$[\text{kg} \cdot \text{m}^{-3}]$
ζ	zeta potential	$[\text{V}]$

Subscripts

0	at time = 0
i	droplet or particle

2	membrane or wall
3	medium
<i>c</i>	continuous phase
<i>d</i>	dispersed phase
<i>Gr</i>	in case <i>Gr</i> is dominant
<i>i</i>	interception
<i>in</i>	inlet
<i>l</i>	local
<i>min</i>	minimal
<i>mod</i>	module
<i>Pe</i>	in case <i>Pe</i> is dominant
<i>tot</i>	total
<i>ves</i>	vessel
<i>z</i>	indicator for droplet size group
∞	in the bulk

References

- 1 M. Hlavacek, Break-up of oil-in-water emulsions induced by permeation through a microfiltration membrane, 1995, Journal of Membrane Science, vol.102, p.1-7.
- 2 H. Unno, H. Saka and T. Akehata, Oil separation from oil-water mixture by a porous poly(tetrafluoroethylene) (PTFE) membrane, 1986, Journal of Chemical Engineering of Japan, vol. 19, no.4, p.281-286.
- 3 K. Ueyama, K. Fukuura and S. Furusaki, Oil-phase permeation behavior of O/W emulsion through a porous polytetrafluoroethylene membrane, 1987, Journal of Chemical Engineering of Japan, vol.20, no.6, p.619-622.
- 4 B.D. Bowen, S. Levine and N. Epstein, Fine particle deposition in laminar flow through parallel-plates and cylindrical channels, 1976, Journal of Colloid and Interface Science, vol.54, no.3, p.375-390.

- 5 **R.H. Davis and D.C. Grant**, Theory for dead end microfiltration, in: *Membrane Handbook*, eds. W.S. W. Ho and K.K. Sirkar, Van Nostrand Reinhold, New York, N.Y, USA, 1992, p. 461-479.
- 6 **D.C. Grant, B.Y.H. Liu, W.G. Fisher and R.A. Bowling**, Particle Capture Mechanisms in Gases and Liquids: An Analysis of Operative Mechanisms in Membrane/Fibrous Filters, 1989, *The Journal of Environmental Sciences*, july/august, p.43-51.
- 7 **C.G. Vinson and S.W. Churchill**, Removal of drops from liquid-liquid dispersions upon flow through screens, 1970, *The Chemical Engineering Journal*, vol.1, p.110-119.
- 8 **Z. Adamczyk, T. Dabros, J. Czarnecki and T.G.M. van de Ven**, Particle transfer to solid interfaces, 1983, *Advances in Colloid and Interface Science*, vol.19, p.183-252.
- 9 **J. Lyklema**, *Fundamentals of interface and colloid science*, vol.1: *Fundamentals*, Academic Press, London, 1991.
- 10 **F.W. Altena and G. Belfort**, Lateral migration of spherical particles in porous flow channels: Application to membrane filtration, 1984, *Chemical Engineering Science*, vol.39, no.2, p.343-355.
- 11 **Z. Adamczyk and T.G.M. van de Ven**, Deposition of particles under external forces in laminar flow through parallel-plate and cylindrical channels, 1981, *Journal of Colloid and Interface Science*, vol.80, p.340-356.
- 12 **P. Walstra**, Estimating Globule-Size Distribution of oil-in-water emulsions by spectroturbidimetry, 1968, *Journal of Colloid and Interface Science*, vol.27, no.3, p.493-500.
- 13 **G. Akay and R.J. Wakeman**, Ultrafiltration and microfiltration of surfactant dispersions: an evaluation of published research, 1993, *TranslChemE*, vol.75-A, p.411-419.
- 14 **P. Lipp, C.H. Lee, G. Fane and C.J.D. Fell**, A fundamental study of the ultrafiltration of oil-water emulsions, 1988, *Journal of Membrane Science*, vol.36, p.161-177.
- 15 **K.L. Rubow, B.Y.H. Liu and D.C. Grant**, Characteristics of ultra-high efficiency membrane filters, *Proceedings of the 33rd Annual meeting of the Institute of Environmental Science*, 1987, p. 383-387.
- 16 **F.M. Othman, M.A. Fahim, G.V. Jeffreys and C.J. Mumford**, Prediction of predominant mechanisms in the separation of secondary dispersions in a fibrous bed, 1988, *Journal of Dispersion Science and Technology*, vol.9, no.2, p.91-113.

3 Transport mechanisms in dispersed phase separators: hydrodynamics

Summary

Separation is investigated of dispersed bromo(hexa)decane droplets ($d_{32} < 10 \mu\text{m}$) stabilized by Tween-40 out of an oil-in-water emulsion by using hydrophobic polypropylene membranes. It has been found previously (chapter 2 of this thesis) that the droplet transport towards the membrane can be modeled by the convective diffusion equation with perfect sink conditions at the membrane surface and presupposing interception to be an important mechanism. To verify the assumption of interception three different module types are investigated in the present chapter; a flat sheet module, a hollow fiber module and a dead end module. The flow velocity is varied as well as the dimensions of the first two module types.

It is confirmed that the experimental permeation data, when expressed as Sh -numbers, can best be described by models which include interception. Generally, the predictions are best at intermediate velocities. Only in case of the hollow fiber modules, the predictions always overestimate the experimental data. It is concluded that the perfect sink condition is met in most cases, hence transport is the rate limiting mechanism. Experimentally, a decrease of Sh with increasing velocity is found for the dead end module, which is not predicted by the models. The time dependent coalescence becomes the rate limiting step at high flow velocities due to the decreased contact time between droplet and membrane. Both a decreased residence time as an increased detachment of droplets from the membrane into the bulk contribute to this effect. If the coalescence time is larger than the contact time, the perfect sink condition is not met and the convective diffusion model should be extended by coalescence models.

Introduction

As mentioned before (chapter 1 and 2) the aim of this thesis is to investigate the possibility to permeate the dispersed phase of an emulsion through the membrane instead of the more commonly applied continuous phase permeation. The membrane area needed for an efficient separation process can be reduced significantly in this way, especially if the volume fraction of the dispersed phase is small. In order for this process to be successful, the droplets have to be transported from the bulk towards the membrane. This transport can be governed by several mechanisms which have been described in chapter 2 (interception, inertial impaction, diffusive capture, gravitational settling and electrostatic deposition). Secondly, droplets have to coalesce with the membrane or with a droplet that is attached to the membrane. This is a time dependent process because of the film drainage of the continuous phase between the droplet and the membrane.

In chapter 2 it is shown that stable (bromo-)hexadecane droplets can indeed be separated from the continuous water phase using an hydrophobic polypropylene membrane in a flat sheet module. Moreover, the process can be modeled using the simplified solutions of the convective diffusion equation with the so called perfect sink assumption. This implies that all droplets arriving at the membrane surface are irreversibly removed by instantaneous coalescence. The main question that is left by the model is the contribution of interception to the total transport. Interception occurs when the combined effect of the location of the flow lines and the droplet size results in contact between the membrane and the droplet. It is the objective of this chapter to gain more knowledge about this mechanism by investigating the effect of several process parameters on both the experimentally determined flux values as on the model predictions. Three different module types have been investigated; a flat sheet module, a hollow fiber module and a dead end module. Variables are the dimensions of the modules and the flow velocity. The mechanism of detachment is introduced, i.e. the removal of drops from the membrane surface back into the bulk. This effect will shorten the contact time between droplet and membrane and thus reduces the chance of coalescence. Therewith, the perfect sink condition might not be valid in case of detachment.

Theory

The investigated modules differ both in hydrodynamics (flow profile and wall shear stress) as in the derivation of the Sherwood number which describes the transport of droplets from the bulk towards the membrane in that particular module. As already discussed in chapter 2, the general definition of Sh [-] used for this process is given by¹:

$$Sh = \frac{j \cdot a}{n_{\infty} \cdot D_{\infty}} \quad (1)$$

where j [$\text{m}^2 \cdot \text{s}^{-1}$] is the flux through the membrane, a [m] is the droplet radius, n_{∞} [m^{-3}] the droplet concentration in the bulk and D_{∞} [$\text{m}^2 \cdot \text{s}^{-1}$] the diffusion coefficient in the bulk. The latter can be calculated by the Stokes Einstein relation $D = kT/6\pi\eta a$, with k [$\text{J} \cdot \text{K}^{-1}$] is the constant of Boltzmann, T [K] the absolute temperature and η [$\text{N} \cdot \text{s} \cdot \text{m}^{-2}$] the dynamic viscosity. The flux, and thus Sh as defined in (1), is averaged over the entire membrane surface. In the following, the solutions of the convective diffusion equation will be described for the three different membrane modules. In all cases it is assumed that colloidal repulsion does not occur and that the hydrodynamic repulsion a droplet experiences in the vicinity of the wall is balanced by the van der Waals attraction force (chapter 2). The three major transport mechanisms determining j are expected to be gravitational settling, Brownian motion and interception, while inertial impaction is neglected. The Sh -number which includes all these transport mechanisms, Sh_{overall} , is given by¹:

$$Sh_{\text{overall}} = \frac{\exp\left(-\frac{1}{6} \cdot Pe \cdot (\delta + 1)^3 - Gr \cdot \delta\right)}{\int_{\delta}^{\infty} \exp\left(-\frac{1}{6} \cdot Pe \cdot (H + 1)^3 - Gr \cdot H\right) dH} \quad (2)$$

with H [-] is the normalized distance between the center of the droplet and the membrane and δ [m] is the normalized primary minimum distance, which is the distance between droplet and membrane at which the sum of the colloidal interactions is maximal

attractive. Both H and δ are normalized by division by a . The gravity number Gr [-] is equal to $4\pi(\rho_d - \rho_w)g \cdot a^4 / (3kT)$, with ρ_d and ρ_w [$\text{kg} \cdot \text{m}^{-3}$] being the densities of the droplet and the medium respectively and g [$\text{m} \cdot \text{s}^{-2}$] the gravity acceleration. The Peclet-number, Pe , denotes the relative magnitude of hydrodynamic and diffusional effects and is dependent on the module type. In chapter 2, only simplified solutions of equation 2 are presented, whereas in the present chapter, calculations will be performed using equation 2 too.

As discussed in chapter 2, several simplified solutions of $Sh_{overall}$ are defined. Firstly, if gravitational settling and interception do not occur, $Sh_{overall}$ can be solved by neglecting the finite size effects (i.e. $a \ll$ thickness of the diffusion boundary layer). This gives Sh_{Pe} , the Sh -number determined by the Peclet number only¹:

$$Sh_{Pe} = K \cdot Pe^{\frac{1}{3}} \quad (3)$$

K [-] is a constant which depends on the module configuration. Secondly, if gravitation is the dominant transport mechanism, $Sh_{overall} = Sh_{Gr} = Gr$. Thirdly, if Pe and Gr are in the same order of magnitude, Sh_{tot} can be defined. Here, it is assumed that the Sherwood numbers of the three transport mechanisms, diffusion, gravitational settling and interception, can be added to give the overall Sherwood number Sh_{tot} :

$$Sh_{tot} = Sh_{Pe} + Sh_{Gr} + Sh_i \quad (4)$$

Sh_i describes the effect of interception and will be discussed further on.

Furthermore, in order to discuss the effect of detachment, the flow profiles and the wall shear stresses are described for the different module types. It has been found that the detachment velocity is a function of the wall shear stress, τ_w [Pa]; $\langle k' \rangle \div (\tau_w)$, with q [-] being a positive constant and $\langle k' \rangle$ [$\text{m} \cdot \text{s}^{-1}$] the logarithmic mean of the detachment velocity^{2,3,4}. One mechanism underlying the detachment is the viscous drag force, F_{drag} [N], that acts to pull a droplet, resting on a flat surface, in the direction of the flow. This force is equal to:

$$F_{drag} = 32 \cdot a^2 \cdot \tau_w \quad (5)$$

Thus, flux differences between modules can partly originate from differences in the wall shear stresses. Inertial lift forces can also contribute to detachment but are usually negligible if $Re_d = a \cdot v \cdot \rho / \eta < 1$, with Re_d [-] being the Reynolds number of the droplets and v [m·s⁻¹] the velocity. This criterion is met in the present study.

Flat sheet module

Hydrodynamics

The velocity at a distance z [m] from the center of the channel (see figure 1) can be described as:

$$v = \frac{3}{2} \bar{v} \cdot \left[1 - \frac{z^2}{b^2} \right] \quad (6)$$

with \bar{v} [m·s⁻¹] being the average fluid velocity and b [m] the half channel height. At $z = b$, the wall shear stress is equal to the shear stress τ [Pa]:

$$\tau = -\eta \cdot \frac{dv}{dz} \text{ and } \tau_w = \frac{3\eta \cdot \bar{v}}{b} \quad (7)$$

Calculation of Sh

Generally, formula 2 can be used to calculate $Sh_{overall}$. For a flat sheet module the Peclet number Pe_{fs} is equal to¹:

$$Pe_{fs} = \frac{3\bar{v} \cdot a^3}{2b^2 \cdot D_\infty} \quad (8)$$

In the absence of gravitational settling and interception Sh_{pe} can be calculated according to equation 3 with K being:

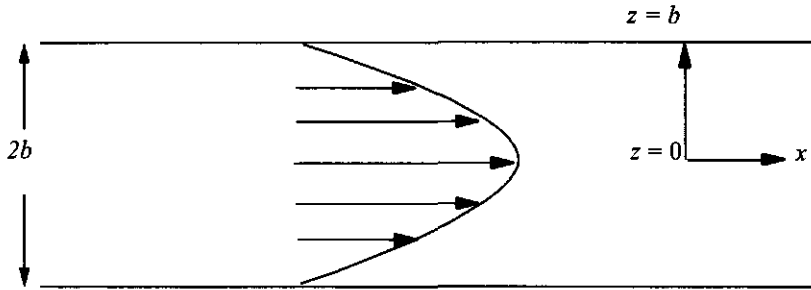


Figure 1, Schematic drawing of the flow profile in a flat sheet module.

$$K_{fs} = \frac{1.017}{\left(\frac{L}{b}\right)^{\frac{1}{3}}} \quad (9)$$

Here, L [m] is the length of the channel. To calculate Sh_p , it is assumed that a certain fraction of the droplets entering the module permeates directly through the membrane because it contacts the membrane. With a membrane on one side of the flow channel only, the interception area fraction A/A , is equal to $(2a \cdot w)/(2b \cdot w)$. Here, A [m²] is the entrance surface area of the module and w [m] is the width of the channel. Therefore,

$$j_{ifs} = \frac{a \cdot \phi \cdot n_{\infty}}{b \cdot O} \text{ and thus } Sh_{ifs} = \frac{a^2 \cdot \phi}{b \cdot O \cdot D_{\infty}} \quad (10)$$

with ϕ [m³·s⁻¹] is the pump delivery and O [m²] the membrane area.

Hollow fiber module

Hydrodynamics

The laminar flow velocity at a distance z [m] from the center of a tube with radius R [m] can be described as

$$v = 2\bar{v}\left(1 - \frac{z^2}{R^2}\right) \quad (11)$$

Figure 1 also holds qualitatively for this situation if b is replaced by R . In this case, τ_w is equal to:

$$\tau_w = \frac{4\eta \cdot \bar{v}}{R} \quad (12)$$

Calculation of Sh

In case of a hollow fiber module equation (2), (3) and (9) are valid if b is replaced by the fiber radius R . Also, Pe changes into:

$$Pe_H = \frac{2\bar{v} \cdot a^3}{R^2 \cdot D_\infty} \quad (13)$$

For a single fiber, denoted by the subscript $1f$, the interception area $A_{i,1f}$ can be defined as:

$$\frac{A_{i,1f}}{A_{1f}} = \frac{(\pi \cdot R^2) - (\pi \cdot (R - 2a)^2)}{\pi \cdot R^2} \text{ giving } \frac{A_{i,1f}}{A_{1f}} = \frac{4a \cdot (R - a)}{R^2} \quad (14)$$

Therefor, the interception flux is equal to:

$$j_{i,1f} = \frac{\phi_{1f} \cdot n}{O_{1f}} \cdot \frac{4a \cdot (R - a)}{R^2} \text{ and thus } Sh_{i,1f} = \frac{\phi_{1f} \cdot 4a^2 \cdot (R - a)}{O_{1f} \cdot R^2 \cdot D_\infty} \quad (15)$$

Since the interception flux of a single fiber is equal to the interception flux of the total module, Sh_{tot} can be calculated by combining equations (3), (4), (13) and (15).

Dead end module

Hydrodynamics

The hydrodynamics in the dead end membrane module used in this research can be best described using the theory of stagnation point flow. This type of flow occurs in case of an impinging jet system (figure 2). A jet of liquid exits through a circular tube with radius R_{tube} [m] with an average velocity \bar{v} into a region bounded by a confinement and an impingement plate. The confinement plate is located parallel and at a distance h [m] from the impingement plate. This system is described by Varennes et al⁵. Although in our dead end module the confinement plate is only the pipe wall, the theory is used to describe the system because only the region very near to the symmetry point P, where the flow closely resembles a stagnation point flow, is considered. If $x < 0.1 \cdot R_{tube}$, stagnation point flow can be described in dimensionless terms as:

$$\frac{v_y}{\bar{v}} = -\bar{\alpha} \cdot \left(\frac{y}{R_{tube}} \right)^2 \quad \text{and} \quad \frac{v_x}{\bar{v}} = \bar{\alpha} \cdot \frac{x}{R_{tube}} \cdot \frac{y}{R_{tube}} \quad (16)$$

or

$$v_y = -\alpha \cdot y^2, \quad v_x = \alpha \cdot x \cdot y \quad \text{with} \quad \alpha = \frac{\bar{\alpha} \cdot \bar{v}}{R_{tube}^2} \quad (17)$$

with v_y and v_x [m·s⁻¹] are the velocities perpendicular and parallel to the membrane respectively, \bar{v} [m·s⁻¹] the average flow velocity in the tube and x and y [m] the distance of the droplet on the axis. The parameter α [m⁻¹·s⁻¹] characterizes the intensity of the stagnation point flow which depends on the cell geometry and the volume flow rate, but does not depend on the radial coordinate x as long as $x < 0.1 \cdot R_{tube}$. Varennes found that in

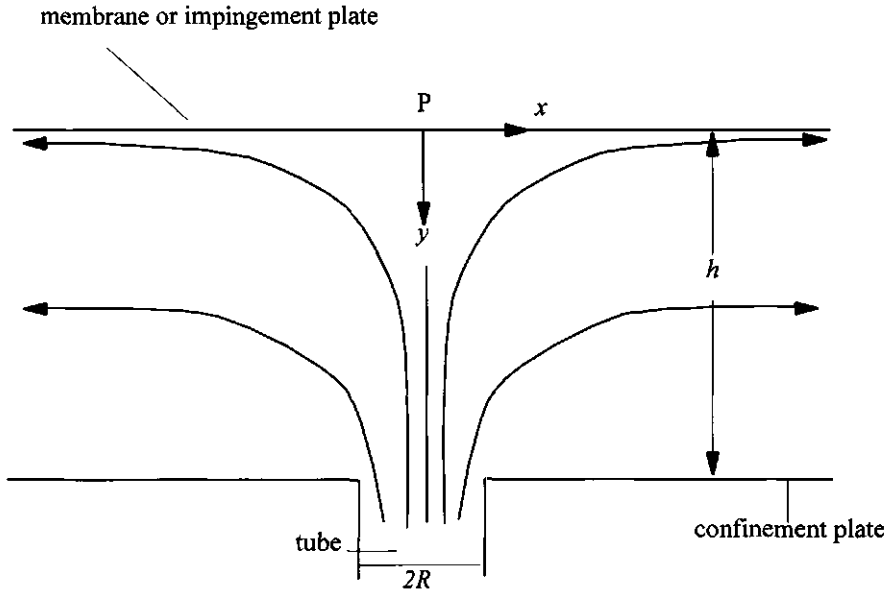


Figure 2. Impinging jet system

his case, where $h = 2.3$ mm and $R = 1$ mm, $\bar{\alpha}$ [-], the dimensionless expression of α , can be estimated by:

$$\bar{\alpha} = 0.8257 + 2.1582 \cdot 10^{-3} \cdot Re - 9.3192 \cdot 10^{-7} \cdot Re^2, \text{ if } Re < 100$$

$$\bar{\alpha} = 0.1 \cdot Re^{0.5}, \text{ if } Re \geq 100 \quad (18)$$

with $Re = \frac{\rho \cdot \bar{v} \cdot 2R}{\eta}$. The wall shear stress follows from combination of $\tau = -\eta \cdot \frac{dv_x}{dy}$ and equation (16):

$$\tau_w = \frac{-\eta \cdot \bar{\alpha} \cdot \bar{v} \cdot x}{R_{tube}^2} \quad (19)$$

Calculation of Sh

Two solutions of the convective diffusion equation have been derived for stagnation point flow¹. If interception and external force fields are absent, Sh_{pe} according to formula 3 is valid with $K = K_{de} = 0.616$ and Pe is equal to

$$Pe_{de} = \frac{2\alpha \cdot a^3}{D_\infty} \quad (20)$$

where α is given by equation (17) and (18). If interception occurs and a density difference exists between the continuous and the dispersed phase, the general model according to formula (2) can be used.

Materials and Methods

The membrane modules

The material properties of the three types of membrane modules that have been used, a flat sheet module, a hollow fiber module and a dead end module, are summarized in table 1. The dimensions can be found in table 2 and figure 3.

Table 1, Material properties of the membrane modules.

	module	material module	membrane material	spacer	potting material	pore size [μm]
flat sheet	own design	polymethyl-methacrylate	polypropylene, Enka, Accurel	polymethyl-methacrylate		0.1
hollow fiber small	Microdyn; MD 020 CP 2N	polypropylene	polypropylene	-	polyurethane	0.2
hollow fiber large	Microdyn MD 020 TP 2N	polypropylene	polypropylene	-	polypropylene	0.2
dead end	own design	polymethyl-methacrylate	polypropylene, Enka, Accurel	polymethyl-methacrylate		0.1

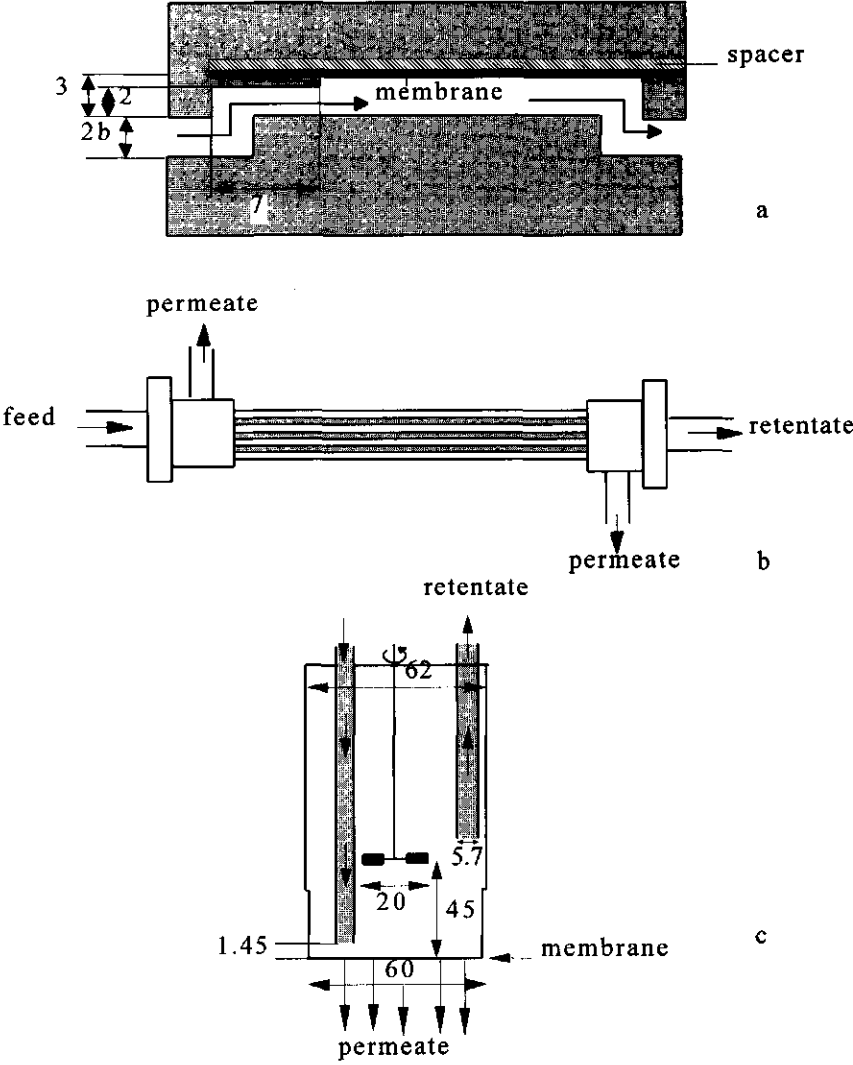


Figure 3, Flat sheet module (a), hollow fiber module (b) and dead end module (c). The dimensions are given in mm.

Table 2, Dimensions of the membrane modules, N [-] denotes the amount of fibers.

	O [m ²]	L [m]	b or R [mm]	N [-]
flat sheet type 1	0.003	0.12	1.5	-
flat sheet type 2	0.003	0.12	0.75	-
flat sheet type 3	0.0015	0.06	1.5	-
hollow fiber type 1	0.1	0.46	0.9	40
hollow fiber type 2	0.04	0.69	2.75	3
dead end	0.0028	0.06 (diameter)	-	-

The modules are placed horizontally using a leveling instrument. In case of the flat sheet module the membrane is situated on the upper side of the channel. The fluid flows parallel to the membrane except at the transit between in- and outlet tube and the module (figure 3a). In the experiments using the hollow fiber modules, the emulsion also flows parallel to the membrane surface (figure 3b). The dead end module is schematically drawn in figure 3c. The membrane is placed at the bottom of the module, which has a volume of $375 \cdot 10^{-6}$ m³. In the vessel, the emulsion is stirred using a 6-bladed turbine stirrer of stainless steel with 6.7 s⁻¹. The blades are $3.0 \cdot 10^{-3}$ m high and $5.6 \cdot 10^{-3}$ m wide. Also, 4 stainless steel baffles with a length of $126 \cdot 10^{-3}$ m are situated in the vessel and two tubes with a diameter of $5.7 \cdot 10^{-3}$ m through which the emulsion is pumped. Thus, the emulsion is flowing directly towards the membrane, simulating impinging jet flow.

Filtering procedures

The filtering procedure using the flat sheet and hollow fiber modules is similar (figure 4a). Before starting an experiment, the membrane is prewet with dodecane (Merck, p.a.) to prevent adsorption of surfactant into the pores of the membrane. The emulsion, which is stirred in a vessel with a magnetic stirrer, is pumped into the module using a gear pump, while the pressure is regulated at 0.05 bar $\pm 10\%$ with a pressure valve on the retentate side. The permeate is collected into a beaker while the retentate is recirculated to the emulsion vessel. During this 3 hours lasting batch process, samples are taken from

the feed to determine the oil concentration. Each experiment is repeated three times starting from a stock emulsion, which is stirred during storage. The membrane unit is rinsed with double distilled water at high velocity in between experiments. In figure 4b, the experimental set up of the dead end module is given. Process conditions are the same as for the flat sheet and hollow fiber module. A pressure of $0.03 \pm 10\%$ bar is applied using air which is humidified with a moisturizer. Samples from the emulsion can be taken using a tap.

Preparation of the emulsions

Emulsions are made by mixing an aqueous solution of $1 \text{ g}\cdot\text{l}^{-1}$ of the nonionic surfactant poly(20)oxyethylene-sorbitan-monopalmitate (Tween-40, Sigma, p.a.) and $2.50 \cdot 10^{-4} \text{ M}$ KCl with specified amounts of bromohexadecane (flat sheet and hollow fiber, ρ is $999 \text{ kg}\cdot\text{m}^{-3}$, Janssen Chimica) or bromodecane (dead end, ρ is $1070 \text{ kg}\cdot\text{m}^{-3}$, Janssen Chimica).

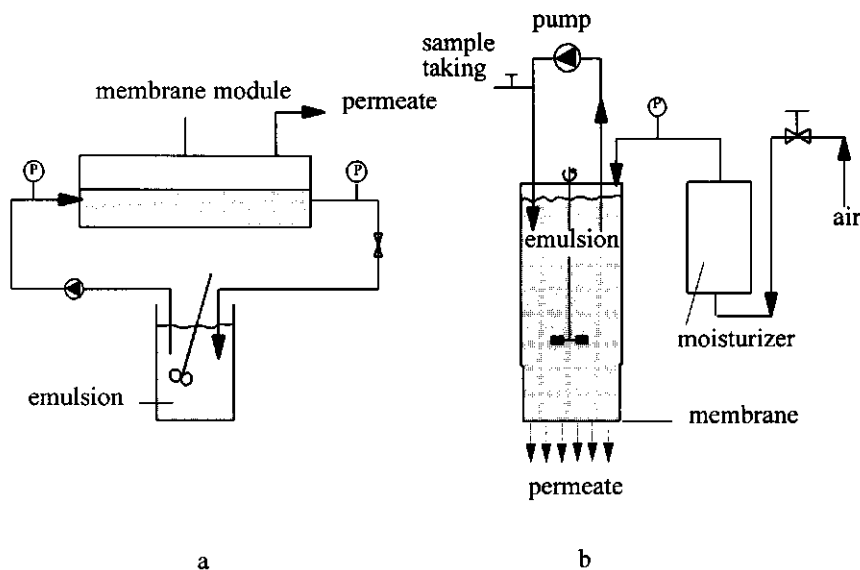


Figure 4, Experimental set up of the flat sheet and hollow fiber modules (a) and the dead end module (b)

Generally, a Silverson mixer, type L4R is used, which is a 4-bladed turbine stirrer that presses liquid through a perforated stator. A volume of 100 ml is mixed during 2 minutes at 1200 rpm. For one experiment, a Condi Labhomogenizer is used. During 15 minutes 100 ml was mixed at 100 bar. All emulsions are stable; no creaming or sedimentation is detected at storage conditions during several days. The droplet size distributions, as measured with both spectroturbidity and dynamic light scattering have been described in chapter 2 of this thesis. The Silverson mixed bromohexadecane emulsions have a d_{32} of 8.5 μm , while the d_{32} of the Silverson mixed bromodecane emulsions is 7.8 μm . The homogenized bromodecane emulsion has a d_{32} of 0.5 μm .

Measurement of the oil concentration in the emulsion

The oil concentration is determined as stated earlier (chapter 2 of this thesis). Ten μl of sample is diluted with 990 μl ethanol (Merck, p.a.) and one μl of this dilution is injected in a Carlo Erba gas chromatograph (GC 6000, vega series) with a 10 m CP-Sil 5 CB capillar column (Chrompack, The Netherlands) and a cold on-column injection system. At the moment of injection the oven temperature is 80 $^{\circ}\text{C}$. After one minute, the temperature is increased at 15 $^{\circ}\text{C}\cdot\text{min}^{-1}$ up to 250 $^{\circ}\text{C}$. The F.I.D detection of bromohexadecane and bromodecane occurs at 370 $^{\circ}\text{C}$. To calculate the concentration, a calibration curve is used.

Determination of Sh

In chapter 2 it is shown that the experimental results can be described with a single fit parameter; the apparent deposition velocity v' [$\text{m}\cdot\text{s}^{-1}$]. With this parameter experiments can be easily compared. In case of the dead end module this fit relation is:

$$n_t = n_0 \cdot \exp\left(\frac{-v' \cdot O}{V_{\text{ves}}} \cdot t\right) \quad (21)$$

with V_{ves} [m^3] is the volume of vessel and t [s] is the time.

Another possibility to express the results is in terms of the Sherwood number, Sh . Sh -values corresponding with formula (1) can be determined by calculating the initial flux which is equal to $(n_0 V_0 - n_i V_i)/(O \cdot t)$ for small values of t . Here, V [m³] is the volume of the emulsion. Assuming that $V_0 = V_i$, this results in $j_0 = V_0(n_0 - n_i)/(O \cdot t)$. The value of n_i can be determined either using the fit procedure or by drawing a tangent in the concentration-time graph. Both methods give similar results and they have been used simultaneously. Sh can then be calculated with d being equal to d_{32} at the beginning of the experiment and $n = n_0$.

Results

The flat sheet module

In figure 5, the experimentally determined Sherwood numbers are plotted against the flow velocity for a flat sheet module type 1. The experiments seem to show a maximum, although not very clear. The initial volume of the emulsion is 200 ml in these experiments. With the filtration time of 3 hours, the difference between n_i and n_0 is very small, explaining the scatter of the measured Sh values.

In figure 5 also the predicted relations of Sh with the flow velocity are presented according to the different models. Because at the entrance of the module the flow might be stagnation point (figure 3a), the stagnation point model has also been tested. The predictions of this model (line d) and of the general model (line a) are in the right order of magnitude. The prediction of $Sh_{p_{cs}}$, which excludes interception, is too low (line b).

The outcome of the stagnation point model is dependent on the value of α . In figure 5, α has been calculated according to formula (18). However, this formula might not be applicable in the system under investigation because the dimensions of h and R are not matching the conditions of Varennes et al⁵. The effect of changing the value of α on Sh is calculated for two flow velocities (figure 6). This sensitivity analysis shows that the

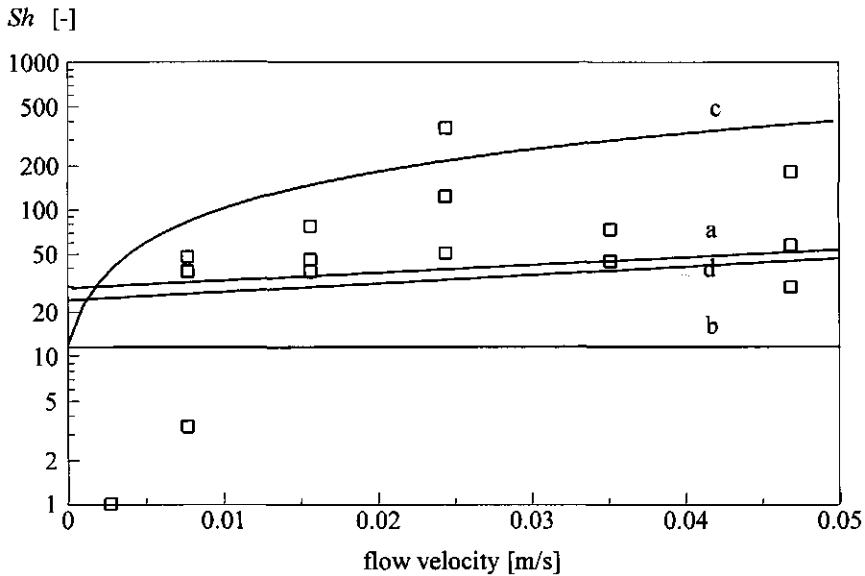


Figure 5, Filtration of Silverson mixed bromohexadecane-in-water emulsions with a flat sheet module type 1; The symbols represent the experimental data with $V_o=200 \cdot 10^{-6} \text{ m}^3$. The lines are the predictions of (a) $Sh_{overall}$ according to equation 2, (b) Sh_{pe} according to equation 3 (c) Sh_{tot} according to equation 4 and (d) $Sh_{overall}$ according to equation 2 with stagnation point flow..

effect is small and at low flow velocities ($Re < 100$, at $\nu = 0.005$) even negligible. Therefore, the results of formula 18 can be used.

Some experiments have been performed with different module dimensions (flat sheet type 2 and 3). Experimentally, no significant change of Sh is measured with decreasing channel height or length. Theoretically, depending on the model used, Sh changes maximal by a factor 1.7 (table 3) which is within the experimental error range. The Sh_{pe} -values, hence without interception, again are all below the experimental values.

These results and those given in figure 5, show that interception contributes significantly to the transport of oil droplets towards the membrane surface.

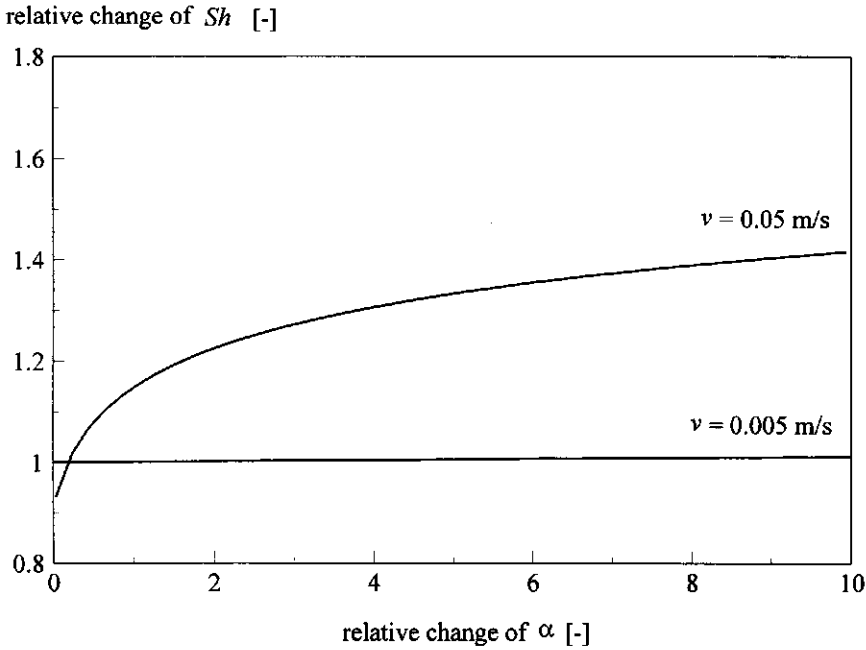


Figure 6, Sensitivity analysis of α on $Sh_{overall}$ $Re=28.5$ at $v=0.005 \text{ m}\cdot\text{s}^{-1}$ and 285 at $v=0.05 \text{ m}\cdot\text{s}^{-1}$.

Table 3, Calculated Sh for the 3 flat sheet module types at a flow velocity of $5\cdot 10^{-3} \text{ m}\cdot\text{s}^{-1}$.

	b [mm]	L [m]	$Sh_{overall}$ equation (2)	$Sh_{overall}$ stagnation point, equation (2) and (20)	Sh_{tot} equation (4)	Sh_{Pe} equation (3)	Sh experimental
type 1	1.5	0.12	72	73	42	12	43 ($v = 8\cdot 10^{-3} \text{ m}\cdot\text{s}^{-1}$)
type 2	0.75	0.12	52	68	42	12	54 ($v = 2.3\cdot 10^{-3} \text{ m}\cdot\text{s}^{-1}$)
type 3	1.5	0.06	72	73	72	12	60 ($v = 3.5\cdot 10^{-3} \text{ m}\cdot\text{s}^{-1}$)

The hollow fiber module

In figure 7, the experimental results of the hollow fiber module type 1 are compared to the theoretical results. The experiments show that Sh decreases with increasing flow velocity. At low velocity, sometimes creaming at the entrance of the module is detected. Moreover, it might be possible that at low velocity the emulsion is not flowing through all fibers because usually the flow profile is not identical in all the fibers of a hollow fiber module⁶. Taking this reduced O into account, even higher values of Sh will be calculated. In contrast to the experimental results, all theories predict an increase of Sh or at least a constant value with increasing velocity. A reason for the deviation between theory and experiment is given further down in the Discussion.

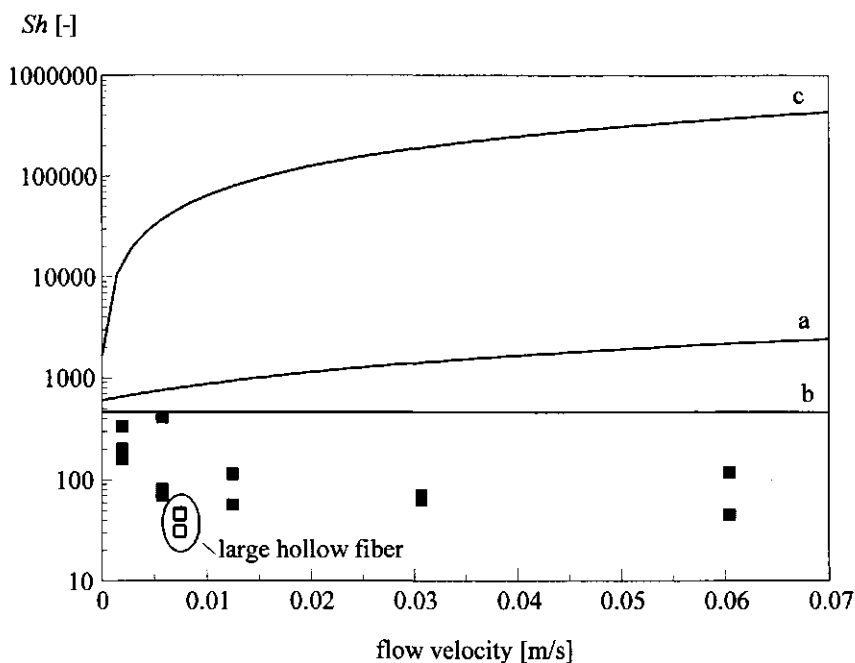


Figure 7, Filtration of Silverson mixed bromohexadecane-in-water emulsions in a hollow fibre module type 1; experimental results (●) compared to theory; (a) $Sh_{overall}$ according to equation 2, (b), Sh_{fm} according to equation 3 and (c) Sh_{tot} according to equation 4.

Also, the type 2 module, with the larger fibers, has been tested at 1 flow velocity which is shown in the figure. The experimental Sh number of type 2 is smaller but within the experimental accuracy. A smaller value is coherent with the predictions although the effect of the latter is much larger than the measured decrease (table 4).

Table 4, Calculated Sh for the two hollow fiber module types at a flow velocity of 0.02 m s^{-1} .

	$Sh_{overall}$ equation (2)	Sh_{tot} equation (4)	Sh_{Pe} equation (3)	Sh experimental
type 1	1260	180000	460	65 ($v = 0.03 \text{ m s}^{-1}$)
type 2	217	6000	35	41 ($v = 0.01 \text{ m s}^{-1}$)

The quantity of our data is too small to draw conclusions about the influence of interception with changing fiber diameter and number. However, Daiminger et al⁷ have shown results with a constant flow velocity and different numbers of identical polypropylene fibers. They found a higher separation efficiency (defined as the fraction of permeated oil after one passage) when increasing the amount of fibers, while the length of the fibers did not have an effect. An explanation of the higher efficiencies with increasing number of fibers can be the increase of the interception area. This supports the conclusion that interception is the dominant transport mechanism in the situation of Daiminger. If gravitational settling or diffusion would be the dominant transport mechanism, an increased separation efficiency would be expected with increasing fiber length. Also, similar to figure 7, Daiminger found a decrease in separation efficiency with increasing flow velocity. This effect will be discussed further on.

The dead end module

From an experimental point of view, the dead end module is the most accurate system to work with because of the well defined flow profile. In figure 8, the experimental results are compared with $Sh_{overall}$ (equation 2), Sh_{tot} (equation 4) and Sh_{Pe} (equation 3) with K_{de} and Pe_{de} . In the figure, the flow velocity is the velocity in the tube. The experimental data

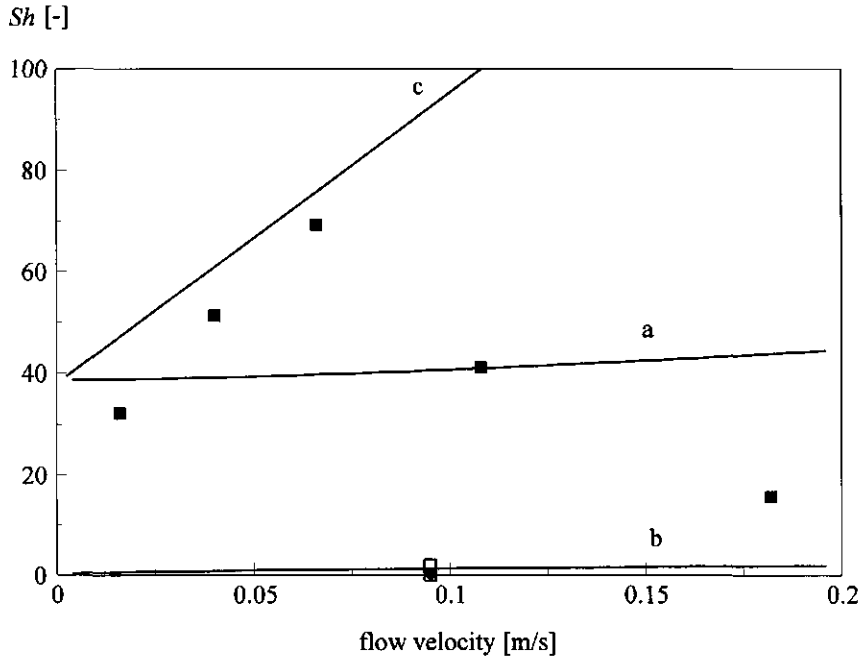


Figure 8, Filtration of bromodecane-in-water emulsions in a dead end module; Comparison of experimental results (\blacksquare Silverson emulsion, $d_{32} = 8.5 \mu\text{m}$ and \blacklozenge homogenized emulsion, $d_{32} = 0.5 \mu\text{m}$) and theoretical results: \square $Sh_{overall}$ and Sh_{pe} for the homogenized emulsion according to equation 2 and 3 resp. , line a: $Sh_{overall}$ for the Silverson emulsion according to equation 2, line b: Sh_{pe} for the Silverson emulsion according to equation 3 and line c: Sh_{tot} for the Silverson emulsion according to equation (4).

clearly show a maximal Sh at a flow velocity of circa $0.075 \text{ m}\cdot\text{s}^{-1}$. At higher and lower velocities Sh decreases. Sh_{pe} (line b) clearly underestimates the experimental Sh -numbers, while the predictions of $Sh_{overall}$ (equation 2, line a) are in the right order of magnitude. Thus, interception is again an important transport mechanism. The comment given in the description of the flat sheet module about the dimensions of h and R and the value of α is

also valid here. If equation 4 is used to calculate Sh_{tot} , the Sherwood-numbers are predicted well at low velocities. At high velocities, the transport is overestimated.

One experiment has been performed with a homogenized emulsion with d_{j2} is 0.5 μm . In this case, both the experimental and the theoretical Sh are significantly lower.

Discussion

In figure 9 the experimental results of three different module types are compared. It can be seen that the order of magnitude of Sh is the same for all modules. This is in accordance with results from literature where Sherwood numbers of 6 different solid particles collector types were in the same order of magnitude¹.

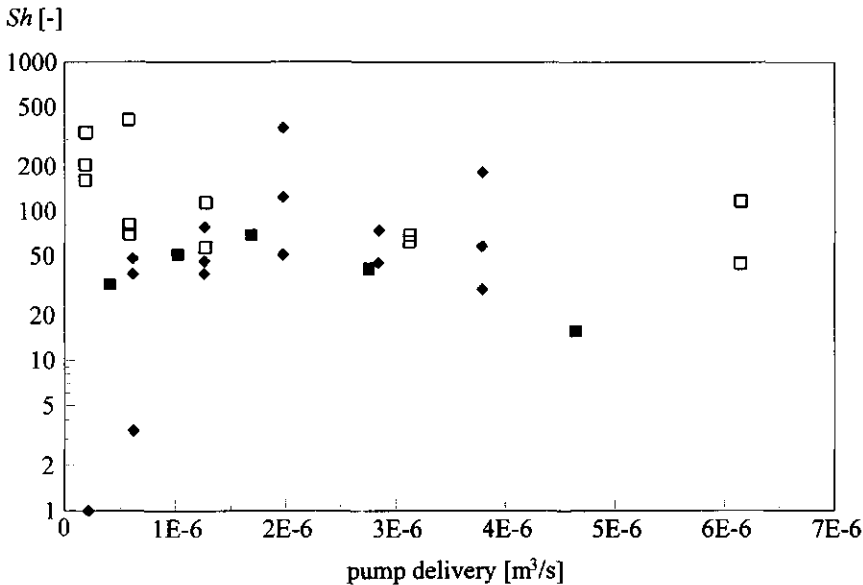


Figure 9, Comparison of the experimental results of \diamond the flat sheet type 1, \square the hollow fiber type 1 and \blacksquare dead end.

Moreover, figures 5, 7 and 8 show that the model data are in the same order of magnitude as the experimental ones, except for the hollow fiber module. However, 2 experimentally observed trends are not predicted: nor the decrease of Sh_{exp} with increasing flow velocity in the hollow fiber module neither the maximum Sh_{exp} for the dead end module and, possible within experimental scatter, for the flat sheet module. It can be hypothesized that at high velocities the perfect sink condition is not met; not all droplets that contact the membrane will permeate. A similar effect was found by Unno et al.⁸ They investigated the filtration of unstabilized oil droplets ($10\text{ }\mu\text{m} < d < 150\text{ }\mu\text{m}$) in a dead end module at different impeller speed ($13\text{--}17\text{ s}^{-1}$). They found a decrease of oil flux with increasing impeller speed. However, at lower impeller speed ($3\text{--}15\text{ s}^{-1}$), Ueyama et al.⁹ found an increasing flux with increasing impeller speed, during the filtration of stabilized droplets ($d < 10\text{ }\mu\text{m}$). Thus, probably an impeller speed can be defined at which the flux is maximal. This shows similarities with figure 8. The reason then might be that at lower velocities the flux increases with velocity because of increasing interception while at further increasing velocity the detachment starts to dominate.

As discussed in the theory, detachment is often related positively to wall shear. In figure 10, the wall shear is given for the three module types. It can be seen that the shear values are highest in case of the hollow fiber. For this module, the predicted Sh -values are much higher than the experimental ones. The latter show a decrease with increasing flow velocity. A similar decrease was found by Daiminger et al.⁷ Both phenomena can be explained by the occurrence of detachment. It must be mentioned that in literature about detachment usually much higher shear forces are applied^{3,4,10,11,12,13}. For example, Hubbe applied shear values up to 100 Pa in the turbulent region. In that research, solid particles first have been deposited on a surface during a certain time (for example 30 minutes). Then, formation of bonds could occur, which is a time dependent process. Afterwards, shear has been applied to reentrain the particles which are situated in the primary energy minimum. The detachment due to shear forces is governed by a convective diffusion transport out of this primary minimum. In the present research, deposition of oil droplets and detachment occurs simultaneously. The time available for bond formation and film

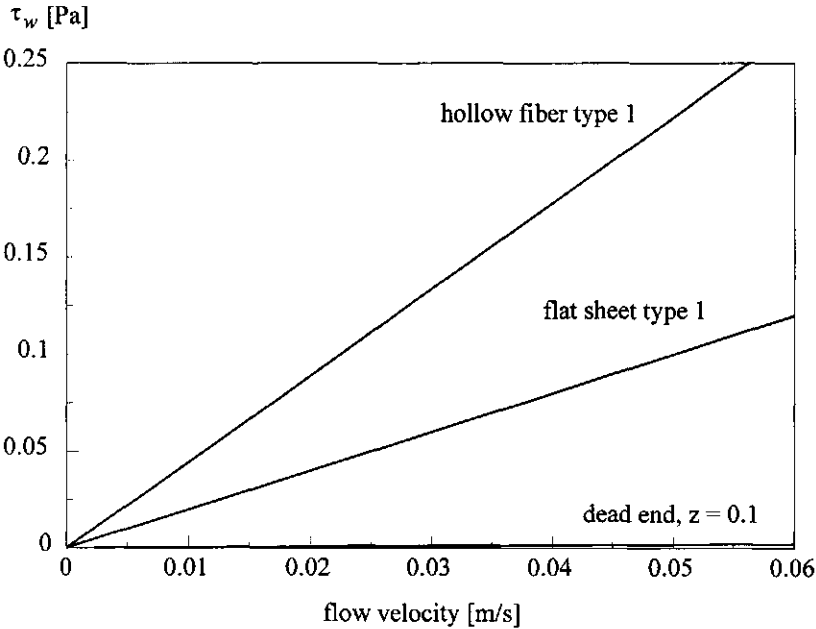


Figure 10, Wall shear versus flow velocity for three module types.

drainage is very limited. Moreover, deposited droplets will not be present in the primary minimum, because usually coalescence has occurred at these short distances and droplets have permeated. Therefor, if droplets are attached to the membrane, they will be in the secondary minimum, if present. This minimum is usually less deep than the primary minimum, resulting in only weak attraction between membrane and droplet. This means that detachment can occur in our system at lower shear values than in the systems described by Hubbe.

The system described by Varennes⁵ is more similar to ours. In stagnation point flow they investigated simultaneously deposition and detachment of solid polystyrene particles. They found a dependency between the distance from the stagnation point (x) and the flux, which is not governed by formula (2); increasing this distance results in a

decrease of deposition. Calculations with equation (19) show that the shear increases with x , pointing again at a positive relation between shear and detachment. Below $Re = 54$, they could not detect any detachment, while with increasing Reynolds numbers the detachment increased. This is in agreement with our data.

Shear might not be the only parameter effecting the contact time between droplet and membrane, but it most likely is a very important one. Another factor can be the residence time of a droplet which is situated near the membrane, t_{res} [-], because the contact time cannot exceed t_{res} . With increasing velocity t_{res} decreases. If t_{res} becomes smaller than the time needed to coalesce, the flux will decrease. In the flat sheet and hollow fiber module L/\bar{v} , which equals the mean residence time, is at least a few seconds. The residence time of a droplet near the membrane in absence of detachment will be larger, as the velocity near the membrane is smaller than \bar{v} (figure 1). In case of the dead end module however, the residence time of a droplet near the membrane is expected to be much smaller because of the stirrer speed.

Daiminger et al. give a similar explanation for the decreasing separation efficiency of oil droplets with increasing velocities⁷. They state that the efficiency is governed by the residence time. If t_{res} is smaller than the time needed to wet the membrane, t_{wet} , which is assumed to be constant, the efficiency will decrease. However, no influence of decreasing L was detected, meaning that $t_{res} > t_{wet}$ also at small L . We think it is important to make a distinction between residence time and contact time, the latter being dependent on effects such as detachment. Moreover, the time needed for coalescence, t_c , should be defined rather than t_{wet} .

In figure 11 the relations between the various time constants and the occurrence of coalescence is depicted schematically for a single droplet. The flow velocity influences both the residence time and the contact time. The coalescence time will be influenced by factors such as surfactant type and concentration, droplet size, temperature and viscosity of dispersed and continuous phase. The coalescence time usually shows a normal distribution¹⁴ which is also expected for the detachment time due to inhomogeneities of the membrane material which effect the interaction energy. For 1 droplet size, coalescence time and detachment time, the coalescence occurrence is either 100% (the perfect sink

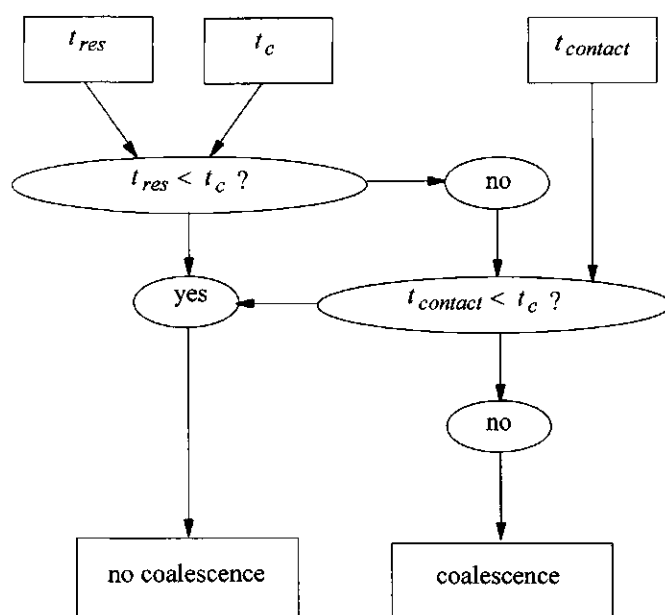


Figure 11, Scheme of the time constants determining the occurrence of coalescence for 1 droplet.

condition is met) or 0% (no coalescence). If the distributions of contact and detachment time are taken into account, as well as the various droplet sizes within an emulsion, the coalescence occurrence can vary between 0 and 100%.

Conclusions

From the experimental results it follows that the different module types have similar experimental Sherwood numbers at moderate flow velocity. This is in agreement with results from literature¹ where Sherwood numbers of 6 different solid particles collector types were in the same order of magnitude. The hollow fiber modules show high Sh at low velocity, probably due to experimental error because of creaming in dead zones. Experiments performed in the dead end module are most accurate.

Comparison between experimental and modeled data of the dead end and flat sheet module leads to the conclusion that interception is an important transport mechanism. Although in case of the hollow fiber module all models overestimate Sh , interception is expected to be important as well since an increase of L does not increase the efficiency of the process significantly.

At high flow velocities the experimental Sh decreases in case of the dead end module. The perfect sink condition, which means that droplets coalesce immediately after contact, is not met under these conditions. Probably, this is also true for the other two module types although the experimental scatter is too large to draw definite conclusions. Moreover, the dead end module shows a maximum Sh at a flow velocity of $0.075 \text{ m}\cdot\text{s}^{-1}$. At lower velocities Sh decreases again because transport becomes rate limiting. Here, coalescence occurrence might be complete.

The models always assume perfect sink conditions and do not take into account the time dependence of the coalescence process. It is important to realize that the coalescence will occur only if the contact time between droplet and membrane is larger or equal to the time needed to coalesce. Models based on the convective diffusion equation with the perfect sink assumption can be applied only if this condition is met. The contact time decreases with increasing flow velocity due to either a decreased residence time or an increased detachment because of increased shear forces. Thus, at high flow velocities the transport models must be extended with coalescence models.

Acknowledgements

The author thanks J. Vente and R.W.M Bakker for performing the experiments. B.H. Bijsterbosch from the department of Physical and Colloid Chemistry is greatly acknowledged for fruitful discussions. Moreover, she wishes to thank the Foundation for Chemical Research in the Netherlands for financial support.

Nomenclature

Symbols

a	droplet radius	[m]
A	entrance surface area	[m ²]
b	half channel height	[m]
d_{32}	volume to surface averaged droplet diameter	[m]
D	diffusion coefficient	[m ² ·s ⁻¹]
F_{drag}	drag force	[N]
g	gravity acceleration	[m·s ⁻²]
Gr	gravity number	[-]
h	distance between confinement plate and impingement plate	[m]
H	distance between center of droplet and membrane normalized by a	[-]
j	flux	[m ² ·s ⁻¹]
k	constant of Boltzmann	[J·K ⁻¹]
k'	detachment velocity	[m·s ⁻¹]
K	constant dependent on module configuration	[-]
L	length of channel	[m]
n	droplet concentration	[m ⁻³]
N	amount of fibers	[-]
O	membrane area	[m ²]

Pe	Peclet number	[-]
q	constant	[-]
R	radius	[m]
Re	Reynolds number	[-]
Sh	Sherwood number	[-]
t	time	[s]
T	absolute temperature	[K]
v	velocity	[m·s ⁻¹]
\bar{v}	average velocity	[m·s ⁻¹]
v'	apparent deposition velocity	[m·s ⁻¹]
V	volume	[m ³]
w	width of channel	[m]
x	coordinate	[m]
y	coordinate	[m]
z	coordinate	[m]
α	parameter which characterizes the intensity of stagnation point flow	[m ⁻¹ ·s ⁻¹]
$\bar{\alpha}$	dimensionless α	[-]
δ	primary minimum distance between droplet and membrane normalized by a	[-]
η	dynamic viscosity	[N·s·m ⁻²]
ϕ	pump delivery	[m ³ ·s ⁻¹]
ρ	density	[kg·m ⁻³]
τ	shear stress	[Pa]
τ_w	wall shear stress	[Pa]

Subscripts

c	coalescence
d	droplet

<i>de</i>	dead end
<i>exp</i>	experimentally
<i>1f</i>	1 fiber in a hollow fiber module
<i>fs</i>	flat sheet
<i>Gr</i>	dominated by <i>Gr</i>
<i>hf</i>	hollow fiber
<i>i</i>	interception
<i>Pe</i>	dominated by <i>Pe</i>
<i>res</i>	residence
<i>tot</i>	total
<i>ves</i>	vessel
<i>w</i>	water
0	initial
∞	bulk

References

- 1 Z. Adameczyk, T. Dabros, J. Czarnecki and T.G.M. van de Ven, Particle transfer to solid surfaces, 1983, *Advances in Colloid and Interface Science*, vol.19, p.183-252.
- 2 M.A. Hubbe, Theory of detachment of colloidal particles from flat surfaces exposed to flow, 1984, *Colloids and Surfaces*, vol.12, p.151-178.
- 3 M.A. Hubbe, Detachment of colloidal hydrous oxide spheres from flat solids exposed to flow, 1. experimental system, 1985, *Colloids and Surfaces*, vol. 16, p.227-248.
- 4 M.A. Hubbe, Detachment of colloidal hydrous oxide spheres from flat solids exposed to flow, 2. Mechanism of release, 1985, *Colloids and Surfaces*, vol. 16, p.249-270.
- 5 S. Varennes and T.G.M. van de Ven, Deposition and detachment of latex particles at glass surfaces exposed to flow, 1987, *PhysicoChemical Hydrodynamics*, vol.9, no.3/4, p.537-559.
- 6 J.K. Park and H.N. Chang, Flow distribution in the fiber lumen side of a hollow fiber module, 1986, *AIChE Journal*, vol.32, p.1937-1947.
- 7 U. Daiminger, W. Nitsch, P. Plucinski and S. Hoffmann, Novel techniques for oil/water separation, 1995, *Journal of Membrane Science*, vol.99, p.197-203.

- 8 **H. Unno, H. Saka and T. Akehata**, Oil separation from oil-water mixture by a porous polytetrafluoroethylene (PTFE) membrane, 1986, *Journal of Chemical Engineering of Japan*, vol. 19, no.4, p.281-286.
- 9 **K. Ueyama, K. Fukuura and S. Furusaki**, Oil-phase permeation behavior of O/W emulsion through a porous polytetrafluoroethylene membrane, 1987, *Journal of Chemical Engineering of Japan*, vol. 20, no.6, p.618-622.
- 10 **J.W. Cleaver and B. Yates**, The effect of reentrainment on particle deposition, 1976, *Chemical Engineering Science*, vol.31, p.147-151.
- 11 **D.F. Sherony, R.C. Kintner and D.T. Wasan**, Coalescence of secondary emulsions in fibrous beds, 1978, *Surface and Colloid Science*, vol.10, p.99-161.
- 12 **A.J. Goldman, R.G. Cox and H. Brenner**, Slow viscous motion of a sphere parallel to a plane wall - II Couette flow, 1967, *Chemical Engineering Science*, vol.22, p.653-660.
- 13 **K. Rietema**, Segregation in liquid-liquid dispersions and its effect on chemical reactions, 1964, *Advances in Chemical Engineering*, vol.5, p.237-302.
- 14 **G. E. Charles and S.G. Mason**, The coalescence of liquid drops with flat liquid/liquid interfaces, 1960, *Journal of Colloid Science*, vol.15, p.236-267.

4 Coalescence in a dispersed phase separator

Summary

Previously, it was shown that small oil droplets ($d_{32} < 10 \mu\text{m}$), stabilized by the non-ionic surfactant Tween-40, can permeate through a hydrophobic membrane (chapter 2 and 3). A continuous oil phase is formed at the permeate side of the membrane. The process can only be successful if the droplets are not only transported from the bulk towards the membrane but also coalesce with the membrane surface. As shown in chapter 2, results obtained in permeation studies could be modeled by assuming the membrane to be a perfect sink, i.e. as soon as a droplet reaches the membrane, it coalesces. We argued that deviations between transport model and experiments at high flow velocities could be due to the fact that contact times were shorter than the time needed for coalescence. In the present chapter the latter phenomenon is investigated in more detail.

Firstly, the coalescence of *large* hexadecane droplets ($d = 1.8 \cdot 10^{-3} \text{ m}$) is studied experimentally, as direct coalescence time measurements of *small* droplets ($d_{32} < 10 \mu\text{m}$) is complicated. Next, the coalescence time, t_c , is modeled theoretically by calculating the time needed to drain the aqueous film between droplet and surface from an initial film height to a film height at which rupture occurs¹. A further complication is the experimental finding that if a solid membrane is inserted into the surface, coalescence times decrease, probably due to surface inhomogeneities.

If the theory is applied to coalescence of small droplets against a liquid surface, the calculated coalescence times are much shorter than 1 second, indicating immediate coalescence. The presence of a membrane will decrease the coalescence times even further. This is in accordance with the experimental

permeation data which could be modeled by assuming ideal (rapid) coalescence. Only in case of the dead end module at high flow velocities coalescence can become rate limiting because of the small contact times. This is in agreement with the observed low permeation rate under these circumstances (chapter 3). Also, in case of high surfactant concentration (if micelles are present in the aqueous phase) coalescence becomes rate determining.

Introduction

In the previous chapters the possibility to use dispersed phase separators to separate emulsion phases has been investigated. An emulsion is pumped along a hydrophobic polypropylene membrane with an average pore diameter of $0.1\ \mu\text{m}$. It has been shown that oil droplets, stabilized by the nonionic surfactant Tween-40, upon contact with the membrane are in most cases able to coalesce with the membrane. Under the influence of a transmembrane pressure difference, the coalesced droplets permeate through the membrane, forming a pure oil phase as the permeate. Thus, separation of the oil and water phase has been achieved in a one step process which is not the case with the more commonly applied conventional coalescer filters.

The overall process can be described by the product of a collision frequency between droplet and membrane and a coalescence probability. The former is determined by various transport mechanisms of droplets from the bulk towards the membrane (chapter 2 of this thesis). The latter is determined by the rate of coalescence. When the droplet approaches the membrane closely, a film forms between droplet and membrane which subsequently drains until a certain critical film thickness h_c [m] is reached. Then, the film ruptures spontaneously and coalescence has occurred. Thus, if the time needed to coalesce, t_c [s] is smaller than the contact time between droplet and membrane, t_{contact} [s], coalescence will occur. If t_c is larger than t_{contact} , coalescence does not occur.

In this chapter, the theory mentioned above will be explored. The coalescence time of large droplets against a liquid interface can be determined both experimentally and theoretically. The coalescence time against a solid membrane interface is expected to

be shorter due to effects of surface inhomogeneities². Next, the theory is extrapolated to small droplets. If the theory predicts $t_c > t_{contact}$, it must be kept in mind that due to the presence of the solid membrane in the interface, the actual t_c is expected to be smaller than the calculated one. Thus, in this case no conclusion about the occurrence of coalescence can be drawn. In the other situation, if t_c is predicted to be smaller than $t_{contact}$, coalescence will certainly occur in the membrane system.

Theory

Drainage

When a droplet has reached the surface, drainage of the film between the droplet and the surface is induced by gravity effects, resulting from a difference in density between the droplet and the surrounding liquid. The flow profile in the film can be described either as plug flow, as Poiseuille flow or as a combination of the two, depending on whether the interfaces are considered to be mobile or rigid. Rigid interfaces can resist shear stresses and thus decrease the drainage velocity¹. Two factors influence the mobility of the interfaces. Firstly, if η_d/η_w , the viscosity ratio between the dispersed and the continuous water phase, is much smaller than 1, the interfaces can be considered to be mobile and the flow will be plug flow. If $\eta_d/\eta_w \rightarrow \infty$, then the interfaces are rigid and the flow is described by the Poiseuille law. Secondly, if the interfaces are covered with surfactant they are considered to be rigid too. During drainage of the film, surfactants will be swept along the interfaces, creating interfacial tension gradients. These act as a stress in the interface, impeding interfacial movement. If no surfactant is present, this effect does not occur and the interfaces are mobile. In the present research $\eta_d/\eta_w = 3.3$ and the droplets are stabilized by surfactant. Thus, the interfaces are rigid and the drainage has to be described by Poiseuille flow.

Several drainage models have been derived, depending on whether the droplet and/or the surface deforms during the process of drainage. Deformation occurs if the

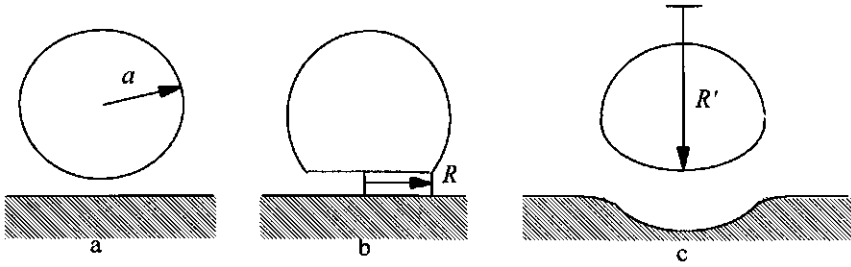


Figure 1, Models of a drop on a liquid surface; a: rigid drop and surface, b: deformable drop and rigid surface, c: deformable drop and surface.

applied external pressure exceeds the internal Laplace pressure, P_L [Pa]^{3,4,5}. Thus, if the gravity force is the only external force, deformation will occur if the hydrostatic pressure difference across the drop, $2a\Delta\rho\cdot g$, is larger than P_L . Here, a [m] is the droplet radius, $\Delta\rho$ [kg·m⁻³] is the density difference between continuous and dispersed phase and g [m·s⁻²] is the gravity acceleration. This can be expressed using the Bond number, $Bo = \Delta\rho\cdot g\cdot a^2/\gamma$ [-], with γ [N·m⁻¹] being the interfacial tension. Deformation occurs when Bo is larger than 0.05. Three situations of deformation are depicted in figure 1. For the case that neither the droplet, nor the surface deforms (figure 1a) Charles et al. derived¹:

$$\left. \frac{dh}{dt} \right|_{rigid} = \frac{-h \cdot F}{6\pi \cdot \eta_w \cdot a^2} \quad (1)$$

with h [m] being the thickness of the film, t [s] the time and F [N] the sum of the forces acting on the film, both colloidal and external. In the simple case of a bare, charged surface, the colloidal forces are the van der Waals attraction, F_{vdW} , the electrostatic force, F_e , and the Born repulsion force, F_B . The external forces that we consider are the gravity force, F_g , and the force due to the Laplace pressure inside the droplet, F_L . The definitions of these forces are summarized in table 1. Allan et al.⁶ showed that in case of droplet-droplet approach, equation (1) remains valid, provided it is multiplied by a factor 4.

Table 1, Forces acting between two droplets; in case of a flat interface $a_2 \rightarrow \infty$.

Force	Definition	Parameter description	Reference
F_g	$\frac{4}{3}\pi \cdot a^3 \cdot \Delta\rho \cdot g$		6
F_B	$\frac{B}{h^7}$	B [N·m ⁷] is the force parameter	7
F_{el}	$4\pi\kappa\epsilon\epsilon_0\zeta_1\zeta_2 \frac{a_1a_2}{a_1+a_2} \cdot \left[\frac{\exp(-\kappa h)}{1 + \exp(-\kappa h)} \right]$	κ [m ⁻¹] is the reciprocal double layer thickness, ϵ [-] is the relative dielectric constant of water, ϵ_0 [C·V ⁻¹ ·m ⁻¹] is the permittivity of the vacuum, ζ [V] is the surface potential; 1 and 2 refer to the droplet and the liquid, respectively.	7
F_{vdw}	$\frac{A_{132} \cdot a_1 \cdot a_2}{6h^2 \cdot (a_1 + a_2)}$	A_{132} [J] is the Hamaker constant of droplet 1 with liquid 2 through	8
F_L	$\frac{2\gamma}{a} \cdot \pi \cdot R^2$	R [m] is the radius of the film.	7

Deformation of the droplet will result in an increased drainage volume, thus leading to a decrease in drainage velocity. For this case, the drainage velocity can be calculated by assuming that the film becomes disc shaped, as depicted in figure 1b. If the surface behaves as rigid, one finds¹:

$$\left. \frac{dh}{dt} \right|_{\text{deformation}} = \frac{-2F \cdot h^3}{3\pi \cdot \eta_w \cdot R^4} \text{ with } R = a^2 \cdot \left[\frac{2\Delta\rho \cdot g}{3\gamma} \right]^{\frac{1}{2}} \quad (2)$$

Here, R [m] is the disc radius. Chappelaer calculated the drainage velocity for the case of a small spherical deformation of both droplet and surface (figure 1c)⁹. He showed that the radius of the deformation R' [m] is equal to $2a$ and that the film radius is equal to the one defined in formula 2 multiplied by a factor $\sqrt{2}$; the contact area between droplet and surface is two times larger for model c than for model b.

In case of model b and c, no pressure gradient exists in the tangential direction over the film due to the Laplace pressure because of the assumption that the curvatures of

the interfaces are identical on both sides of the film. It must be stated that all above mentioned models are simplifications of reality. For example, they assume the film height to be uniform. However, since the pressure in the flowing film must drop in the radial direction of the flow, going from a maximum value in the center to the bulk pressure at the edge, the radii of curvature must vary and the film can not be uniform in thickness; it must have a 'dimple' in the center. Because more realistic models are very complex we have chosen to apply the simplified ones.

Film rupture

Drainage occurs until a certain critical film height, h_c , is reached. Then, spontaneous rupture can occur. The reason for this is the presence of disturbances in the film due to thermal motion or external vibrations, leading to the formation of waves. The first effect of these waves is an enlargement of interfacial area resulting in an increase of the interfacial free energy. Secondly, in the thin part of the wave the interaction energy increases while in the thick part of the film the interaction energy decreases. If the total of these energies is negative, the wave will grow until the growth velocity becomes larger than the drainage velocity. Then, rupture occurs¹⁰. Vrij et al.¹¹ proposed the following equation for h_c in case of rigid interfaces;

$$h_{c,rigid} = 0.267 \cdot \left(\frac{A_{132}^2 \cdot R^2}{6\gamma \cdot P} \right)^{\frac{1}{7}} \quad (3)$$

with P [Pa] the pressure difference over the film. In case of an undeformable droplet and surface, P is assumed to be equal to the Laplace pressure inside the droplet and R can be calculated to be equal to $\sqrt{h_c \cdot (2a - h_c)}$. Here, the assumption is made that if the center of the film reaches the critical film height, the thickness at the outside of the film is equal to $2h_c$. If $a \gg h_c$ equation (3) becomes:

$$h_{c,rigid} = 0.159 \cdot \left(\frac{A_{132} \cdot a}{\gamma} \right)^{\frac{1}{3}} \quad (4)$$

In case of a deformable droplet according to model b and c, P will be governed by the gravitational force:

$$h_{c,deformation} = 0.267 \cdot \left(\frac{A_{132}^2 \cdot R^4 \cdot \pi}{6\gamma \cdot F_g} \right)^{\frac{1}{7}} \quad (5)$$

Incorporation of steric repulsion

If surfactants are present drainage is hindered either due to steric repulsion (in case of nonionics) or due to electrostatic repulsion (in case of charged surfactants). Groeneweg et al.³ suggest to replace the total film thickness h in equation (1) by $h-h_{2e}$ as the flow resistance is determined by the thickness of the liquid part of the film. Here, h_{2e} [m] is the combined thickness of the two emulsifier layers.

Initial film thickness

Knowing the drainage velocity, the time needed to reach h_c can be calculated if the film height at which the calculation starts, h_i [m], is defined. This time is equal to the coalescence time. Dahlquist et al.¹² define h_i to be 100 nm, while others suggest that $h_i = 0.38 \cdot a$.¹³ Jaeger et al.¹⁴ consider that drainage starts if the external driving force is equal to the force resisting drainage. Similar, in our case we define h_i to be the film height at which the drainage velocity (equation 1 or 2) is equal to the creaming velocity $F_g/(6\pi \cdot \eta_w \cdot a)$. It is assumed that at this distance the colloidal interaction forces are negligible compared to the gravitational force, so F in (1 and 2) is F_g . Thus, h_i is equal to a for model 1 and $(R^4/4a)^{\frac{1}{3}}$ for model b and c (assuming deformation has already occurred). Naturally, during the drainage also other forces than F_g will become noticeable.

Summarizing, the coalescence time can be calculated according to the schedule given in figure 2.

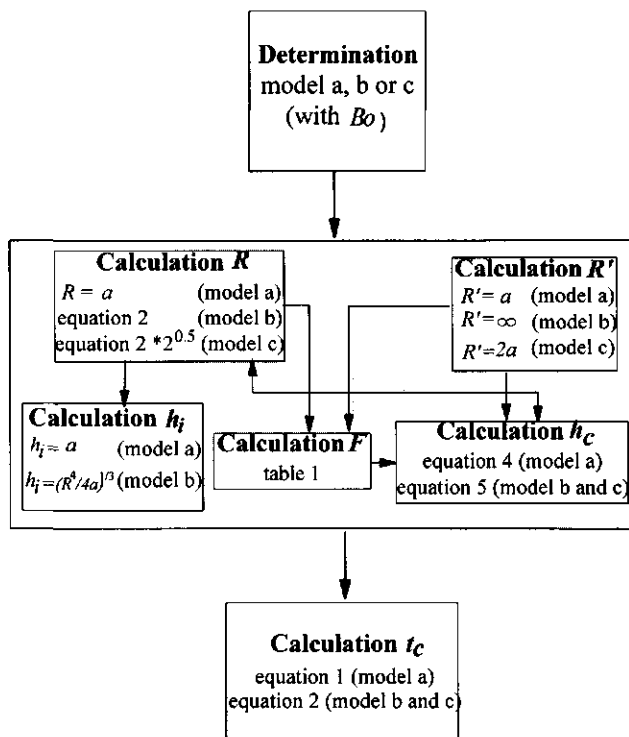


Figure 2, Scheme to calculate the coalescence time t_c .

Materials and Methods

Coalescence of large oil droplets against a liquid surface

In order to measure the coalescence time of hexadecane droplets against a surface of pure hexadecane, an experimental set up as drawn in figure 3 is used. A teflon beaker is filled with surfactant solution with on top a layer of hexadecane. The temperature is controlled at 25 °C by using a thermostated box. At the bottom of the vessel a hexadecane droplet with a volume of $3 \pm 0.05 \mu\text{l}$ ($d = 1.8 \text{ mm}$) is injected by an injection needle. The droplet is allowed to rest for a few seconds at the tip of the needle, before it is removed by a

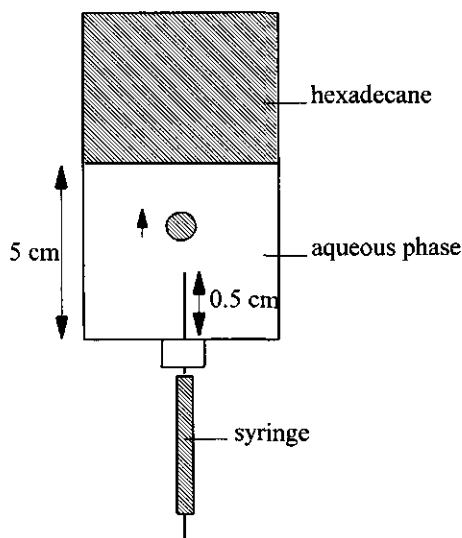


Figure 3, Experimental set up for the measurement of coalescence times of oil droplets against a hexadecane surface.

small tap against the needle. Then, the droplet rises towards the interface where it stays and coalesces after a certain time. The time between arrival at the interface and coalescence is measured using a stopwatch. From literature it is known that these measured coalescence times are normally distributed, probably due to fouling and other disturbances in the interface. Therefore, the coalescence times of at least 30 droplets have been measured for each model system.

Coalescence of large oil droplets against a membrane

To measure coalescence times of oil droplets against a membrane, a similar technique has been used as described above for the measurement of coalescence against a liquid surface. Instead of a beaker, a flat-sheet, transparent perspex membrane module with an internal volume of 100 ml has been used (figure 4). The module consists of two parts

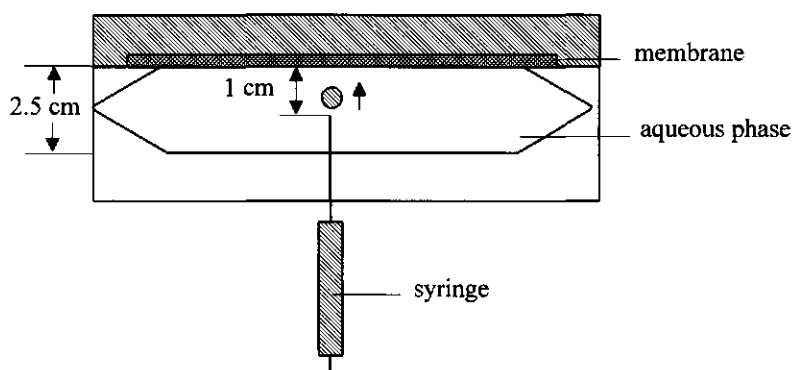


Figure 4, Experimental set up to measure coalescence times of oil droplets against a membrane.

between which the pretreated membrane can be pinned. The two parts are fixed by an iron frame. At the bottom part, an injection needle can be inserted. The experimental procedure is identical to the one described above.

Coalescence of a secondary emulsion against a liquid surface

A double-stirred, glass vessel as described by Scholtens et al.¹⁵ is filled with 225 ml of Silveson mixed emulsion (figure 5). Then, 100 ml of *n*-decane (p.a, Merck, density is $729 \text{ kg}\cdot\text{m}^{-3}$) is put on top, while care is taken that emulsion and organic phase do not mix. The vessel is covered with teflon and tape to avoid any evaporation. Both phases are stirred with stainless steel stirrers, at a rotational speed of 1.5 s^{-1} . Care is taken to keep the interface as stable as possible. Inside the vessel, stainless steel baffles are present. During an experiment, which is performed at $25 \pm 1 \text{ }^\circ\text{C}$, samples from both phases are taken at suitable intervals using a pipette.

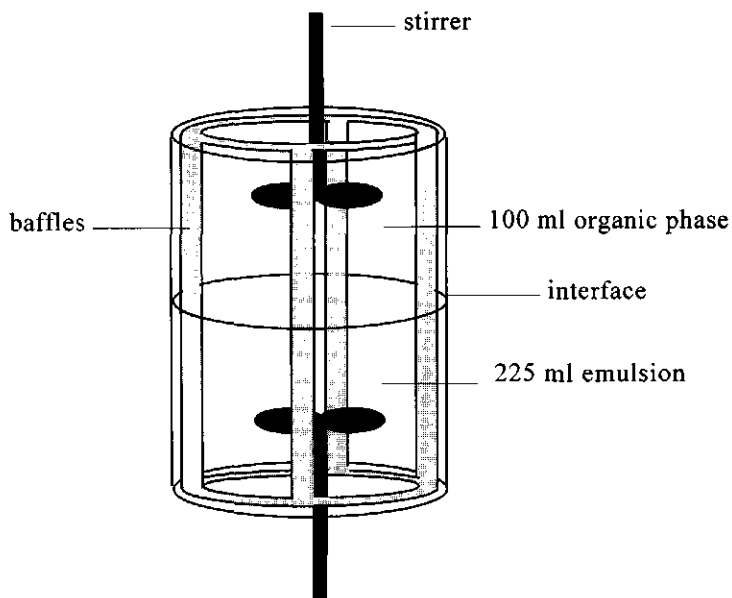


Figure 5, The double-stirred vessel.

Coalescence of a secondary emulsion against a membrane

The coalescence of droplets of a secondary emulsion against a membrane is measured indirectly by filtering experiments in a flat sheet module as described before (chapter 2 and 3 of this thesis). The module, with a length of 0.12 m, a channel height of 3 mm and a membrane area of $3.24 \cdot 10^{-3} \text{ m}^2$ is placed horizontally using a leveling instrument. The membrane, which is situated on the upper side of the channel, is made of polypropylene with an average pore diameter of $0.1 \text{ }\mu\text{m}$ (Enka, Accurel). The fluid flows parallel to the membrane except at the in- and outlet. Before starting an experiment, the membrane is prewet with dodecane (Merck, p.a.) to prevent adsorption of surfactant into the pores of the membrane. The emulsion, which is stirred in a vessel with a magnetic stirrer, is pumped into the module using a gear pump, while the pressure is regulated at $0.05 \pm 10\%$ Pa with a pressure valve on the retentate side. The permeate is collected into a beaker

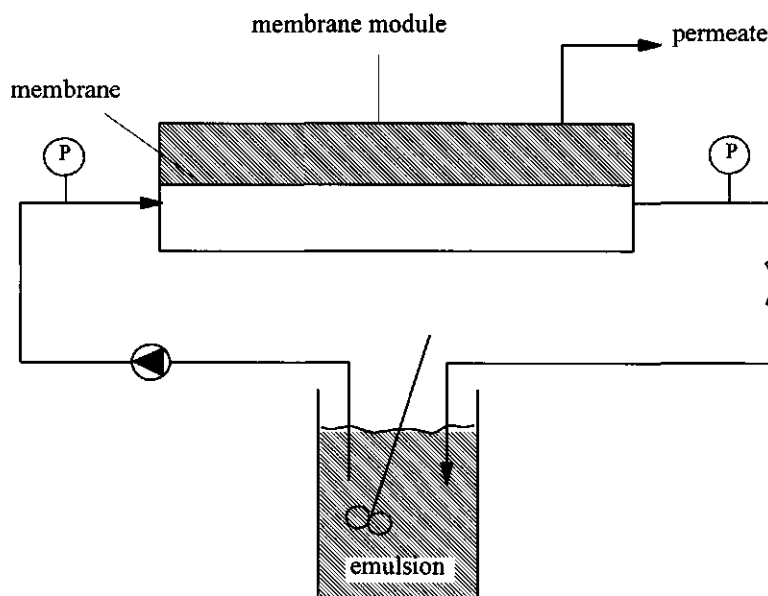


Figure 6, Set up of the filtering experiments.

while the retentate is led back to the vessel containing the emulsion. The temperature is controlled at 25 °C in a thermostated box. During an experiment, samples are taken from the feed to determine oil concentration and droplet size distribution. In figure 6 the system is given.

Preparation of the emulsions

Emulsions are made by mixing $2.50 \cdot 10^{-4}$ M KCl aqueous surfactant solution with specified amounts of hexadecane or bromohexadecane (Janssen Chimica, density is 773 and 999 kg·m⁻³ respectively). Three types of surfactants (Sigma, p.a.) have been used in different concentrations, their properties are summarized in table 2. Two types of mixers have been used. Firstly, a Silverson mixer is a 4-bladed turbine stirrer that presses liquid

Table 2, Properties of surfactants used in the research

surfactant	SDS	Tween 40	Triton X-100
type	anionic	nonionic	nonionic
M [g·mol ⁻¹]	288	1258	646
Critical Micelle Concentration [kg·m ⁻³]	2.31	0.14	0.18
formula	CH ₃ (CH ₂) ₁₁ -SO ₃ Na	polyoxyethylene(20)-sorbitan-monopalmitate	C ₆ H ₁₇ -C ₆ H ₄ -O-(CH ₂ -CH ₂ O) ₁₀ H

through a perforated stator. A volume of 100 ml is mixed during 2 minutes at 1200 rpm. Also, a Condi Labhomogenizer has been used. A volume of 100 ml is mixed during 15 minutes at 100 bar. All emulsions are stable; no creaming or sedimentation has been detected during several days. The droplet size distributions, as measured with both spectroturbidity and dynamic light scattering have been described earlier (chapter 2 of this thesis). The Silverson mixed emulsions have a d_{32} of 8.5 μm , while the homogenized emulsions have a d_{32} of circa 0.5 μm .

Measurement of the oil concentration in the emulsion

The oil concentration is determined as stated earlier (chapter 2 of this thesis). Ten μl of sample is diluted with 990 μl ethanol (Merck, p.a.) and one μl of this dilution is injected in a Carlo Erba gas chromatograph (GC 6000, vega series) with a 10 m CP-Sil 5 CB capillar column (Chrompack, The Netherlands) and a cold on-column injection system. At the moment of injection the oven temperature is 80 °C. After one minute, the temperature is increased at 15 °C·min⁻¹ up to 250 °C. The F.I.D detection of hexadecane and bromohexadecane occurs at 370 °C. To calculate the concentration, a calibration curve is used.

Determination of surface tension

The Wilhelmy plate method has been used to measure the surface tension between a surfactant solution and the oil phase⁸. On top of the surfactant solution a layer of

hexadecane is put. Then, a Wilhelmy plate is brought vertically into contact with the horizontal interface and the force which is exerted on the plate by the interface is measured.

Viscosity measurements

The viscosity of the surfactant solutions is measured using a Ubbelohde capillary viscometer⁸. By measuring the time needed for a known volume of liquid to flow through the capillary the viscosity can be calculated if the radius of the capillary and the density of the fluid are known.

Results and Discussion

Coalescence of large oil droplets against a liquid surface.

For each surfactant type, three experiments have been performed with different surfactant concentration, namely 0.1, 1 and 5 times the critical micelle concentration (CMC). For all solutions, the measured viscosity is equal to $1 \cdot 10^{-3} \pm 0.01 \cdot 10^{-3} [\text{N} \cdot \text{s} \cdot \text{m}^{-2}]$. Thus, the viscosity of the continuous phase is constant for all experiments. The surface tensions of the various surfactant solutions against hexadecane are given in table 3.

Table 3, Surface tension, γ [$\text{mN} \cdot \text{m}^{-1}$] between surfactant solutions and hexadecane.

concentration (C/CMC)	SDS	Tween 40	Triton X-100
0	53.3	53.3	53.3
0.1	7.5	13.1	12.4
1	3.6	7.8	4.4
5	2.9	6.1	1.5

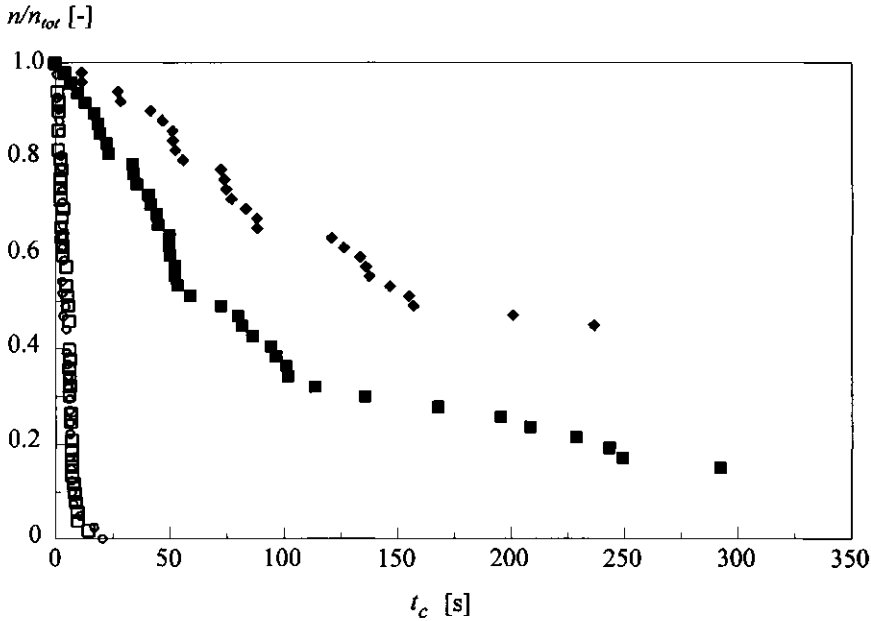


Figure 7, The amount of hexadecane droplets that has not yet coalesced (n) divided by the total amount of hexadecane droplets of which t_c has been measured (n_{tot}) as a function of the coalescence time. Coalescence occurs against an interface of an aqueous solution with different Tween-40 concentrations and pure hexadecane; \circ no surfactant present, \square 0.1-CMC, \blacksquare 1.0-CMC and \blacklozenge 5.0-CMC.

The results of the coalescence rate measurements for the Tween-40 model system are shown in figure 7. The figure shows that the coalescence times increase with increasing surfactant concentration; the droplets become more stable due to an increased steric hindrance of the Tween molecules.

For the other two surfactant types similar experiments have been performed. The results are summarized in table 4 in which the values of the half life time $t_{0.5}$ [s] and $t_{0.9}$ [s] are given. The half life time is the time at which 50% of the tested droplets has

Table 4, Values of $t_{0.5}$ [s] and $t_{0.9}$ [s] for the coalescence of hexadecane droplets against a hexadecane surface with different surfactant types and concentrations in the aqueous phase.

surfactant concentration (C/CMC)	SDS		Tween-40		Triton X-100	
	$t_{0.5}$	$t_{0.9}$	$t_{0.5}$	$t_{0.9}$	$t_{0.5}$	$t_{0.9}$
0	4.3	8	4.3	8	4.3	8
0.1	5.3	29	5.6	9	8.1	33
1	26.3	270	65.6	300	65.9	287
5	50.1	160	157.5	237*	-	-

* This value represents $t_{0.6}$ in stead of $t_{0.9}$

coalesced, thus $n/n_{tot}=0.5$. At $t_{0.9}$, 90% of the tested droplets has coalesced while 10% of the droplets has a coalescence time that is larger than $t_{0.9}$.

Next, the three models from figure 1 are used to calculate the theoretical coalescence times. The value of A_{132} is set at $1 \cdot 10^{-26} \text{ J}^{10}$. Because Van de Pas¹⁶ estimates a chain length of $1.9 \cdot 10^{-9} \text{ m}$ in case of a tail of 11 oxyethylene units, h_{2e} is chosen to be $7 \cdot 10^{-9} \text{ m}$ and $4 \cdot 10^{-9} \text{ m}$ for Tween-40 (20 units) and Triton (11 units) respectively. In all cases the droplets can deform as Bo is larger then 0.05. Thus, model a, which assumes rigid droplets, is inappropriate. Calculations using this model predict coalescence times that are smaller than 1 second due to the contribution of the Laplace pressure on the film drainage.

More realistic are models b and c, although they highly overestimate the drainage times. In order to improve the predictions, an extra force, F' , is added to the total force of equation 2. Such a supplementary force will exist if the curvatures of the interfaces of the film are not completely identical. A pressure gradient due to the Laplace pressure will then exist, although not as large as in case of model a. Of course, F' might also compensate for other mechanisms which are not taken into account in models b and c. The minimal and maximal value of F' are determined for model b, using the experimental results without the presence of surfactant. In this case, F_g is $7 \cdot 10^{-6} \text{ N}$ and $F_{vdW}(h_c)$ is $3 \cdot 10^{-9}$

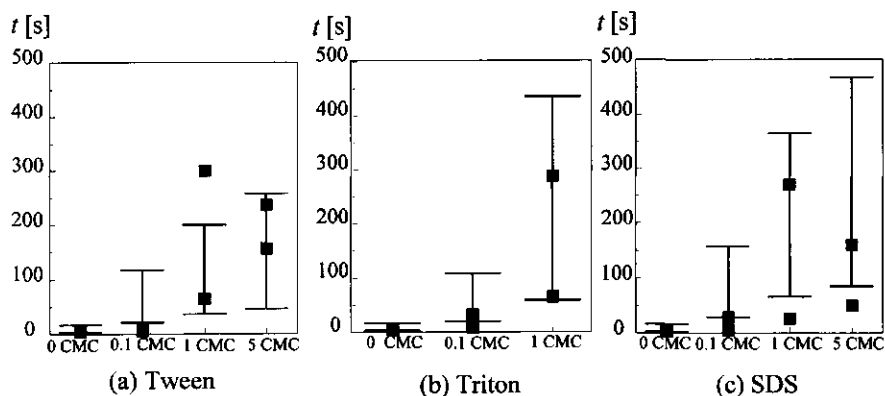


Figure 8, Comparison of experimentally determined $t_{a,5}$ and $t_{a,9}$ values with theoretical t_c -values according to model b for (a) Tween, (b) Triton and (c) SDS at different surfactant concentrations. The vertical lines represent the theoretical range of t_c while the squares are the experimental values. For the calculations the following constants are used: $d=1.9\cdot 10^{-3}\text{m}$, $A_{132}=1\cdot 10^{-20}\text{J}$, $\Delta\rho=227\text{ kg}\cdot\text{m}^{-3}$, $\zeta=0.038\text{V}$ and $5\cdot 10^{-5}<F'<3\cdot 10^{-4}\text{N}$.

N. Only if $5\cdot 10^{-5}\text{ N} < F' < 3\cdot 10^{-4}\text{ N}$, the calculated t_c varies between 4.1 and 22.3 s, which is in accordance to the experimental values (figure 7). Please note that F' is still smaller than F_L in case of model a, thus not unrealistic. Since F' is dominant and cannot be measured separately, the model really is a fit model. If it is assumed that F' is independent of γ , the minimal and maximal values of F' can be used to determine the minimal and maximal coalescence time for all experiments. The results are shown in figure 8. The figure shows that the majority of the experimental data lies in the theoretical range, although there is a tendency of overestimation. Calculations based on model c showed similar results.

Several remarks have to be made here. Firstly, F' might vary with γ and thus with surfactant concentration. A decrease of γ results in a more flexible interface and thus in a

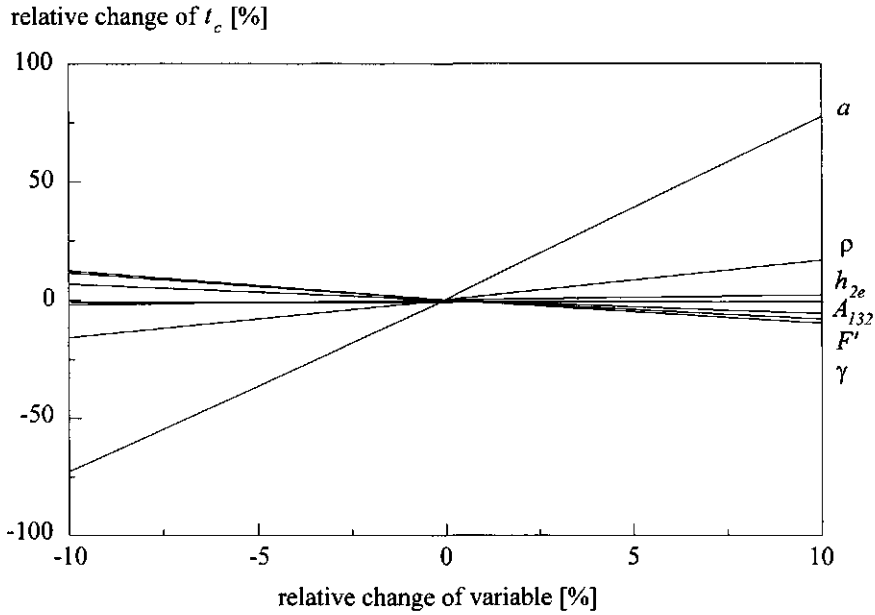


Figure 9, The influence of changing the values of several variables on the calculated coalescence time.

change of curvature of the film. Moreover, a decrease of γ can affect the droplet size of the droplet leaving the tip of the injection needle. Also, small variations of $\Delta\rho$, A_{132} and h_{2e} affect the calculations, which is shown in figure 9. Here, the effect of changing the variables by 10 % on the relative change of the calculated coalescence time is shown. As can be seen, the effect of changing the droplet size is largest; a small decrease results in a significantly lower prediction. The decrease of ρ and h_{2e} also diminishes the coalescence time, while the effect of changing A_{132} , γ and F' is inverse.

Coalescence of large oil droplets against a membrane

In order to investigate the effect of the presence of a membrane in the interface where coalescence takes place, coalescence times have been measured in a flat sheet, transparent membrane module. The results of the experiments, both with and without the polypropylene membrane, are shown in figure 10. Coalescence times decrease dramatically if the membrane is placed in the interface. One of the reasons for this effect might be the inhomogeneities of the membrane material². A more detailed discussion about the influence of surface roughness is given in chapter 6 of this thesis.

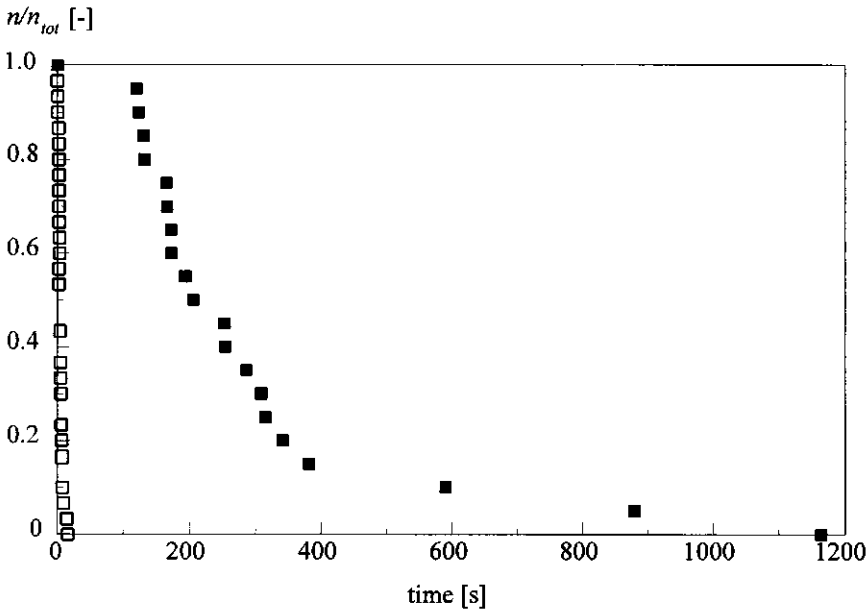


Figure 10, Coalescence times measured in a transparent membrane module with (\square) and without (\bullet) a polypropylene membrane with an average pore diameter of $0.1 \mu\text{m}$ as the surface. The aqueous phase contains a Tween-40 concentration of 14 CMC.

Coalescence of small droplets

Above, it is verified that the coalescence theory predicts the order of magnitude of the coalescence times for large oil droplets against a liquid surface. When the theory is applied to small droplets (e.g. $a = 0.2 \mu\text{m}$) with Tween-40 as surfactant, the calculated coalescence times are much smaller than 1 s. The reason for this is that h_i and h_c are so small that the attractive F_{vdW} is large and dominates the process. Although changing the main parameters (α , ρ , γ and h_{2e}) does influence the calculations, always $t_c \ll 1$ s. In some cases the calculations break down because either $h_c - h_{2e} < 0$ or $h_i < h_c$. Then, the coalescence time is estimated by calculating the time for most rapid growth of a wave in the film at a certain film thickness¹¹: $\tau = 96 \cdot \pi^2 \cdot \eta \cdot \gamma \cdot A_{132}^{-2} \cdot h^5$. If $h = h_c$, $\tau \ll 1$. At film heights smaller than h_c , τ will even be smaller. In conclusion, drainage theory shows that coalescence of small droplets against a liquid surface occurs fast. This is in contrast to the findings of Dickinson et al.¹⁷, who found a negative relation between droplet size and t_c . However, the diameter of the droplets they studied was not smaller than $2 \mu\text{m}$ and a protein was used to stabilize the emulsion. Therefore, the effect of steric hindrance was much larger and these results are difficult to compare to ours.

In the experiments with the double stirred-vessel the contact time of a droplet against the decane surface is expected to be only a fraction of a second. Thus, both contact time and coalescence time are in the same order of magnitude. Figure 11 shows that upon increasing the density difference between the dispersed and continuous phase, an increase of the oil removal rate is observed. It can be argued that the presence of a density difference contributes to an increase of the contact time, so that coalescence can occur.

During filtration, the coalescence times will be smaller than the calculated ones, due to the presence of the membrane. Based on an average residence time of a droplet in the flat sheet module of 10 s, under laminar flow conditions, the contact time should at least be a few seconds. Thus, $t_c < t_{\text{contact}}$ and coalescence will occur. In case of the dead end module as discussed in chapter 3 however, the contact times will be much smaller because of the presence of a stirrer (similar to the situation of the double stirred vessel). If it is assumed that a droplet contacts the membrane only at the surface parallel to the tube

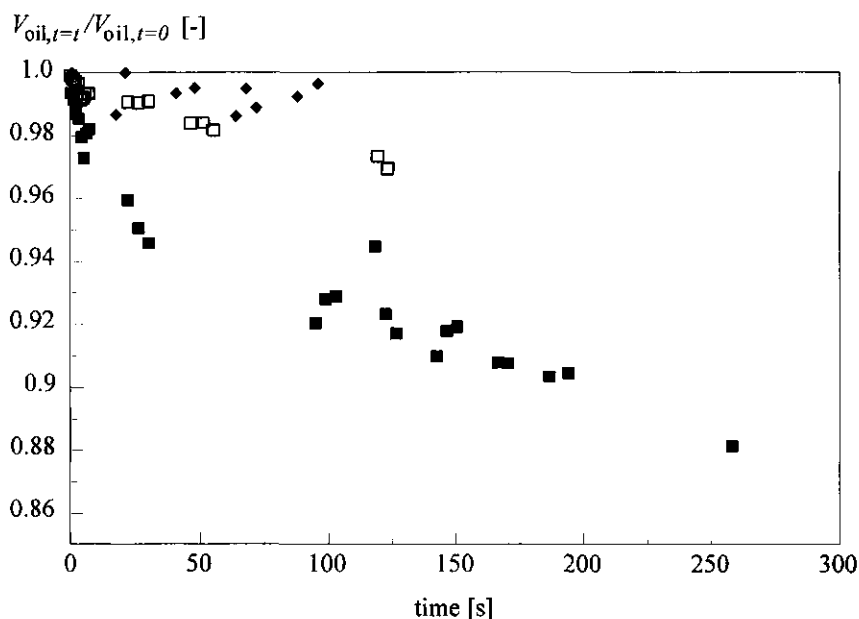


Figure 11, Profiles of the oil removal in the double stirred vessel out of Silverson-mixed emulsions, stabilized by 1 g/l Tween-40 with 3 different emulsified oil phases: ■ 100 % hexadecane, □ 65% hexadecane and 35% bromohexadecane and ◆ 50% hexadecane and 50% bromohexadecane.

through which the emulsion is pumped (see figure 3c in chapter 3), the contact time varies between 0.1 and 0.03 seconds, depending on the flow velocity. Thus, in case of the dead end module t_c and $t_{contact}$ are in the same range and coalescence can become limiting. This is in agreement with the observations in chapter 3 that at high velocities the permeation rate in the dead end module decreases (figure 8, chapter 3) with increasing velocity.

Figure 12 shows 3 filtration experiments of homogenized hexadecane emulsions prepared with different Tween-40 concentrations in the aqueous phase, using the flat sheet module. The permeation behavior of the emulsions with initially a Tween-40 concentration of 1

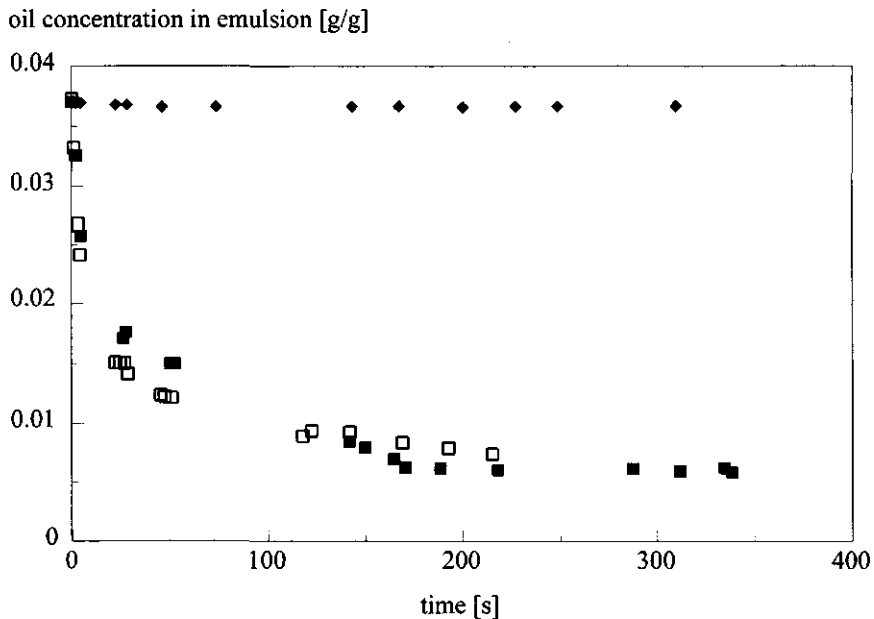


Figure 12, Filtration experiments with homogenized hexadecane-in-water emulsions stabilized by Tween-40 in the flat sheet module with an average flow velocity of $0.01 \text{ m}\cdot\text{s}^{-1}$. The surfactant concentration in the aqueous phase before emulsification is \blacksquare 1 CMC, $d_{32}=0.3 \text{ }\mu\text{m}$ \square 5 CMC $d_{32}=0.1 \text{ }\mu\text{m}$ and \blacklozenge 10 CMC, $d_{32}=0.1 \text{ }\mu\text{m}$.

CMC and 5 CMC is similar and can be modeled by the convective diffusion equation if the droplet size distribution is known (e.g. figure 9 in chapter 2 of this thesis). This model only takes into account the transport mechanisms while it is assumed that the membrane behaves as a perfect sink. As soon as a droplet reaches the membrane it permeates through the membrane, meaning that coalescence occurs immediately. This is in accordance with $t_c < t_{\text{contact}}$.

If the initial Tween-40 concentration is increased up to 10 CMC, no permeation is detected at all. A higher Tween concentration results in a smaller droplet size which can

result in a slower transport to the membrane (chapter 2 of this thesis). However, this effect cannot explain the absence of permeation. An explanation might be the presence of micelles in the aqueous phase after emulsification. The micelles in the film might hinder the drainage process in case of small droplets because the micelle diameter is in the same order of magnitude as the film thickness (nm). Groeneweg et al. found a similar stabilizing effect of the presence of micelles on droplet-droplet coalescence ($d_{j2} < 10 \mu\text{m}$)³. In case of large droplets this effect is not expected (figure 10) because of the larger film thickness. Another reason for the absence of permeation at high surfactant concentration might be the hindered film rupture.

In figure 12, micelles will not be present at the two lower Tween-40 concentrations because of the adsorption of surfactant molecules on the oil droplets. It can be calculated (assuming a total oil-water interface of 25 m^2 and a minimal covered surface area of $120 \cdot 10^{-20} \text{ m}^2$ per molecule) that in case of an initial 5 CMC concentration, the amount of Tween molecules is just too low to cover the oil interface completely. Due to this adsorption the actual Tween-40 concentration in the aqueous phase is lower than the critical micelle concentration. Since the surfactant molecules prefer the oil-water interface strongly over the bulk, micelles will only be present at the highest surfactant concentration.

One experiment with an initial SDS-concentration of 5 CMC has been performed in which no permeation is observed. For SDS it can be calculated (assuming a minimal covered surface area of $53 \cdot 10^{-20} \text{ m}^2$ per molecule) that already at an initial concentration of 5 CMC the actual amount of SDS in the bulk after emulsification exceeds the CMC, even under the assumption that the complete interfacial area is covered with surfactant molecules. Thus, micelles will be present in the aqueous phase, hindering the coalescence process.

Conclusions

The order of magnitude of the coalescence times of large oil droplets against a liquid surface with varying surfactant types and concentrations can be modeled by the theory which assumes a disk shaped deformation of the oil droplet if a supplementary force is defined. The presence of this force can result from a difference between the curvature of the droplet and the surface. Coalescence against a solid membrane surface occurs faster than against a liquid surface, probably because of surface roughness.

If the model is applied to small droplets, calculated coalescence times against a liquid surface are smaller than 1 second. Coalescence against a membrane is expected to occur even faster. This means that coalescence is ideal, i.e. as soon as a droplet reaches the solid or liquid surface it coalesces. This is in accordance with previous research (chapter 2 and 3 of this thesis) where filtration experiments of stable, secondary emulsions could be modeled by assuming perfect sink conditions, which means that as soon as a droplet contacts the membrane, it coalesces and disappears out of the emulsion. Hence, the model presumes transport limitation.

The residence time of an oil droplet in a flat sheet module naturally depends on the flow velocity but is in most cases at least a few seconds in the present research. Therefore, the order of magnitude of $t_{contact}$ is also assumed to be seconds resulting in $t_c < t_{contact}$; coalescence occurs. It is now clear that, in case of a flat sheet module and an initial Tween-40 concentration of 1 g/l the perfect sink condition is justified. In case of the dead end module however, the contact times are very short, due to different hydrodynamics. In this case it is possible that $t_c > t_{contact}$ and coalescence is rate limiting. This explains the observed decrease in permeation rate with increasing flow velocity using the dead end module in chapter 3. Moreover, coalescence limitation occurs, even in the flat sheet module, at high surfactant concentrations.

Acknowledgements

The author wishes to thank H. Donkers, V. Rafajlovska and C. Hassink for performing the experiments. B.H. Bijsterbosch from the department of Physical and Colloid Chemistry is greatly acknowledged for fruitful discussions. Moreover, she thanks the Foundation for Chemical Research in the Netherlands for financial support.

Nomenclature

a	droplet radius	[m]
A_{132}	the Hamaker constant of droplet 1 with liquid 2 through medium 3	[J]
B	force parameter	[N·m ⁷]
Bo	Bond number	[-]
CMC	critical micelle concentration	[kg·m ⁻³]
d	diameter	[m]
d_{32}	volume to surface average droplet diameter	[m]
F	force	[N]
F'	supplementary force	[N]
F_B	Born repulsion force	[N]
F_{el}	electrical repulsion force	[N]
F_g	gravity force	[N]
F_L	Laplace force	[N]
F_{vdW}	van der Waals attraction force	[N]
g	gravity acceleration constant	[m·s ⁻²]
h	film thickness	[m]
h_c	critical film thickness	[m]
h_i	initial film thickness	[m]
h_{2e}	combined thickness of 2 emulsifier layers	[m]
n	amount of droplets that has not yet coalesced	[-]

n_{tot}	total amount of droplets of which t_c is measured	[-]
R	radius of the film or disc	[m]
R'	radius of deformation	[m]
P	pressure	[Pa]
P_L	Laplace pressure	[Pa]
t	time	[s]
t_c	coalescence time	[s]
$t_{contact}$	contact time between droplet and membrane	[s]
$t_{0.5}$	half life time of coalescence	[s]
$t_{0.9}$	time at which 90% of the droplets has coalesced	[s]
γ	interfacial tension	[N·m ⁻¹]
ϵ	dielectric constant of water	[-]
ϵ_0	the permittivity of the vacuum	[C·V ⁻¹ ·m ⁻¹]
η	dynamic viscosity	[N·s·m ⁻²]
κ	the reciprocal double layer thickness	[m ⁻¹]
ρ	density	[kg·m ⁻³]
τ	characteristic time for most rapid growth of a wave in the film layer	[s]
ζ	the surface potential	[V]

Subscripts

d	droplet
w	continuous water phase
1	droplet
2	membrane or wall
3	medium

References

- 1 G.E. Charles and S.G. Mason, The coalescence of liquid drops with flat liquid-liquid interfaces, 1960, *Journal of Colloid Science*, vol. 15, p.236-267.
- 2 Z. Adamczyk, T. Dabros, J. Czarnecki and T.G.M. van de Ven, Particle transfer to solid surfaces, 1983, *Advances in Colloid and Interface Science*, vol.19, p.183-252.
- 3 F. Groeneweg, F. van Voorst Vader and W.G.M. Agterof, The dynamic stability of w/o emulsions from vegetable oil, 1993, *Chemical Engineering Science*, vol.48, no.2, p.229-238.
- 4 G.D.M. MacKay and S.G. Mason, The gravity approach and coalescence of fluid drops at liquid interfaces, 1963, *The Canadian Journal of Chemical Engineering*, vol.11, p.203-212.
- 5 E. Nakache, P. Longaive and S. Aiello, Determination of a coalescence parameter related to the stability of emulsions with polymeric surfactants, 1995, *Colloids and Surfaces A: Physicochemical and Engineering Aspects*, vol.96, p.69-76.
- 6 R.S. Allan and S.G. Mason, Particle motion in sheared suspensions; XIV Coalescence of liquid droplets in electric and shear fields, 1962, *Journal of Colloid Science*, vol.17, p.383-408.
- 7 T. Dabros and T.G.M. van de Ven, Surface collisions in a viscous fluid, 1992, *Journal of Colloid and Interface Science*, vol.149, no.2, p.493-505.
- 8 P. Hiemenz, *Principles of colloid and surface chemistry*, 1977, M. Dekker, New York, 516 p's.
- 9 D.C. Chappelaer, Models of a liquid drop approaching an interface, 1961, *Journal of Colloid Science*, vol.16, p.186-190.
- 10 P. Becher, *Encyclopedia of Emulsion Technology*, 1983, vol.1, M. Dekker Inc., New York, p.725.
- 11 A. Vrij and J.T.G. Overbeek, Rupture of thin liquid films due to spontaneous fluctuations in thickness, 1968, *Journal of the American Chemical Society*, vol.90, no.12, p.3074-3078.
- 12 E. Dahlquist and F. Setterwall, Parametric experiments and modeling of a cross-flow coalescence filter, 1993, *Separation Technology*, vol.3, p.198-211.
- 13 P.A. Arp and S.G. Mason, Orthokinetic collisions of hard spheres in simple shear flow, 1976, *Canadian Journal of Chemistry*, vol.54, p.3769-3774.
- 14 P.T. Jaeger, J.J.M. Janssen, F. Groeneweg and W.G.M. Agterhof, Coalescence in emulsions containing inviscid drops with high interfacial mobility, 1994, *Colloids and Surfaces A: Physicochemical and Engineering Aspects*, vol.85, p.225-264.
- 15 B.J.R. Scholtens, S. Bruin and B.H. Bijsterbosch, Liquid-liquid mass transfer and its retardation by macromolecular adsorption, 1979, *Chemical Engineering Science*, vol.34, p.661-670.
- 16 J. van de Pas, A study of the physical properties of lamellar liquid-crystalline dispersions, 1993, PhD-thesis.

-
- 17 E. Dickinson, B.S. Murray and G. Stainsby, Coalescence kinetics of protein-stabilised emulsion droplets, in: *Gums and Stabilisers for the Food Industry 4*; Proceedings of the 4th International Conference held at Wrexham, Wales, 1987, eds. G.O. Phillips, P.A. Williams and D. Wedlock, p.463-471.

5 Performance of a dispersed phase separator enhanced by an electric field

Summary

In previous research it was shown that small ($d_{32} < 10 \mu\text{m}$), stable oil droplets can permeate through hydrophobic membranes, forming a continuous oil phase as the permeate. In most cases the permeation is transport limited, i.e. the transport of oil droplets from the bulk towards the membrane can be optimized. Therefor, in this research an additional, external force is applied by creating an electric field over the emulsion. As oil droplets are slightly negatively charged, the transport can be enhanced by placing the anode near the membrane. It is important to avoid the presence of large resistances between the electrodes other than the emulsion. If such a large resistance exists, the electric field will be situated mainly over the phase containing this resistance, at the cost of the electric field over the emulsion.

Three systems are investigated. Firstly, the anode is placed at the feed side of the membrane. The extraction of oil droplets out of the emulsion is successful; if the voltage is increased from 0 to 20 V, the velocity at which droplets disappear out of the emulsion is increased 1200 times. However, not all droplets permeate through the membrane and a layer of concentrated emulsion near the anode is formed.

In the second system, the anode is placed at the permeate side of the membrane, while the resistance of the permeate is decreased by using an organic phase (DCE) with an apolar electrolyte (TBAI). Here too, the permeation is enhanced, although the electric field over the emulsion is 100 times lower than in the first system due to the resistance of the DCE-phase. This results in a lower electrophoretic velocity. Application of the system in practice is difficult because of the pollutional aspects of DCE and TBAI.

In the third system, the anode together with an aqueous phase is placed at the permeate side of the membrane. Droplets that coalesce with the membrane can be pushed through the membrane by means of a pressure pulse. In the permeate large droplets are found which can easily be separated using a settler. Thus, all systems show indeed an enhanced extraction. However, we think that only systems 1 and 3 are scaleable.

Introduction

Previously, the separation of small oil droplets ($d_{32} < 10 \mu\text{m}$), stabilized by the non ionic surfactant Tween-40 out of oil-in-water emulsions using a hydrophobic polypropylene membrane has been investigated (chapter 2 of this thesis). At the retentate side of the membrane an emulsion is circulated. If a droplet is transported to the membrane and coalesces onto the membrane it permeates to the continuous oil phase at the permeate side. In principle, this separation method is to be preferred over the removal of the continuous water phase by hydrophilic membranes in case of a low volume fraction of oil. Therefore, the oil weight fraction of the emulsions under consideration is always lower than 0.06. It was shown, that the droplets can be separated, although the experimental flux values are low. The separation mechanism consists of 2 steps: transport of the droplets from the bulk towards the membrane and coalescence of the droplets with the membrane. In most cases, the process is transport limited. Thus, in order to increase the efficiency of the process, transport must be optimized. As stated before, the main transport mechanisms are *interception*, *impaction*, *diffusion*, *gravitation* and *electrostatic attraction*. In the present chapter, the effect of the application of an additional transport factor, namely an *electric field force*, is investigated.

Electric separation techniques have been in commercial use for nearly 70 years¹. Some important applications are electrical emulsion breaking, electrofiltration of fine suspensions and continuous flow electrophoresis. Demulsification of water in oil emulsions can be achieved with both dc fields², pulsed dc fields and ac fields^{3,4}. The process of emulsion breaking proceeds in 3 stages. During the first stage, small droplets

coalesce and grow into larger droplets which settle in the next stage. The final stage involves coalescence of large drops with the continuous phase. The presence of an electric field probably promotes all stages. Two main mechanisms can be distinguished⁵. Firstly, coalescence can be enhanced due to induced dipoles of the droplets. Induced polarization forces occur in water-in-oil emulsions. Here, the dispersed phase is relatively high conducting, resulting in polarized droplets which can form chains and increase the coalescence probability. Another effect of polarization forces occurs if the field is nonhomogeneous, i.e. the field lines converge or diverge. One side of the droplet experiences a higher field force than the other side, resulting in a net force towards the convergence of the ac or dc field. The droplets start to travel, enhancing the chance of collision. This mechanism is called dielectrophoresis. Secondly, coalescence will be enhanced by an electric field if the droplets have a net charge. The droplets will travel between the electrodes, thus increasing the chance of collision and coalescence (electrophoresis). If the charged, dispersed phase is immovable the presence of an external field will force the continuous phase to flow; this process is called electro osmosis.

In the present research, polarization effects are assumed to be negligible because the dispersed phase consists of a low conducting oil phase. As a result, the electrolyte concentration in the droplets is low and so is polarization. Moreover, due to the high electrolyte concentration in the continuous phase, the small polarization forces between the oil droplets will be buffered. However, because oil droplets have a net negative charge, electrophoresis will happen⁶. If an anode is placed in the module at the side of the membrane, the transport of droplets towards the membrane will be enhanced. Unfortunately, if the anode is placed on the permeate side of the membrane, problems are expected because of the low conductivity of the continuous oil phase on this side. As a result, the potential difference and thus the electric field is mainly situated over the permeate instead of over the emulsion. Therefore, 3 different systems have been investigated. In the first, the anode is placed on the feed side of the membrane. Here, the only function of the membrane is to separate the continuous oil and water phases. In the second system, the anode is placed on the permeate side, but the conductivity of the oil

phase is increased by using hydrophobic ions. In the third system, where the anode is placed on the permeate side too, an aqueous phase is circulated on the permeate side. Here, the membrane acts as a conventional coalescer to enlarge the droplets.

Theory

Surface charge

A colloidal particle can be charged by specific adsorption of positively and/or negatively charged ions (cations and anions respectively) on the surface of the particle⁶:

$$\sigma_0 = F \cdot (\Gamma_+ - \Gamma_-) \quad (1)$$

with σ_0 [$\text{C}\cdot\text{m}^{-2}$] is the surface charge, F [$\text{C}\cdot\text{mol}^{-1}$] is the Faraday constant and Γ_+ and Γ_- [$\text{mol}\cdot\text{m}^{-2}$] are the adsorbed amounts of cations and anions respectively. An excess of one type of ion on the surface can be caused by either an excess of that ion type in the bulk or by specific adsorbance due to non electrostatic forces (e.g. van der Waals attraction and interaction of dipoles). Generally, anions show higher affinity for the interface than cations in case of an oil-water interface due to polarization effects. The surface charge causes a surface potential, ψ_0 [V] which can be approximated by:

$$\Psi_0 = \frac{\sigma_0}{\epsilon \cdot \kappa} \quad (2)$$

if $\psi_0 < 25$ mV. Here, ϵ [$\text{C}\cdot\text{V}^{-1}\cdot\text{m}^{-1}$] is the dielectric constant which is equal to the product of the relative dielectric constant ϵ_r [-] and the dielectric constant of the vacuum, ϵ_0 [$\text{C}\cdot\text{V}^{-1}\cdot\text{m}^{-1}$] and κ [m^{-1}] is a constant. For aqueous systems κ can be calculated by:

$$\kappa = \sqrt{10 \cdot c \cdot z^2} \quad (3)$$

Here, κ is expressed in nm^{-1} , c [$\text{mol}\cdot\text{l}^{-1}$] is the electrolyte concentration and z [-] is the valence of the ions. Moreover, κ [m^{-1}] is the reciprocal double layer thickness. This double layer is formed due to the presence of ions in the bulk. The counterions, i.e. the ions with an opposite charge to the surface, concentrate near the surface. In this way, the surface charge is compensated. Equation 3 shows that an increase of the electrolyte concentration compresses the double layer. If the ions are considered to have no volume and if $\psi_0 < 50$ mV, the potential as a function of the distance from the surface can be estimated by:

$$\Psi_x = \Psi_0 \cdot e^{-\kappa x} \quad (4)$$

with x [m] being the distance from the surface. Because the surface potential cannot be measured, the potential at the plane of shear, the ζ -potential, is often used as an estimation. The distance between the surface and the plane of shear is usually a few water

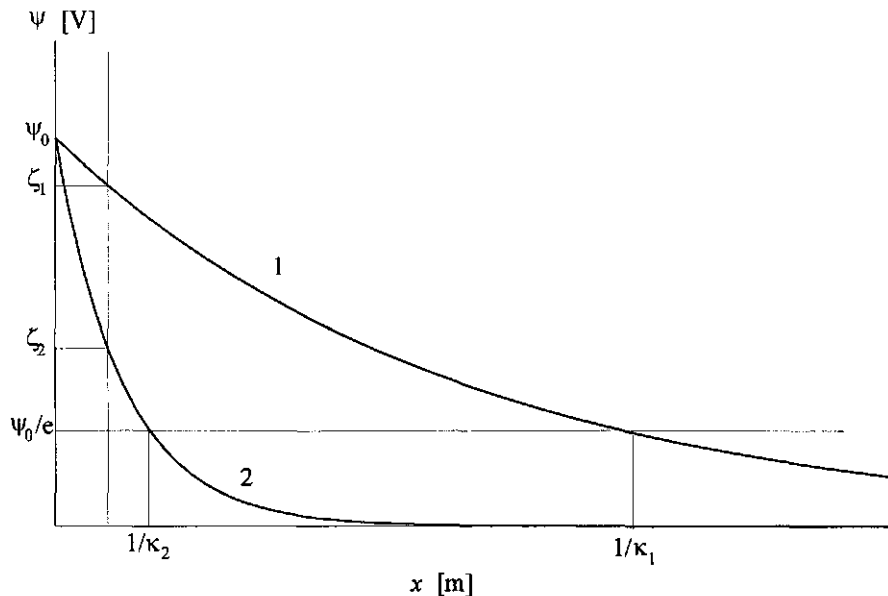


Figure 1, Potential as a function of distance from the surface of an oil droplet, (1) low electrolyte concentration and (2) high electrolyte concentration.

molecules thick. The ζ -potential is a good estimation for ψ_0 if the electrolyte concentration is low. At high electrolyte concentration, ζ is much smaller than ψ_0 (figure 1).

Electrophoresis

Generally, the electrophoretic velocity, v_e [$\text{m}\cdot\text{s}^{-1}$], is given by⁷:

$$v_e = \frac{\epsilon \cdot E \cdot \zeta}{\eta} \cdot f(\kappa, a) \quad (5)$$

with E [$\text{V}\cdot\text{m}^{-1}$] is the electric field, η [$\text{N}\cdot\text{s}\cdot\text{m}^{-2}$] is the dynamic viscosity and a [m] is the droplet radius. In case of large, non conducting droplets with a thin double layer ($\kappa \cdot a \gg 1$), $f(\kappa, a) = 1$. In the other case, if ($\kappa \cdot a \ll 1$), $f(\kappa, a) = 2/3$.

The electric field between two electrodes is equal to the ratio of the potential difference, V [V], and the distance between the electrodes, d [m]:

$$E = \frac{V}{d} \quad (6)$$

If several phases are present in series between the electrodes (e.g. an emulsion, a membrane and a organic phase), a potential difference V_i exists over each phase i and $V_{tot} = \sum V_i$. Also, Ohm's law holds:

$$V_i = I \cdot R_i \text{ and } R_{tot} = \sum R_i \quad (7)$$

I [A] being the flow strength and R [Ω] the resistance. The latter is determined by:

$$R_i = \frac{d}{O \cdot \kappa_{sp,i}} \quad (8)$$

Here, O [m^2] is the surface area of the electrode and $\kappa_{sp,i}$ [$\Omega^{-1}\cdot\text{m}^{-1}$] is the specific conductivity of the solution in phase i . Combination of equation 6, 7 and 8 gives:

$$E_i = \frac{I}{O \cdot \kappa_{sp,i}} \quad (9)$$

Thus, if a potential difference is applied over the membrane module, I and $\kappa_{sp,i}$ can be measured and E_i can be calculated. Then, the electrophoretic velocity can be calculated with equation 5. Problems are encountered if one of the phases between the electrodes is a continuous oil phase with a κ_{sp} of almost 0, resulting in a very small electric field in the emulsion phase. Therefore, in some of our experiments κ_{sp} of the oil phase is increased by addition of electrolytes which can dissociate in non-aqueous solutions^{8,9}. An important variable for dissociation of electrolytes in solutions with a low dielectric constant is the sum of the radii of both anion and cation. The higher this sum, the better the electrolyte is soluble.

Effect of electrophoresis on the permeation flux

The experimentally determined flow velocity through the membrane, v' [$\text{m}\cdot\text{s}^{-1}$], is a product of the transport velocity of oil droplets towards the membrane, $v_{transport}$ [$\text{m}\cdot\text{s}^{-1}$], and the coalescence probability P_c . If not all droplets that contact the membrane coalesce, P_c will be smaller than 1.

$$v' = v_{transport} \cdot P_c \quad (10)$$

If an electric field is applied, $v_{transport}$ is determined by the sum of the 'conventional' transport mechanisms (chapter 2 and 3) and electrophoresis. Since only the electrophoresis mechanism is dependent on the electric field, formula 11 is valid:

$$\frac{dv'}{dE} = \frac{\varepsilon \cdot \zeta \cdot f(\kappa, a)}{\eta} \cdot P_c \quad (11)$$

Thus, if experiments are performed at different electric field values and v' is measured, P_c can be determined by the tangent of the graph of v' against E .

Materials and Methods

Preparation of the emulsions

Emulsions are made by mixing an aqueous solution of $1 \text{ g}\cdot\text{l}^{-1}$ of the nonionic surfactant poly(20)oxyethylene-sorbitan-monopalmitate (Tween-40, Sigma, p.a.) and $2.5\cdot 10^{-4} \text{ M}$ KNO_3 with specified amounts of n-hexadecane (Merck, p.a., density is $773 \text{ kg}\cdot\text{m}^{-3}$). The oil concentration in the emulsions is always smaller than 6 weight percent. A mixture of 100 ml is homogenized during 15 minutes using a Condi Labhomogenizer. The pressure, which can not be adjusted, is circa 100 bar.

Filtration experiments

In all cases, a hydrophobic polypropylene membrane (Enka, Accurel) with an average pore size of $0.1 \mu\text{m}$ is placed in a flat sheet, cross flow module. The length of the module is 0.12 m, the channel height is $3\cdot 10^{-3} \text{ m}$ and the effective membrane area is $3.24\cdot 10^{-3} \text{ m}^2$. The height of the permeate chamber is $1\cdot 10^{-3} \text{ m}$. The module is placed horizontally using a leveling instrument. The emulsion (100 ml), which is stirred in a vessel with a magnetic stirrer, is pumped through the module using a gear pump with a velocity of $0.01 \text{ m}\cdot\text{s}^{-1}$. The retentate is led back to the vessel. A transmembrane pressure is regulated with a pressure valve on the retentate side of the module. Two electrodes are placed in the module with a surface area identical to the membrane surface area (except the anode in system 1). A d.c. field is applied by a generator (15 W), the voltage is measured by a voltmeter and the amperage by a galvanometer. A conductivity meter measures the specific conductivity of the emulsion. During this batch process, samples are taken from the feed to determine the oil concentration.

System 1: anode on the feed side of the membrane

A perspex module is placed in such a way that the membrane is situated on the upper side of the feed chamber. In the bottom plate of the module, a stainless steel electrode (cathode) is implanted. The anode, a $0.5\cdot 10^{-3} \text{ m}$ thick, stainless steel plate of which 50%

of the surface area is perforated, is placed on the feed side of the membrane (figure 2). The permeate is collected into a beaker. The transmembrane pressure is 0.03 bar.

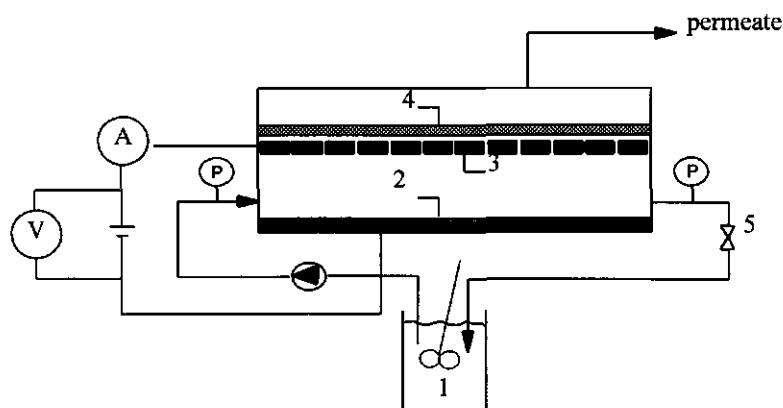


Figure 2, Experimental system with the anode on the feed side: (1) vessel containing the emulsion, (2) cathode, (3) anode, (4) membrane and (5) pressure valve.

System 2: Anode with an organic phase on the permeate side

In this system, the anode is situated on the permeate side of the membrane. A volume of 250 ml dichloroethane (DCE, $\epsilon_r = 10.6$, $\rho = 1250 \text{ kg}\cdot\text{m}^{-3}$ with 10^{-3} M tetra-*n*-butylammonium iodide (TBAI) is pumped on the permeate side with a velocity of $0.06 \text{ m}\cdot\text{s}^{-1}$. The transmembrane pressure is 0.06 bar. Because the density of DCE is higher than that of the emulsion, the teflon module is arranged in such a way that the membrane is situated on the lower side of the feed chamber (figure 3). In the vessel containing the DCE phase, 150 ml distilled water is put on top to avoid evaporation of DCE. During most experiments, the electric field in the emulsion, E_{emulsion} , and thus the ratio $\frac{I}{\kappa_{sp}}$ in the emulsion, is kept as constant as possible by regulating the voltage.

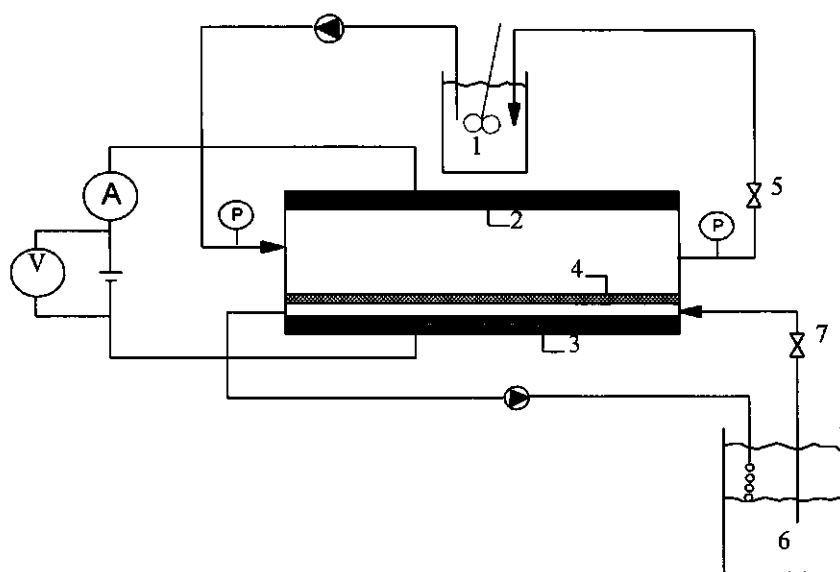


Figure 3, The experimental setup in case the anode is placed at the permeate side of the membrane and a solution of TBAI in DCE is recycled at the permeate side; (1) vessel containing the emulsion, (2) cathode, (3) anode, (4) membrane, (5) pressure valve, (6) vessel containing the DCE-phase with water on top and (7) 3 way valve to take DCE samples.

System 3: Anode with an aqueous phase on the permeate side

Identical to system 2, the anode is placed on the permeate side of the membrane. The membrane is situated on top of the feed chamber. The transmembrane pressure in the perspex module is 0.35 bar for most experiments (1 experiment was performed at 0.1 bar). On the permeate side, 150 ml of an aqueous $2.5 \cdot 10^{-4}$ M KNO_3 solution is recycled at a velocity of $0.06 \text{ m} \cdot \text{s}^{-1}$. During an experiment the membrane pores are filled with oil. This results in an increase of the resistance of the membrane phase, because of the low κ_{sp} of the oil. Therefore, similar to system 2, the voltage is regulated to keep $E_{emulsion}$ constant. When the maximal voltage is reached, a vacuum pulse on the permeate side is applied by closing valve 7 (figure 4) to remove the oil out of the pores. This results in a decrease of the resistance of the membrane phase and thus an increase of $E_{emulsion}$. The pressure at the

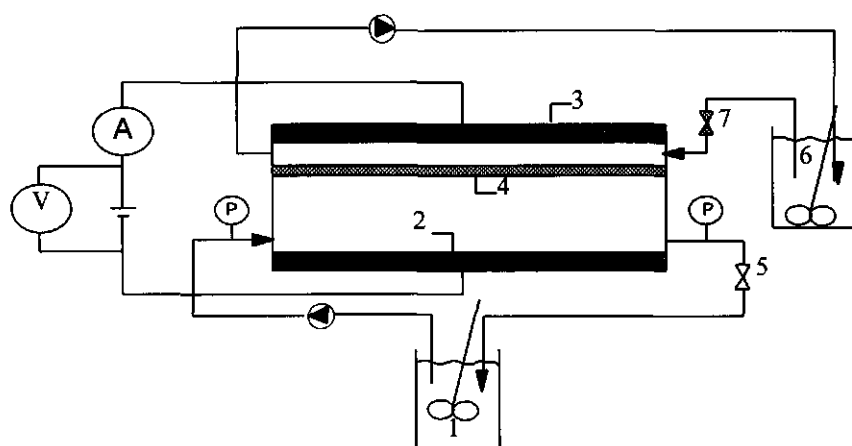


Figure 4, Experimental setup of the system with a anode on the permeate side of the membrane while an aqueous phase is recycled at the permeate side; (1) vessel containing the emulsion, (2) cathode, (3) anode, (4) membrane, (5) pressure valve, (6) vessel containing the aqueous phase and (7) valve to create vacuum on the permeate side.

permeate side becomes -0.02 bar and I is allowed to increase up to a value of $5 \cdot 10^{-3}$ A. Then, the vacuum is stopped, the voltage is set to the desired value and the experiment is continued. This process is repeated constantly.

Procedure to fit the data

In chapter 2 it was shown that the experimental results can be fitted with a single fit parameter; the apparent deposition velocity v' [$\text{m} \cdot \text{s}^{-1}$]. It indicates the efficiency of the separation process and can be used to easily compare experiments.

Measurement of the oil concentration in the emulsion

The oil concentration is determined as stated earlier (chapter 2 of this thesis). Ten μl of sample is diluted with 990 μl ethanol (Merck, p.a.) and one μl of this dilution is injected in a Carlo Erba gas chromatograph (GC 6000, vega series) with a 10 m CP-Sil 5 CB capillar column (Chrompack, The Netherlands) and a cold on-column injection system. At the moment of injection the oven temperature is 80 $^{\circ}\text{C}$. After one minute, the temperature is increased at 15 $^{\circ}\text{C}\cdot\text{min}^{-1}$ up to 250 $^{\circ}\text{C}$. The F.I.D detection of hexadecane occurs at 370 $^{\circ}\text{C}$. To calculate the concentration, a calibration curve is used.

Determination of the droplet size

The dynamic light scattering method is used to determine the droplet size. The variation of intensity of scattered laser light (wave length of 634 nm) in time is measured so the average diffusion coefficient can be calculated. With the Stokes-Einstein relation the volume averaged diameter, d_{30} , can be derived, which is usually somewhat smaller than the average volume/surface droplet diameter.

In case of system 2, the influence of adding different concentrations of TBAI-ions after emulsification on the droplet size is investigated. The samples are stored during 17 hours at 4 $^{\circ}\text{C}$. No influence of the TBAI concentration on the droplet size could be measured.

Determination of the ζ -potential

A Malvern Zetasizer III is used to determine the ζ -potential. Samples are diluted using the aqueous solution with which the emulsions are prepared until the oil concentration in the sample is 0.001 % (w/w). An electric field is applied over a capillar and the electrophoretic mobility U [$\text{m}^2\cdot\text{s}^{-1}\cdot\text{V}^{-1}$] of a droplet is measured by the Laser-Doppler effect. Because $U = \frac{v_e}{E}$ the ζ -potential can be calculated (equation 5).

For system 2, it is checked whether the presence of TBAI-ions influences the ζ -potential of the emulsion. Measurements are performed by diluting the emulsion with an aqueous solution of $2.5\cdot 10^{-4}$ M KNO_3 and different concentrations of TBAI. No effect

of TBAI on the ζ -potential was found up to a TBAI concentration of 10^{-4} M. At a concentration of 10^{-3} M, the ζ -potential decreases. Two effects are important. Firstly, the high electrolyte concentration buffers the charge of the droplet. Secondly, the hydrophobic TBA^+ -ion is expected to adsorb on the oil-surface more than the I^- -ion, thus compensating the negative charge of the oil surface.

Results and Discussion

The surface to volume averaged droplet diameter, d_{32} , equals $0.4 \mu\text{m}$. The ζ -potential of the oil droplets in an emulsion prepared as discussed in Materials and Methods is $-22 \cdot 10^{-3}$ V. Thus, the oil droplets are indeed charged and the application of an electric field should enhance permeation. The specific conductivity, κ_{sp} , of the emulsion is $40 \mu\Omega^{-1}\text{cm}^{-1}$. This is equal to the conductivity of a $2.5 \cdot 10^{-4}$ M KNO_3 solution; the presence of oil does not effect κ_{sp} . If changes of κ_{sp} occur during an experiment, they cannot be caused by a decrease of oil concentration in the emulsion.

System 1: Anode on the feed side of the membrane

The effect of increasing the voltage from 0 to 20 V after 5 hours of filtration can be seen in figure 5. The figure clearly shows a large increase of the permeation rate after the electric field is applied; the apparent deposition velocity has increased 1200 times from $1.1 \cdot 10^{-7}$ up to $1.3 \cdot 10^{-4} \text{ m}\cdot\text{s}^{-1}$.

During the experiment with constant V , I decreases from $2.2 \cdot 10^{-2}$ to $4.1 \cdot 10^{-3}$ A while κ_{sp} is constant. Therefore, E_{emulsion} decreases (from $1.4 \cdot 10^3$ to $2.3 \cdot 10^2 \text{ V}\cdot\text{m}^{-1}$) as does v_e . This effect must be caused by an increase of the total resistance. During the experiment, a cream layer is detected near the anode. This means that oil droplets cumulate near the electrode but are not removed into the permeate. As the amount of oil droplets increases in this layer, the oil-in-water emulsion might even change into a water-in-oil emulsion. This effect might be responsible for the increase of R_{tot} . An

explanation for the presence of the cream layer might be the increased surfactant concentration near the anode. Initially, droplets coalesce and the oil-water interfacial area decreases subsequently. Therefore, the surfactant concentration in the water phase near the anode increases. These surfactant molecules will (partly) diffuse back into the bulk, but they might also adsorb on remaining oil droplets, thus stabilizing them.

The electrophoretic velocity, calculated according to equation 5 with ϵ_r of water is 80 and ϵ_0 is $8.9 \cdot 10^{-12} \text{ F} \cdot \text{m}^{-1}$, decreases from $4.2 \cdot 10^{-5} \text{ m} \cdot \text{s}^{-1}$ to $8.1 \cdot 10^{-6} \text{ m} \cdot \text{s}^{-1}$. Here, $f(\kappa, a)$ is assumed to be 1, as κ^{-1} is 20 nm for a $2.5 \cdot 10^{-4} \text{ M KNO}_3$ solution and d_{32} is $0.4 \text{ } \mu\text{m}$ leading to $\kappa \cdot a = 10$. Thus, during the whole experiment, v_e is significantly higher than the apparent deposition velocity without an electric field. This means that electrophoresis can be successfully used to increase the separation efficiency of stable oil droplets by

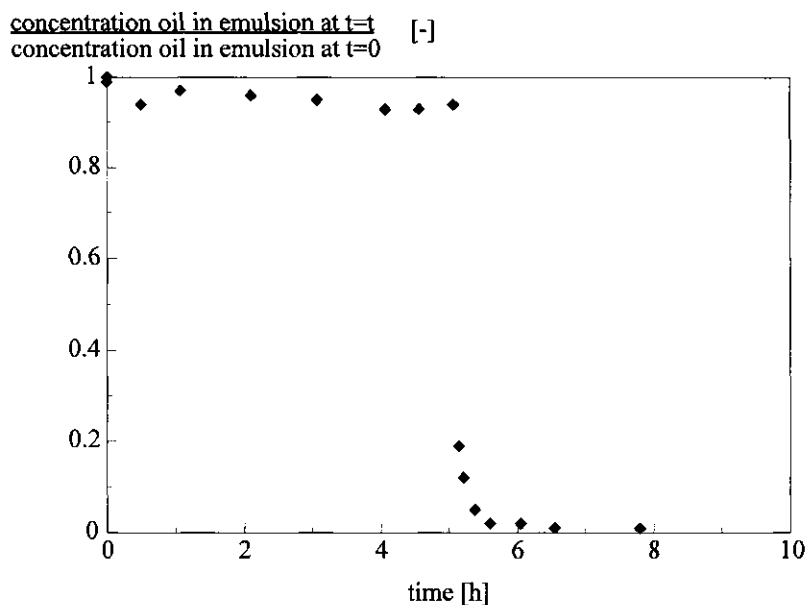


Figure 5, Experimental results in system 1; during the initial 5 hours no electric field is present ($v=1.1 \cdot 10^{-3} \text{ m} \cdot \text{s}^{-1}$), after 5 hours a voltage of 20 V is applied ($v=1.3 \cdot 10^{-4} \text{ m} \cdot \text{s}^{-1}$).

membranes. However, as not all droplets permeate through the membrane, another design is necessary to improve the oil removal.

System 2: Anode with an organic phase on the permeate side

Before experiments are started, it is verified that the presence of TBAI-ions does not affect the stability of the emulsion droplets. No influence of the ions on droplet size and ζ -potential of the emulsion has been measured (see Materials and Methods).

One filtration experiment has been performed in which no effort is made to keep the field strength in the emulsion constant (figure 6). The oil concentration in the emulsion decreases in time, while the hexadecane concentration in the DCE-phase increases. No cream layer as in system 1 is detected near the membrane surface. During the first 6 hours, $E_{emulsion}$ decreases from 90 to 10 V·m⁻¹, after which a steady state is reached. This decrease of $E_{emulsion}$ is caused by a decrease of $R_{emulsion}$ and/or an increase of R_{DCE} (equation 8 and 9). The κ_{sp} of the emulsion phase is measured to change from 40 $\mu\Omega^{-1}\cdot\text{cm}^{-1}$ initially to 140 $\mu\Omega^{-1}\cdot\text{cm}^{-1}$ after 56 hours filtration with a potential of 20 V. The κ_{sp} of the DCE phase decreases from 31.3 to 1.5 $\mu\Omega^{-1}\cdot\text{cm}^{-1}$. This indeed results in a decrease of $E_{emulsion}$.

Several processes are responsible for these changes of κ_{sp} . Firstly, the TBAI molecules will divide themselves over the DCE-phase, the emulsion and the water phase on top of the DCE. This will lead to an increased conductivity in the emulsion and a decreased conductivity in the DCE-phase. As the partitioning coefficient of TBAI in water versus DCE is measured to be 4, this effect contributes largely to the increased conductivity in the emulsion. Secondly, the reaction at the electrodes causes formation of (OH)⁻ out of H₂O at the cathode in the emulsion and I₂ out of I⁻ at the anode in the DCE-phase. In the emulsion, this causes an increase of κ_{sp} . However, (OH)⁻-ions will be transported towards the DCE phase because of the decreasing I⁻-concentration due to the anode reaction. Because OH⁻-ions have a lower solubility in DCE than I⁻-ions, κ_{sp} in the DCE phase decreases. Also, the charge effects due to the electrode reactions will be compensated by transport of TBA⁺-ions towards the cathode and/or OH⁻-ions from the

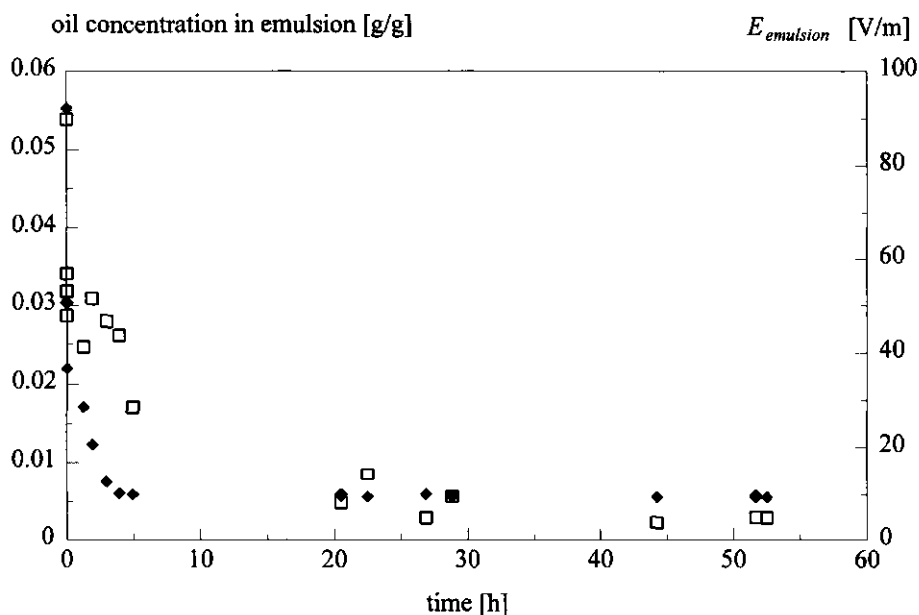


Figure 6, Experimental results of system 2 with $V = 20$ V, □ oil concentration in the emulsion [w/w] and ◆ electric field over the emulsion, $E_{emulsion}$ [$V \cdot m^{-1}$].

emulsion to the anode. As TBA^+ dissolves much better in water than OH^- dissolves in DCE, the main mechanism will be transport of TBA^+ . A final remark concerns the formation of I_2 at the anode. During the experiment, the DCE-phase becomes saturated with I_2 . Because iodine does hardly dissolve in water it precipitates at the DCE-water interface in the vessel.

Next, experiments are performed at different, constant $E_{emulsion}$ -values, by keeping the ratio $\frac{I}{K_{sp}}$ in the emulsion constant. Figure 7a shows an increased permeation when an electric field is applied. However, the apparent deposition velocity in case of an electric field is much smaller than in case of system 1. The reason is, that in system 2 the electric field over the emulsion (maximal $35 V \cdot m^{-1}$) is much lower than in system 1 (average of

$44 \cdot 10^2 \text{ V} \cdot \text{m}^{-1}$) due to the relatively high resistance of the DCE phase. Therefore, the maximal v_e in system 2 is only $5.4 \cdot 10^{-7} \text{ m} \cdot \text{s}^{-1}$. Nevertheless, this is twice as much as the deposition velocity without an electric field. Thus, in system 2 also the electric field significantly improves the permeation.

Finally, in figure 7b the coalescence probability, P_c , is determined as described in equations 10 and 11 with $\varepsilon = 7.12 \cdot 10^{-10} \text{ C} \cdot \text{V}^{-1} \cdot \text{m}^{-1}$, $\zeta = -22 \cdot 10^{-3} \text{ V}$, $f(\kappa, a) = 1$ and $\eta = 1 \cdot 10^{-3} \text{ N} \cdot \text{s} \cdot \text{m}^{-2}$; $P_c = 1.18$. Theoretically, P_c cannot be larger than 1. However, a three points measurement will not give a very accurate estimation of P_c . In figure 7b, the best fit ($P_c = 1.18$) and a fit with $P_c = 1$ is given. One can see that both lines are good estimations. An other reason for the high P_c -value can be a small error in the determination of the ζ -potential. During this measurement the amount of adsorbed surfactant molecules onto the oil droplets differs from that in the original emulsion. Measurements of the

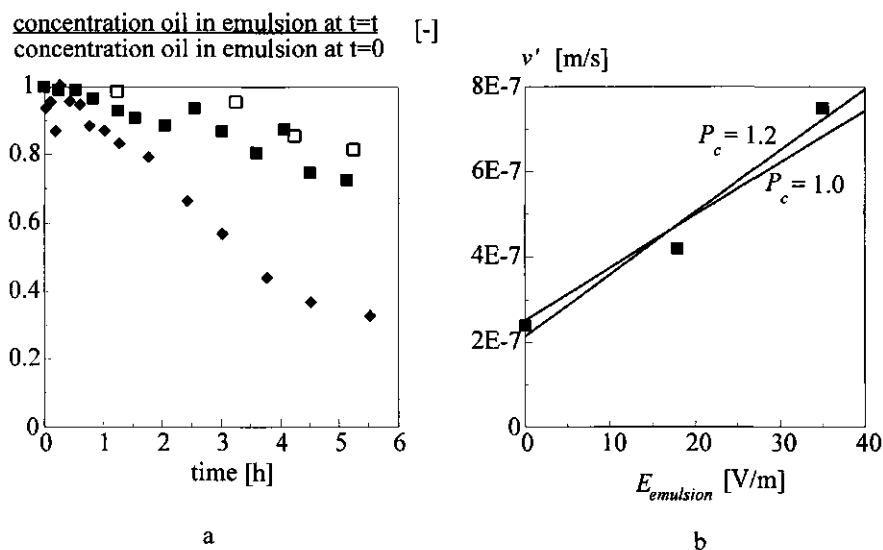


Figure 7, Experimental results of the DCE-system (a) oil concentration against time with $\square E_{emulsion} = 0 \text{ V} \cdot \text{m}^{-1}$, $\blacksquare E_{emulsion} = 18 \text{ V} \cdot \text{m}^{-1}$ and $\blacklozenge E_{emulsion} = 35 \text{ V} \cdot \text{m}^{-1}$ and (b) v' against $E_{emulsion}$

ζ -potential with different amounts of surfactant in the dilution solution show a positive relation between a decrease of surfactant concentration and a increase of ζ -potential. If P_c is determined with a ζ -potential of $-20 \cdot 10^{-3}$ V in stead of $-22 \cdot 10^{-3}$ V, $P_c = 1$.

It is clear that the system is still transport limited, despite of the presence of an electric field. If the electric field could be increased, the permeation can be improved. However, the maximal workable $E_{emulsion}$ in system 2 is $35 \text{ V} \cdot \text{m}^{-1}$ since at higher E , the TBAI molecules are almost completely removed out of the DCE phase. This results in a high R_{DCE} and thus a low $E_{emulsion}$. Moreover, at high E_{tot} strong gas development at the electrodes occurs.

System 3: Anode with an aqueous phase on the permeate side

In this system an aqueous phase is situated on the permeate side. Droplets, which coalesce against the membrane, can be transported towards the permeate by applying a pressure pulse. If no such pulse is applied, a cream layer of concentrated emulsion is detected on the feed side of the membrane, similar to system 1, and I drops to 0. If pulsation is applied, such a cream layer still occurs but also large droplets ($a = 0.1\text{-}1 \text{ mm}$) can be detected in the permeate, which can be easily separated using a settler. Thus, the system can be compared to a conventional coalescer which also acts to enlarged the droplets.

The total resistance is equal to the sum of the resistance in the emulsion, the resistance in the membrane and the resistance in the permeate. During an experiment the membrane resistance, which depends on the ratio of the amount of pores filled with water and the amount of pores filled with oil, is variable. In time, the amount of pores filled with oil increases, resulting in a higher $R_{membrane}$ and a lower electric field over the emulsion. The electrophoretic velocity of the oil droplets will decrease. In order to 'open' oil filled pores, the Laplace pressure inside the pores must be overcome by applying a transmembrane pressure. The higher the transmembrane pressure, the more pores will open, which is advantageous for the separation efficiency. Also, an increase of the pulse frequency and pressure will have a similar effect.

Apart from a flux towards the permeate side, a water flux from the permeate towards the feed, against the transmembrane pressure, is observed. This is caused by the occurrence of electro osmosis in the membrane pores and/or the cream layer. Electro osmosis can occur in charged capillaries when the ions in the electrical double layer are transported under the influence of an electric field and drag the aqueous phase with them. In our case, the charges of the oil droplets in the cream layer and of the oil wetted membrane pores are negative. Thus, the positive ions in the double layer will move towards the cathode in the emulsion, resulting in a water flux in that direction. The water flux will hinder the transport of oil droplets in the opposite direction. This osmosis effect can be balanced by increasing the transmembrane pressure.

The apparent deposition velocities of 4 experiments with different settings for $E_{emulsion}$ are shown in figure 8. Here, $E_{emulsion}$ is kept constant. To calculate the deposition velocity, corrections are made for the amount of droplets in the cream layer. For example, after 6 hours filtration at $E_{emulsion} = 17 \text{ V}\cdot\text{m}^{-1}$, 34% of the total oil volume has permeated and 32% is present in the cream layer just in front of the membrane. Only the permeated amount is used to determine v' . The figure shows a positive relation between $E_{emulsion}$ and v' . The experiment at $5 \text{ V}\cdot\text{m}^{-1}$ is performed at a transmembrane pressure of 0.1 bar, while during the other experiments a transmembrane pressure of 0.35 bar is applied. It is clear that this influences the results highly because of the effect of the pressure on $R_{membrane}$ and on the electro osmosis flux.

If equation 11 is applied, using the experiments at 0.35 bar only, a P_c of only 0.25 is calculated, indicating coalescence limitation. This is in agreement with the presence of the cream layer. However, the electrophoretic velocities are similar to those in the transport limited system 2, since the $E_{emulsion}$ values are similar. Thus, the reason for the coalescence limitation of system 3 cannot be an extremely high transport velocity. Because not only electrophoresis depends on E , but also the electro osmosis effect the system is more complicated than equation 11 assumes. Probably, the reason for the coalescence limitation will be the occurrence of electro osmosis, which hinders the approach of oil droplets towards the interface where coalescence occurs.

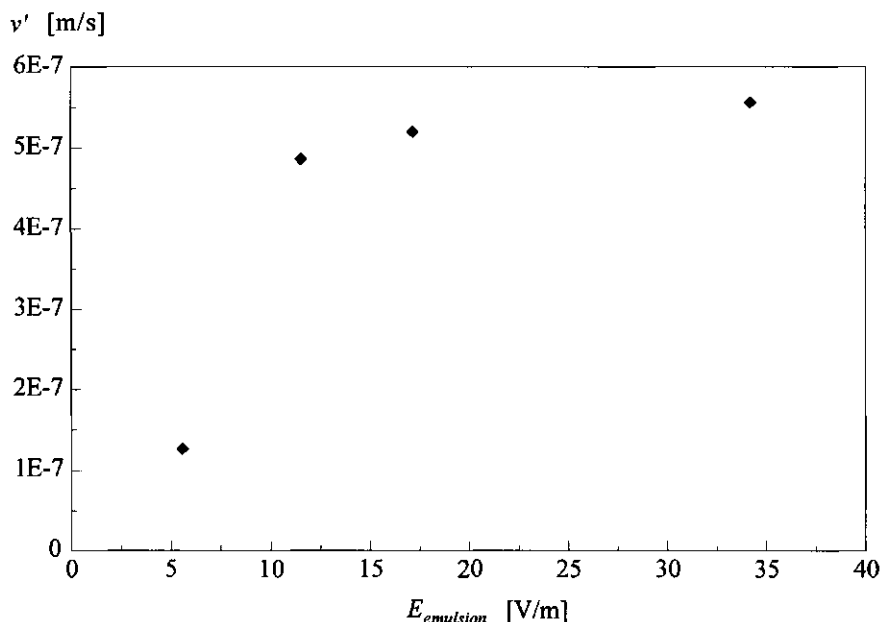


Figure 8, The apparent deposition velocity as a function of $E_{emulsion}$ for system 3. The transmembrane pressure is 0.1 bar for the experiment at $E_{emulsion} = 5 \text{ V}\cdot\text{m}^{-1}$ and 0.35 bar for the other experiments.

Concluding Remarks

The application of an electric field can significantly improve the permeation of small oil droplets through hydrophobic membranes. The transport velocity of the negatively charged droplets from the bulk towards the membrane is enhanced by electrophoresis. This effect is largest in case the anode is placed on the feed side of the membrane. Here, an increase of the apparent deposition velocity with a factor of 1200 can be reached if the voltage is increased from 0 to 20 V. The electric field ($44 \cdot 10^2 \text{ V}\cdot\text{m}^{-1}$ averaged) is situated completely over the emulsion phase, as no other large resistances exist. The only limitation which will arise is the formation of a cream layer near the anode. Thus, the droplets are extracted out of the bulk but not all permeate through the membrane.

If the anode is placed on the permeate side of the membrane, efforts must be made to decrease the resistance at the permeate side in order to successfully apply an electric field over the feed. The use of electrolytes that can dissolve in organic fluids is an answer to this problem. If $E_{emulsion}$ is increased from 0 to 35 V·m⁻¹ the apparent deposition velocity increases with a factor 2. The system is transport limited, indicating that higher permeation rates can be achieved if the electric field is increased. However, at higher voltages the TBAI-ions are almost completely removed out of the DCE into the emulsion, making it impossible to increase $E_{emulsion}$.

In the final system under investigation in this research, the membrane is successfully used to enlarge the droplet size. Here, the anode is placed on the permeate side of the membrane. Simultaneously, an aqueous phase is pumped at the permeate side. Oil droplets will coalesce onto the membrane and can be released by manipulating the transmembrane pressure and the pressure during pulsing. The major disadvantage of the system is the occurrence of electro osmosis of water from the permeate towards the membrane, thus hindering droplet transport in the opposite direction.

Summarizing, system 1 and 3 are promising methods to enhance emulsion separation, not only on lab scale, but also on industrial scale. Application of system 2 is difficult, mainly because of the pollutional effects of TBAI and DCE.

The advantage of system 1 is the direct separation of the continuous oil phase but efforts must be made to prevent the occurrence of a cream layer against the anode. This can be done by increasing the flow velocity of the feed or by regularly removing the cream layer and recirculate it into the original emulsion. Also, the anode can be adjusted, for example by enlarging the pores, by hydrophobization or by decreasing the distance between anode and membrane. System 3 is in fact an efficient conventional coalescer; the droplets are enlarged but an additional process is necessary in order to separate the phases (e.g. a settler). The system can also be used as an electro filter to concentrate the emulsion at the membrane side of the feed channel. The concentrated emulsion can be collected and processed further. In this case the membrane prevents the undesirable coalescence against the anode, as observed in system 1.

Acknowledgements

The author wishes to thank P. Vermeiden and E. van der Ent for performing the experiments. B.H. Bijsterbosch from the department of Physical and Colloid Chemistry is greatly acknowledged for fruitful discussions. Moreover, she thanks the Foundation for Chemical Research in the Netherlands for financial support.

Nomenclature

a	droplet radius	[m]
c	electrolyte concentration	[mol·l ⁻¹]
d	distance between the electrodes	[m]
d_{32}	surface to volume averaged droplet diameter	[m]
E	electric field	[V·m ⁻¹]
F	constant of Faraday	[C·mol ⁻¹]
I	flow strength	[A]
O	surface area electrode	[m ²]
P_c	coalescence probability	[-]
R	resistance	[Ω]
U	electrophoretic mobility	[m ² ·s ⁻¹ ·V ⁻¹]
v'	apparent deposition velocity	[m·s ⁻¹]
v_e	electrophoretic velocity	[m·s ⁻¹]
$v_{transport}$	transport velocity	[m·s ⁻¹]
V	potential difference	[V]
x	distance	[m]
z	valence	[-]
ϵ	dielectric constant	[C·V ⁻¹ ·m ⁻¹]
ϵ_0	dielectric constant of the vacuum	[C·V ⁻¹ ·m ⁻¹]

ϵ_r	relative dielectric constant	[-]
η	dynamic viscosity	[N·s·m ⁻²]
κ	reciprocal double layer	[m ⁻¹]
κ_{sp}	specific conductivity	[Ω^{-1} ·m ⁻¹]
σ_o	surface charge	[C·m ⁻²]
ζ	potential at the plane of shear	[V]
Γ	adsorbed amount of ions	[mol·m ⁻²]
ψ_o	surface potential	[V]

Subscripts

<i>i</i>	indicator for phase
<i>tot</i>	total

References

- 1 K.J. Ptasiński and P.J.M. Kerkhof, Electric field driven separations: Phenomena and Applications, 1992, Separation Science and Technology, vol.27, no.8&9, p.995-1021.
- 2 T.J. Willims and A.G. Bailey, Changes in the size distribution of a water-in-oil emulsion due to electric field induced coalescence, 1986, IEEE Transactions on industry applications, vol.22, 1A-22, no.3, p.536-541.
- 3 S.S. Wang, C.J. Lee and C.C. Chan, Demulsification of water-in-oil emulsions by use of a high voltage ac field, 1994, Separation Science and Technology, vol.29, no.2, p.159-170
- 4 R.S. Allan and T.G. Mason, Effects of electric fields on coalescence in liquid-liquid systems, 1961, Transactions of the Faraday Society, vol.57, p.2027-2040.
- 5 L.C. Waterman, Electrical coalescers, 1965, Chemical Engineering Progress, vol.61, no.19, p.51-57.
- 6 P. Becher, Encyclopedia of Emulsion Technology, vol.1, 1983, M. Dekker, New York, 725 p's.
- 7 P.C. Hiemenz, Principles of colloid and surface chemistry, 1977, M. Dekker, New York, 516 p's.
- 8 P.C. van der Hoeven and J. Lyklema, Electrostatic stabilization in non-aqueous media, 1992, Advances in Colloid and Interface Science, vol.42, p.205-277.
- 9 B. Kratochvil and H.L. Yeager, Conductivity of electrolytes in organic solvents, 1972, Topics in current chemistry, vol.27, Nonaqueous Chemistry, F. Boschke, Springer Verlag, Berlin.

6 General Discussion

In this thesis the separation of emulsion phases by using dispersed phase separators is investigated. While conventional coalescer filters need an additional separation process to remove the enlarged droplets out of the emulsion (e.g. settlers), the dispersed phase separators studied in the present research integrate coalescence and separation. The dispersed phase on the feed side is transferred to a continuous permeate phase.

The process can be described in 2 steps: firstly the droplets have to be transported from the bulk towards the membrane and secondly they have to coalesce and permeate. The transport mechanisms are investigated both experimentally and theoretically (chapter 2 and 3). The influence of several parameters, such as oil properties (chapter 2) and hydrodynamics (chapter 3) have been researched. In chapter 4 the coalescence mechanism is discussed and it is concluded that in most situations the system is transport limited. Therefor, in chapter 5, electrophoresis is applied successfully as an additional transport mechanism.

In this chapter, the dispersed phase separator will be compared to conventional emulsion separation methods. Problems encountered by applying the system in practice will be discussed. This includes some new results concerning the coalescence which have not been discussed in the other chapters.

State of the Art

Chapter 2 and 3 show that it is indeed possible to separate stable, dispersed oil droplets out of the bulk of a secondary emulsion into a continuous permeate phase by recycling the emulsion along a hydrophobic polypropylene membrane. The investigated model system consists of a (bromo-)hexadecane in water emulsion with maximal 6 weight percent dispersed phase. The oil droplets generally have a diameter smaller than 10 μm ($0.5 < d_{32} < 12.4 \mu\text{m}$) and are stabilized by the non-ionic surfactant Tween-40. The emulsions are stable; i.e. no creaming of oil occurs during several days of storage. The underlying thought while choosing this model system is the possible attractiveness of application of dispersed phase separators for the purification of waste waters such as cutting and cleaning fluids, which typically contain 5-10% oil¹. Moreover, we focus on small, stable droplets because of the challenge to separate these emulsions.

Literature about emulsion filtration generally concerns the permeation of the continuous phase²⁻⁷. Others investigated the possibility to permeate the complete emulsion through the membrane⁸⁻¹⁰. During the permeation, the oil droplets are enlarged and can be separated using settlers. Thus, the membrane acts as a conventional coalescer and separation of the 2 phases cannot be reached in a single step.

Some research groups investigated the possibility to permeate the dispersed phase only (similar to our studies). However, either they studied unstabilized emulsions with large droplets ($d = 10\text{-}150 \mu\text{m}$)¹¹ or they investigated stable emulsions with droplet sizes similar to ours but with much larger oil volume fractions ($>25\%$)^{9, 12, 13}. Moreover, the emphasis in these studies was highly experimental; a profound theoretical explanation of the observations was not given. In the present thesis it is shown that the theories developed for collectors of solid particles can be used to explain the transport behavior of emulsion droplets in membrane modules. The effect of changing parameters such as droplet size, density of the dispersed phase, flow rate and module design can be explained using this theory. Thus, optimization of the dispersed phase separator is possible as long as the system is transport limited. This is true for our model emulsion except at high flow velocities in the dead end module. At these conditions, the contact

time of a droplet and the membrane is smaller than the time needed to coalesce. Hence, the system is coalescence limited. If the droplets are larger and/or less stable, transport limitation is valid again. However, in practice all kinds of impurities will be present in oil containing waste waters, such as grease, heavy metals, salts, other surfactants etc.^{1, 6}. These impurities might effect the coalescence behavior, which will be discussed later.

Performance of the Dispersed Phase Separator

In table 1, the dispersed phase separator is compared qualitatively to the conventional coalescers and continuous phase membrane filtration. As mentioned before, the advantage of the dispersed phase separator compared to conventional coalescers is the integrated coalescence and separation of the dispersed phase. Moreover, the pores of coalescers tend to clog heavily, making a frequent, time consuming cleaning procedure necessary^{13,14}. In case of dispersed phase separators, clogging is expected to occur less, because of the cross flow direction of the feed. In both the conventional and the dispersed phase separators, a pure oil phase is produced, while the retentate consists of a diluted oil-in-water emulsion. The latter can be reused or disposed if the oil concentration is low enough. As discussed in chapter 1, in order to dispose waste water in the North Sea, the

Table 1, Comparison of continuous phase membrane filtration, dispersed phase separators and conventional coalescers, in case of oil-in-water emulsion treatment.

	continuous phase filtration	dispersed phase separator	conventional coalescer
permeate	Pure water.	Pure oil.	Pure oil (after settling).
retentate	Concentrated emulsion.	Diluted emulsion.	Diluted emulsion.
additional process necessary	Yes, retentate.	No.	Yes, permeate.
fouling/clogging	Yes, due to concentrated emulsion and permeation of water soluble foulants.	No, not in case of model system. In practice yes, but limited due to the cross flow set up.	Yes, due to impurities in the emulsion.

oil concentration may not exceed the value of 40 ppm, which is in case of a hexadecane-in-water emulsion $5 \cdot 10^{-4}$ g/g (or $0.5 \text{ g} \cdot \text{l}^{-1}$). Figures 4 and 5 of chapter 2 show that these values are not yet reached after 200 hours of filtration of 100 ml emulsion with a $3.24 \cdot 10^{-3} \text{ m}^2$ membrane. However, if an electrical field is applied to enhance the transport of droplets towards the membrane (e.g. figure 5, chapter 5) already after 1 hour filtration the oil concentration in the retentate is low enough. Hence, once the system is optimized, it should be able to meet the legislation restrictions. In the next paragraph, possibilities for optimization will be discussed.

In case of the filtration of the continuous phase, the permeated water phase will be oil free. However, the retentate is a highly concentrated oil-in-water emulsion, which tends to foul the membrane irreversibly¹. Replacement of the membrane will then be necessary. Moreover, this concentrated retentate is difficult to dispose and has to be processed further. The flux values during the continuous phase filtration generally vary between 1 and $100 \text{ l} \cdot \text{m}^{-2} \cdot \text{h}^{-1}$ (i.e. $2.8 \cdot 10^{-7}$ – $2.8 \cdot 10^{-5} \text{ m} \cdot \text{s}^{-1}$)^{1, 15 16}. The flux values of the dispersed phase separator are 100 times smaller (chapter 2 and 3 of this thesis). This means that only under certain conditions the dispersed phase separator is feasible. The membrane area needed to completely separate an oil-in-water emulsion in a given time (1 hour) can be calculated roughly per liter separated oil for both systems assuming a constant flux (figure 1). It must be mentioned that up to now, complete separation of both phases has not been achieved in either membrane system. For both systems calculations are performed using a minimal and a maximal flux. The figure shows, that at low oil concentrations the dispersed phase separator becomes advantageous.

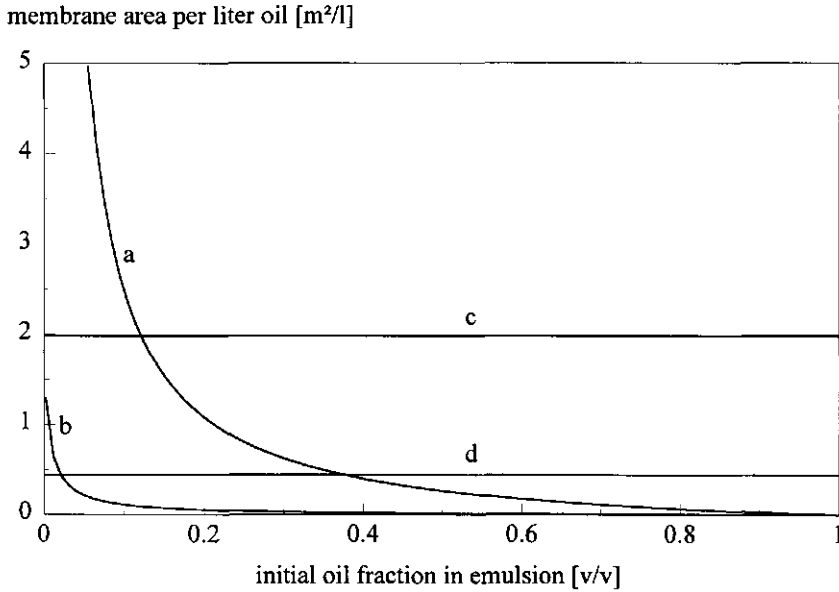


Figure 1. Estimation of the membrane area needed to separate an oil-in-water emulsion into 2 pure phases in 1 hour as a function of initial oil fraction in the emulsion. For a conventional filtration system the continuous phase permeates at a flux of (a) $3 \cdot 10^{-6} \text{ m} \cdot \text{s}^{-1}$ and (b) $30 \cdot 10^{-6} \text{ m} \cdot \text{s}^{-1}$ and in case of a dispersed phase separator the dispersed phase flux equals (c) $0.1 \cdot 10^{-6} \text{ m} \cdot \text{s}^{-1}$ and (d) $0.6 \cdot 10^{-6} \text{ m} \cdot \text{s}^{-1}$ (chapter 2 and 3).

In figure 2, an example of a calculation of the membrane area for a dispersed phase separator is given as a function of the final oil concentration in the retentate. In the figure it is assumed that the flux declines linearly with the oil concentration in the emulsion, with a maximum value similar to figure 1. Therefore, the removal of oil droplets becomes more difficult in time. Naturally, this effect is more pronounced in case of a more realistic, faster flux decline in which the effect of droplet size is incorporated (chapter 2).

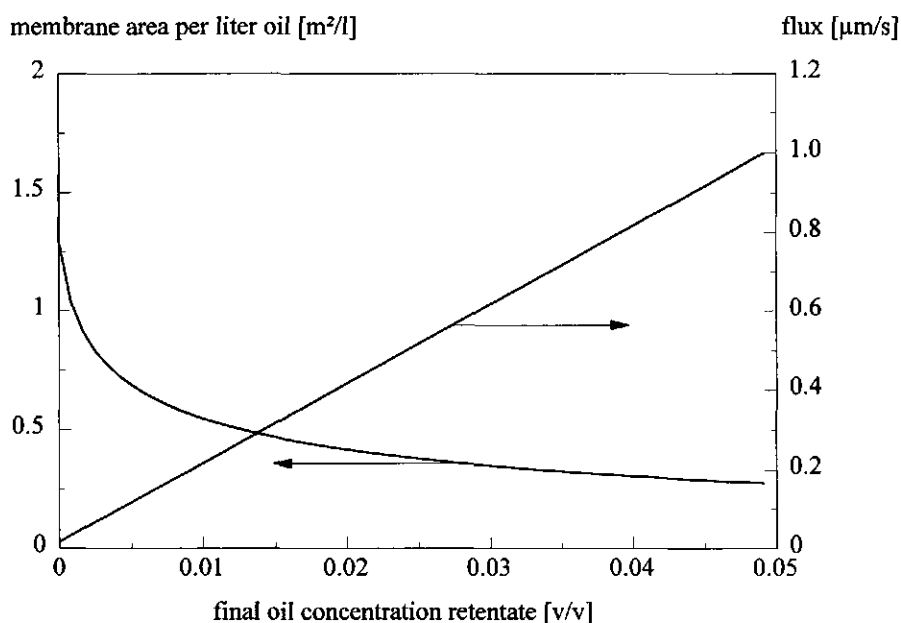


Figure 2, Example of a calculation of the membrane area needed for the separation of an oil-in-water emulsion (1 liter) with an initial oil concentration of 5% (v/v) as a function of the final oil concentration of the retentate for a dispersed phase separator. The total filtration time is set at 1 hour. It is assumed that the flux declines linearly with the oil concentration.

Optimization in case of Transport Limitation

Oil properties

In chapter 2 the positive effect of increasing *droplet size* on the permeation rate is discussed. Thus, the presence of coalescence improving material in the feed channel can improve the performance of the dispersed phase separator. Some experiments have been performed in which a fibrous teflon sheet (normally used as retentate spacer) is placed on

the feed side of the membrane. Indeed, this results in enlargement of the oil droplets and a significantly enhanced permeation rate.

Also, the effect of the *density difference* between the continuous and the dispersed phase is discussed in chapter 2. An increase of this variable results in an increased permeation rate. However, the density difference is a given condition of the emulsion and cannot be optimized. Increasing the density difference effect by applying centrifugational forces (e.g. rotating membranes) seems to be too costly for this type of application. The effect of *oil viscosity* on the transport behavior has not been studied because it is not expected to have a large impact^{7,17} and it will not be discussed further.

Hydrodynamics

In chapter 2 and 3, it is concluded that interception is an important transport mechanism in the dispersed phase separator. Thus, improving the interception will lead to an increase of the permeation efficiency. Interception occurs if the location of the streamlines and the droplet size results in contact between membrane and droplet. Module design must be focused on increasing the membrane area which is contacted by the incoming streamlines. For example, a cross flow module as proposed by Knops et al.¹⁸ might be advantageous (figure 3). Here, the module is packed with hollow fibers and the flow direction is perpendicular to these fibers. Therefor, the interception area is very large. A disadvantage of this module type is the increased probability of clogging if impurities are present in the emulsion. Another possibility to enhance transport is to use flow channels with a diameter similar to or smaller than the droplet diameter. In this way, contact between the droplets and the membrane is guaranteed. However, again clogging will be a problem. Disturbance of the flow pattern causing turbulence will increase the interception too. This can be achieved for example by building small barriers in the feed channel (turbulence promoters) or increasing the flow velocity. Of course, if the retentate is recirculated, increasing the cross flow velocity will always result in an increased intercepted volume per time unit.

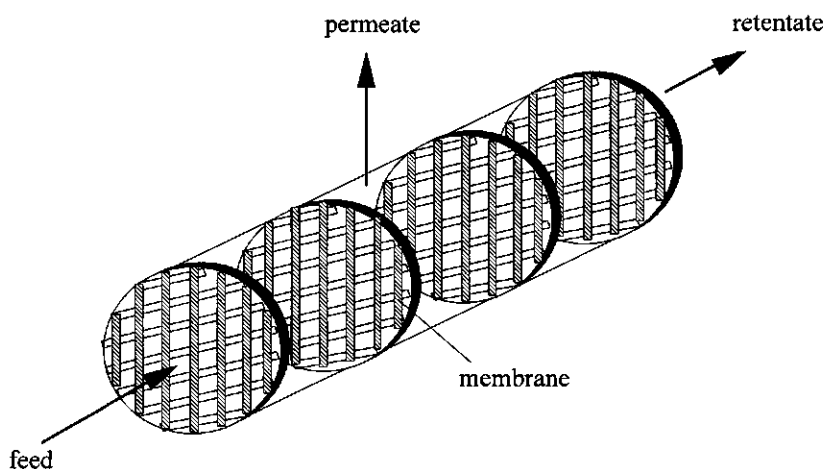


Figure 3, An idea to increase the interception area: cross flow module with flow perpendicular to the packed hollow fibers¹⁸.

Additional external forces

As discussed in chapter 5, the application of an electric field can successfully increase the transport of oil droplets from the bulk towards the membrane. Another possibility might be the replacement of the anode by a positively charged membrane. Also centrifugal forces can be applied, for example in a rotating membrane module, although this is a highly energy consuming method. The use of spiral modules¹⁹ or the design of winded channels can improve the impaction mechanism too.

Some Aspects in case of Coalescence Limitation

Industrial emulsions will always contain all kinds of impurities, which affect the coalescence behavior of the dispersed phase. It is widely accepted that impurities such as sand and dust tend to prevent coalescence²⁰. These large particles can be removed using a prefilter before the dispersed phase separator is applied. However, the presence of large amounts of surface active agents will cause problems. It is shown in chapter 4 that coalescence becomes rate limiting if the surfactant concentration in the bulk is high. Also, it is possible that due to adsorption of surfactants onto the hydrophobic membrane surface, the surface will become less hydrophobic²¹. This might result in a change of coalescence behavior, although in literature no consensus about the influence of coalescer surface properties is reached. For example, Sareen et al.²² state that the influence of *wettability* of the coalescer material by the dispersed phase does not influence the coalescence behavior, while others found opposite results^{23, 24}. Austin et al.²⁵ make a distinction between primary and secondary emulsions. In case of the former *wettability* is important, while for small, secondary droplets it is not. Thus, it is expected that as long as the membrane material is preferably wetted by the oil phase, changes in *wettability* will not have a large impact on the performance of our system. However, if the membrane becomes hydrophilic, water will permeate through the membrane and no separation of the oil and water phase can be achieved.

Another important characteristic of conventional coalescers is the ζ -potential of the coalescer material^{14,26} while also *surface roughness* is mentioned in this context^{20,22,27}. In the present research some experiments have been performed in which the oil phase is colored with Sudan Red. For example, filtration experiments in the dead end module of chapter 3 show that red coloring and thus coalescence only occurs at specific spots of the membrane (at the edges, in the center and at the top of bubbles in case the inserted membrane sheet is not completely flat). Similar results are obtained in the cross flow module. Here, red spots develop at the entrance of the module where a perspex plate is situated (figure 2, chapter 2) and at particular spots of the membrane. Finally, some

experiments have been performed in which an emulsion is stirred in the presence of small membrane parts, with a surface area of circa 1 cm^3 . Here, red coloring of the membrane parts always starts at the edges of the membrane. These results indicate that inhomogeneities of the surface properties enhance coalescence. In the following, the results of more detailed experiments concerning the surface roughness of the membrane material are discussed.

Coalescence time measurements of large droplets as a function of surface roughness

Firstly, the surface roughness of two nodular polypropylene membranes (Enka, Accurel, d_{pore} are 0.1 and 0.2 μm) and of a stretched polypropylene membrane (Micron Separations Inc, d_{pore} is 0.45 μm) has been investigated using the technique of Atomic Force Microscopy (AFM, Digital Instruments, Nanoscop III). A flexible tip is placed at a distance of a few nanometers from the membrane surface and is moved horizontally. Due to changes in colloidal forces, the tip moves in the vertical direction. This movement is measured and can be transformed into a two or three dimensional picture of the surface²⁸. A typical scan is covering a surface of 10 by 10 μm . The results are shown in figure 4 in which a lighter color indicates a larger height. The pictures show that an increase of the average pore size results in a coarsening of the surface structure. This means that the larger the pore size, the less becomes the number of height differences per surface area unity. However, the size of the height difference increases. This is consistent with the data in table 2. Here, per membrane type 4 different spots of membrane are scanned and per spot the average and the maximal height is measured. The data are best reproducible in case of the nodular membrane with the small pore size. The 4 measurements of the stretched membrane show large deviations. This means that the characteristic length of the surface roughness is larger than the scanned surface area.

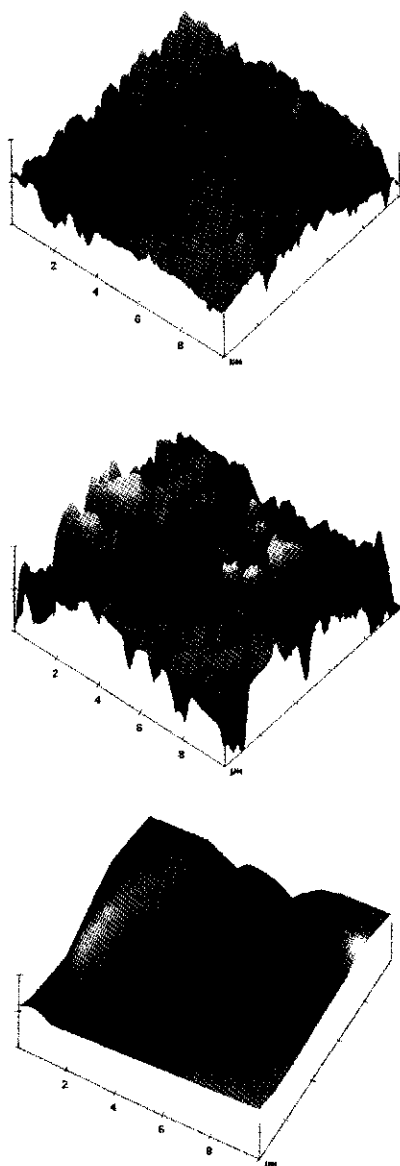


Figure 4. AFM scans of polypropylene membranes; (a) nodular membrane, d_{pore} is $0.1\ \mu\text{m}$, (b) nodular membrane, d_{pore} is $0.2\ \mu\text{m}$ and (c) stretched membrane, d_{pore} is $0.45\ \mu\text{m}$. The values of d_{pore} have been indicated by the suppliers. The scale of the vertical axes is $500\ \text{nm}$ for figure a and b and $2000\ \mu\text{m}$ for figure c.

Table 2, Measured values of average and maximal roughness height of 3 polypropylene membrane surfaces using AFM.

membrane type and pore diameter	nodular, 0.1 μm	nodular, 0.2 μm	stretched, 0.45 μm
range of average heights of 4 measurements	73-78 nm	91-190 nm	61-413 nm
maximal height (averaged over 4	300 nm	1240 nm	1519 nm

Next, coalescence time measurements similar to those described in chapter 4 are performed (figure 4, chapter 4). A membrane, prewetted with dodecane, is inserted into a transparent flat sheet module. The aqueous phase in the chamber of the module contains $2 \text{ g}\cdot\text{l}^{-1}$ Tween-40 and $2.5\cdot 10^{-4} \text{ M}$ KCl. At the bottom of the module a hexadecane droplet ($d = 1.8 \text{ mm}$) can be released from the tip of an injection needle. The time between arrival of the droplet at the membrane interface and coalescence is measured for at least 30 drops. The results are shown in figure 5. The coalescence times clearly differ per membrane type; the larger the pore size is, the smaller the coalescence times become. Thus, in case of large droplets coalescence is increased by large height differences of the membrane surface, probably caused by a decrease of the film thickness which has to drain. This will be discussed later.

Coalescence measurements of small droplets using reflectometry.

As discussed in chapter 4, direct coalescence time measurement of small oil droplets is troublesome. Filtration experiments of secondary hexadecane-in-water emulsions, which are influenced not only by coalescence but also by transport mechanisms, show no clear relationship between the membrane properties and the measured oil flux. Therefore, a more direct method to measure the coalescence behavior of small droplets is needed. In case of coalescence against a liquid oil-water surface, a microscopic method is available²⁹. This method might be applicable in case of a solid surface too if proper adjustments are made.

In the following, some preliminary results concerning a new method, based on reflectometry, are given. With a reflectometer usually the adsorption of surface active

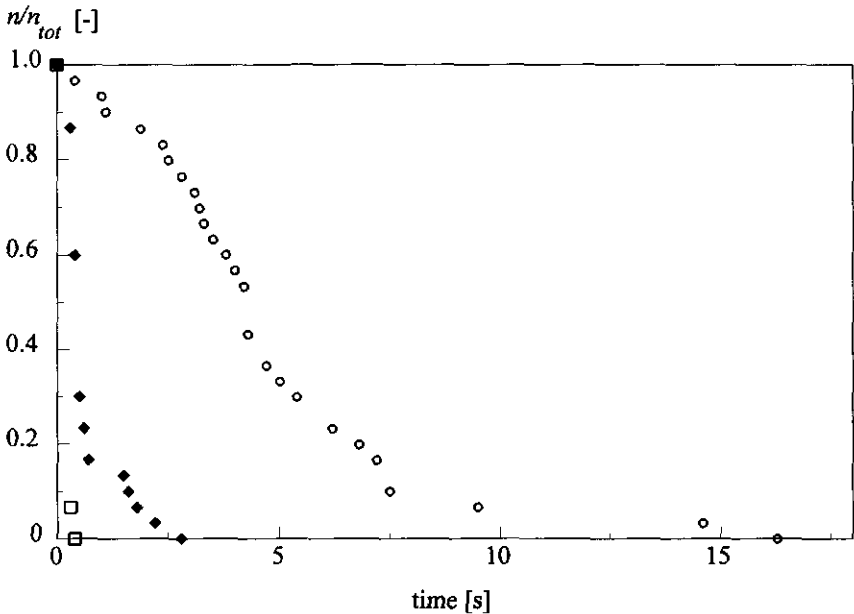


Figure 5, Coalescence time measurements of hexadecane drops against three different polypropylene membranes; \circ nodular membrane, d_{pore} is $0.1\text{ }\mu\text{m}$, \diamond nodular membrane, d_{pore} is $0.2\text{ }\mu\text{m}$ and \square stretched membrane, d_{pore} is $0.45\text{ }\mu\text{m}$. n [-] is the amount of droplets that has not yet coalesced, n_{tot} [-] is the total amount of droplets measured.

agents, such as proteins and soaps, onto solid surfaces is determined by flowing a solution along a surface and measuring the change of the reflection intensity of a polarized laser beam³⁰. The latter is directed at the stagnation point where the solution contacts the surface. The reflected intensities, I [cd], of the perpendicular (subscript s) and parallel (subscript p) components are continuously measured and electronically combined to give the output signal S [-], which is equal to:

$$S \approx \frac{I_p}{I_s} \tag{1}$$

The change in signal, ΔS [-] caused by adsorption is defined by

$$\Delta S = \frac{S_2 - S_1}{S_1} \quad (2)$$

where the subscripts 1 and 2 indicate before and after adsorption. If the sample is an emulsion and droplets coalesce against the surface, a change in the polarization ratio (and hence in S) of the reflected laser beam is expected as well. In this way, the effect of different surface roughnesses on the coalescence of secondary oil droplets can be measured qualitatively. In figure 6, the system is depicted. The surface is an oxidized silicon wafer (Wacker Chemitronic GmbH), which is hydrophobized using dimethyldichlorosilane. After hydrophobization, the wafer has a surface tension ($27 \cdot 10^{-3} \text{ N} \cdot \text{m}^{-1}$) which is approximately equal to that of the polypropylene membrane ($29 \cdot 10^{-3} \text{ N} \cdot \text{m}^{-1}$)^{21, 31}. Electron microscope observations show that such silicon surfaces are very

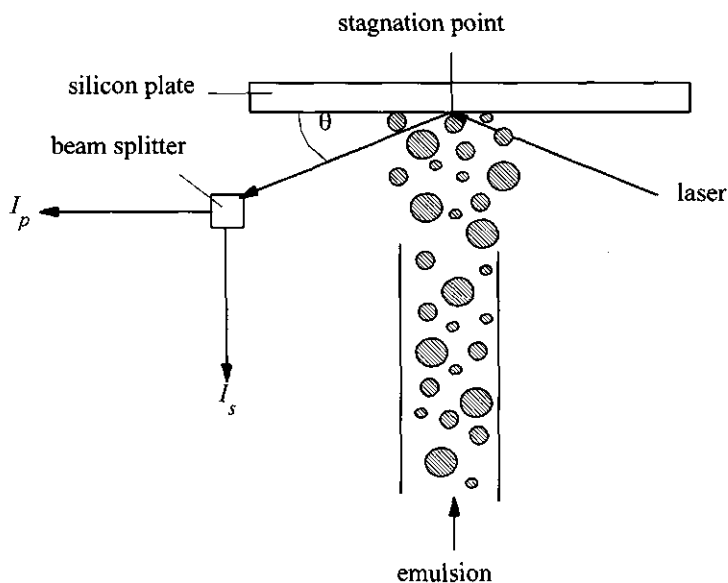


Figure 6, Principle of reflectometry, not to scale

smooth. Therefore, before hydrophobization, the surface is roughened by either using abrasive paper (Superflex, P320) or by softly scraping the surfaces with silicon powder by dimpling the plate during 48 hours into a stirred, aqueous solution containing $40 \text{ g}\cdot\text{l}^{-1}$ silicon powder. Afterwards, the surface is rinsed with water thoroughly. These surfaces can not be scanned using AFM, either because of the high roughness (sandpapered surface) or because of the presence of remaining silicon powder particles (silicon treated surface). In case of the sandpapered surface, observations with a metal microscope show that $\pm 25 \%$ of the surface is covered with scratches of 1 to $50 \mu\text{m}$ depth. The roughness of surface treated with silicon powder is expected to be in between that of untreated and sandpapered silicon.

The results of some preliminary experiments are shown in figure 7. Firstly, the ΔS of a diluted homogenized hexadecane-in-water emulsion at a smooth, hydrophobized silicon surface (line c) is compared to that of an aqueous $0.01 \text{ g}\cdot\text{l}^{-1}$ Tween 40 solution against a smooth surface (line a). The ΔS is similar for both experiments, indicating that in case of the emulsion experiment the observed increase of ΔS is caused by Tween adsorption. The higher noise in the emulsion experiment is due to the fluctuations caused by scattering by oil droplets in the laser beam. One experiment has been performed with a Silverson mixed emulsion, which has a broader droplet size distribution (chapter 2). This indeed results in a significantly higher noise, which supports the idea of scattering by oil droplets.

If a sandpapered surface is inserted into the reflectometer, the ΔS in case of a Tween-40 solution is slightly larger than with a smooth surface (line b). It is important to mention that at some spots of the sandpapered wafer a high initial S is measured, while at other spots the initial S is low. Hence, one can conclude that an inhomogeneous surface has been prepared. Some spots are rough, which results in a high scatter and a low reflectivity while other spots are smooth with low scatter and high reflectivity. If a smooth spot is situated at the stagnation point in the reflectometer and the sample is an emulsion, the results are the same as those obtained with an untreated silicon wafer (line c). However, if a rough spot is monitored, a spectacular increase of ΔS can be observed in

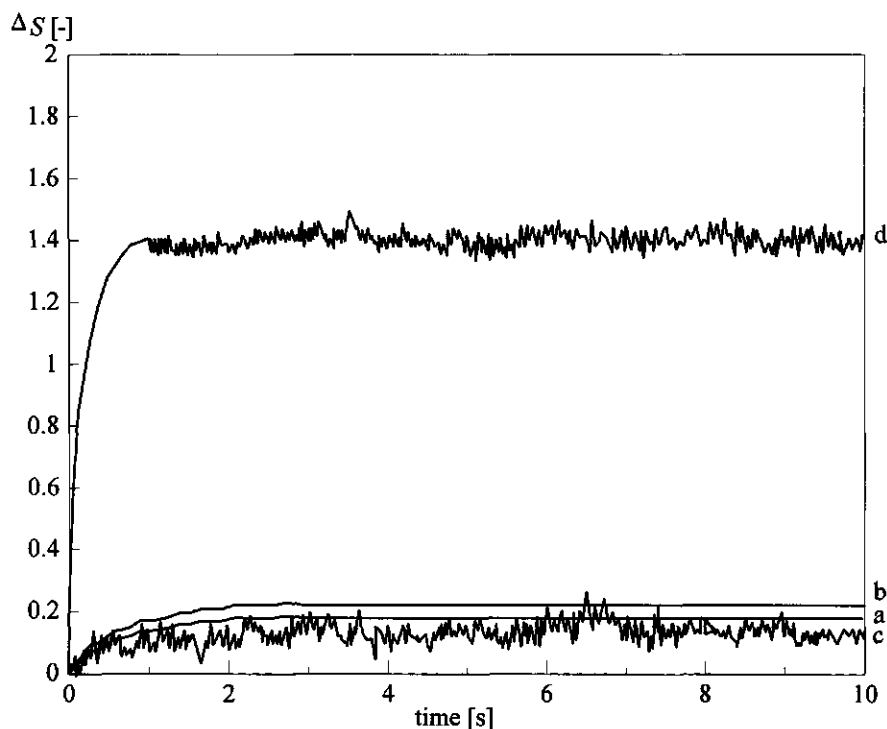


Figure 7, Results of the reflectometric experiments using hydrophobized silicon surfaces with a surface tension of $27 \cdot 10^{-3} \text{ N} \cdot \text{m}^{-1}$; aqueous Tween 40 solution ($0.01 \text{ g} \cdot \text{l}^{-1}$) against (a) a smooth and (b) a sandpapered surface and a homogenized, Tween-40 stabilized hexadecane-in-water emulsion against (c) a smooth and (d) a sandpapered surface. Before an experiment is started, the original emulsion, containing $1 \text{ g} \cdot \text{l}^{-1}$ Tween and $2.5 \cdot 10^{-4} \text{ M}$ KCl is diluted 100 times with double distilled water.

case of an emulsion (line d). This means that another component than Tween-40 must interact with the surface. It is reasonable to assume that this component is the oil phase.

In case of the silicon-powder-treated surface 4 emulsion experiments are performed. Three of them show a ΔS -curve similar to that of Tween adsorption onto a smooth surface (line c). In the fourth experiment an increased ΔS has been observed, comparable to the emulsion experiment against a sandpapered surface (line d). It is most

likely that the roughness as a result of scratching with silicon powder is too small to have an effect on the coalescence behavior but that the presence of some remaining silicon particles can increase the coalescence. Thus, adsorption of particles onto a (membrane) surface might be used to increase the coalescence.

The above shows that reflectometry is a promising method to gather in a relatively simple way knowledge about the influence of surface properties on the coalescence of small oil droplets. It shows in a qualitative way a clear relationship between surface roughness and coalescence. It must be possible to study other factors too, such as surface charge and surface tension.

Surface roughness related mechanisms affecting coalescence

First of all, it is important to mention that the dimensions of the surface roughness should be related to those of the droplets and other length scales in the theory of interaction. For example, seen from a large distance, a surface can appear smooth, while at distances at which colloidal interactions become noticeable, the surface contains large irregularities³². Relevant dimensions of the surface roughness are the height differences between the 'valleys' and the 'mountain tops' (H_{surface}) and the sharpness of the latter determined by the curvature (C_{surface}). Depending on the surface roughness and droplet dimensions, several mechanisms affect coalescence (figure 8). Firstly, if the diameter of the droplet, d_{droplet} is smaller than or equal to H_{surface} , a droplet can be caught into a 'valley'. The contact time between droplet and membrane will increase, resulting in a higher coalescence probability (see also chapter 4). Secondly, a small peak on the surface ($d_{\text{droplet}} \gg H_{\text{surface}}$) can result in a launching of the droplet away from the interface³³. Condition for this mechanism is a horizontal movement of the droplet along the surface, which is the case in our dispersed phase separator. The third mechanism concerns the disturbance of the aqueous film between droplet and surface during drainage by surface roughnesses. If C_{surface} is in the same order of magnitude as d_{droplets} differences in film thickness will occur, resulting in pressure differences. Depending on the shape of the plot of the total colloidal pressure versus the film thickness, this pressure will either increase (i.e. become more

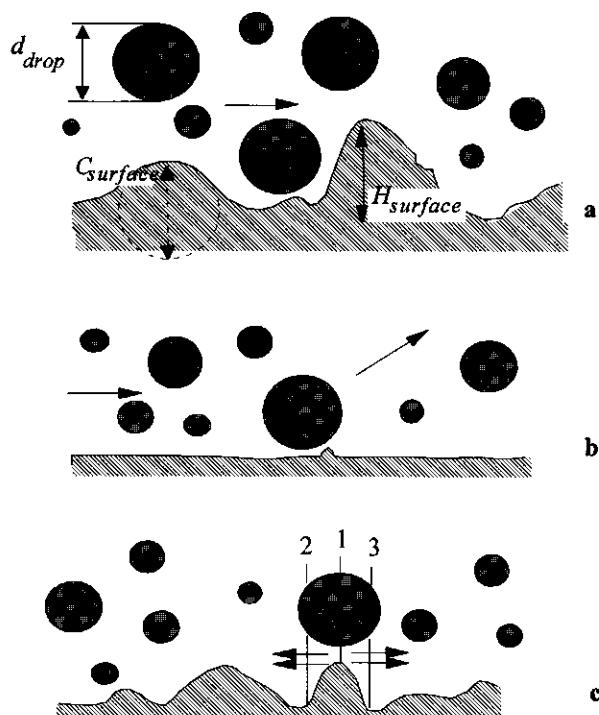


Figure 8, Mechanisms of surface roughness on coalescence; (a) capture of a droplet, (b) removal of a droplet with a horizontal movement and (c) film thickness disturbances, the film pressure at 1 is higher than at 2 and 3.

repulsive) or decrease (i.e. become more attractive) with decreasing film thickness (chapter 4). An enhanced film drainage will occur in the direction of the decreased pressure. The time needed to reach the critical film thickness at which rupture occurs spontaneously will consequently change. This effect increases with increasing $C_{surface}$ and $H_{surface}$ because of an increased pressure difference within the film. If the droplet interface deforms under the influence of the roughness, the film thickness will change less. However, in this case an increased Laplace pressure in the film exists. If this Laplace pressure exceeds the colloidal pressure in the area of deformation, the film will break and coalescence occurs.

Considering table 2 and figure 4, one can conclude that for both nodular membranes $H_{surface}$ is in the same order of magnitude (or slightly smaller) as the droplet diameter of secondary emulsions. Moreover, the curvatures of the tops are strong (small $C_{surface}$); sharp points can be distinguished. This indicates that the mechanism of both capture (a) and film disturbance (c) are likely to occur.

Film disturbance will also occur in case of the coalescence experiments with the large droplets ($d_{droplet} = 1.8$ mm). The stretched membrane enhances coalescence most, which can be explained by the large $H_{surface}$ resulting in high pressure differences in the film. The reflectometric experiments cannot be discussed because of the lack of data about the surface roughness of the silicon plates on microscopic level. The only conclusion can be that roughness clearly improves the coalescence.

Optimization in case of coalescence limitation

In case of coalescence limitation, several methods are available to enhance the process. For example, the addition of certain chemicals is often applied³⁴. *Electrolytes* decrease the double layer thickness and thus the repulsion between droplets (chapter 4) while *concentrated acids* can protonate polar groups at the surface of the droplets, thus decreasing the negative charge. Positively charged *metal complexes*, which are formed after addition of ferro or alumina ions, enhance flocculation of oil droplets. *Polymers* can simultaneously adsorb at multiple droplets, forming a bridge which leads to flocculation too. The addition of small *solid particles* can have similar effects. For example, Boode³⁵ reports the occurrence of partial coalescence of oil droplets due to the presence of fat crystals. If small, hydrophobic particles are present in the aqueous film which has to drain, film rupture is enhanced because of the low wettability of the particle by water. Hydrophilic particles can form bridges between oil droplets, causing flocculation. However, also Pickering stabilization can occur based on steric hindrance of adsorbed particles on the droplet surfaces.

A disadvantage of all these additions is the necessary removal afterwards in order to obtain a pure oil and water phase. A modification of the membrane material with

similar destabilizing effects is more attractive. For example, some publications about conventional coalescers report a positive effect of coating polypropylene fibers with N-aminoethyl-aminopropyl-trimethoxysilane^{7, 14}. In this way, the surface charge becomes slightly positive (ζ -potential is ± 80 mV). An attractive electrostatic force arises, which will result in an enhanced drainage velocity (see also chapter 4). Another possibility which is investigated in the present research, is to increase the membrane surface roughness by adsorption of destabilizing, solid particles. For this purpose, organophilic boehmite needles (AlOOH), which are coated with a polymer (polyisobutene modified with a polar anchor group), are used^{36, 37}. These rods are about 200 nm long, 10 nm wide and 8 nm thick, determined by transmission electron microscopy. Their density is $2.1 \cdot 10^3$ kg·m⁻³. Firstly, it is checked whether these needles are capable of destabilizing a hexadecane-in-water emulsion, stabilized by Tween-40. Mixing 9 ml emulsion with 1.5 ml 1 g·l⁻¹ boehmite-in-dodecane solution at 25 °C results in a clear destabilization; after 2 hours a pure aqueous phase is obtained with on top a flocculated oil phase. In this experiment, the amount of rods ($\pm 4 \cdot 10^{13}$) is in the same order of magnitude as the amount of oil droplets ($\pm 1 \cdot 10^{13}$). A blank experiment with a pure dodecane phase shows no such destabilization. Next, efforts are made to impregnate the rods on a nodular membrane ($d_{\text{pore}} = 0.1 \mu\text{m}$). This is done by filtration of a boehmite-in-dodecane solution (at different boehmite concentrations) through the membrane during 15 minutes. The hypothesis is that a part of the rods are kept by the membrane and form sharp points at the membrane surface. Unfortunately, at the time these experiments have been performed, the AFM-scans of the membrane surfaces were not available yet. Looking at figure 4, it is clear that the needles will disappear into the membrane surface roughness itself. The rods are simply too small, which explains why no difference is found between the oil fluxes before and after membrane modification. Thus, although reflectometric experiments show that increasing the surface roughness is promising, the implementation has not yet been achieved. Further research concerning this subject should concentrate on selecting larger particles.

Concluding Remarks

This thesis shows that dispersed phase separators can be used to simultaneously destabilize secondary oil-in-water emulsions and separate the two pure phases. Comparison of dispersed phase separators with conventional coalescers and continuous phase filtration shows that application of dispersed phase separators will be most attractive in case of low initial oil concentration. Feasibility of the dispersed phase separators will improve if efforts are made to decrease the remaining oil fraction in the retentate.

This thesis shows that the transport mechanisms responsible for droplet movement from the bulk towards the membrane can be modeled using theories developed for solid particle collectors. The influence of several process variables is discussed and based upon this knowledge the process can indeed be optimized. This can be achieved, among others, by adjusting the flow profile to improve the interception mechanism.

In case of the model system under investigation coalescence occurs fast and does not limit the separation efficiency. However, in practice coalescence is expected to cause problems, due to the presence of all kinds of impurities. Although coalescence can be improved using chemical or mechanical additions, it is more attractive to focus on coalescence improving properties of the membrane material. In this way, the advantage of a single process for both destabilization and phase separation is kept. Therefore, it is important to investigate the behavior of oil droplets against solid interfaces more profoundly. Some preliminary experiments (coalescence time and reflectometry measurements) indicate the importance of surface roughness. Therefore, artificial roughening of the surface is expected to increase the coalescence probability. However, a more detailed elaboration is needed in order to be able to optimize the coalescence mechanism.

Acknowledgements

Most experiments discussed in this chapter are performed by K. Hering and C. Hassink. During the reflectometric experiments and the AFM measurements, assistance has been given by R. Fokkink and M. Giesbers of the Department of Physical and Colloid Chemistry of the Agricultural University of Wageningen. B. H. Bijsterbosch of the same department contributed fruitful ideas during several meetings. The boehmite particles were kindly provided by A.P. Philipse and C. Pathmamanoharan of the Van 't Hoff Laboratory for Physical and Colloid Chemistry of the Utrecht University. Finally, the author wants to thank the financial support of the Foundation for Chemical Research in the Netherlands.

Nomenclature

$C_{surface}$	curvature of the roughness	[m]
d	diameter	[m]
$H_{surface}$	height difference of the surface roughness	[m]
I	reflected intensity	[cd]
n	amount of droplets that has not yet coalesced	[-]
n_{tot}	total amount of droplets of which the coalescence time is measured	[-]
S	output signal of the reflectometer	[-]

Subscripts

1	before adsorption
2	after adsorption
p	parallel
s	perpendicular

References

- 1 **L. Yüksel, R. Sedelies, U. Müller and B. Spei**, A new concept in the economical treatment of waste emulsions: chemical breaking and membrane filtration, 1991, *Industrie Minérale-Mines et Carrières-Les Techniques*, vol.7, p.126-131.
- 2 **G.K. Anderson and C.B. Saw**, Oil/water separation with surface modified membranes, 1987, *Environmental Technology Letters*, vol.8, p.121-132.
- 3 **F. Vigo, C. Uliana and P. Lupino**, The performance of a rotating module in oily emulsions ultrafiltration, 1985, *Separation Science and Technology*, vol.20, no.2, p.213-230.
- 4 **K. Scott, I.F. McConvey and A. Adhamy**, Application of crossflow microfiltration to emulsion separation in extraction processes, 1992, *Journal of Membrane Science*, vol.72, p.245-257.
- 5 **P. Lipp, C.H. Lee, A.G. Fane and C.J.D. Fell**, A fundamental study of the ultrafiltration of oil-water emulsions, 1988, *Journal of Membrane Science*, vol.36, p.161-177.
- 6 **R.L. Goldsmith, D.A. Robberts and D.L. Burre**, Ultrafiltration of soluble oil wastes, 1974, *Journal of Water Pollution Control Federation*, vol.46, no.9, p.2183-2192.
- 7 **E. Dahlquist**, Demulsification of O/W emulsions by filtration with special emphasis on cross flow filtration, 1991, Ph.D. thesis, Department of Chemical Engineering, Royal Institute of Technology, Stockholm, 197 p's.
- 8 **J. Murkes**, Cross flow filtration of emulsions combined with coalescing; a new coalescer concept, 1986, *Proceedings of the 5th World Filtration Congress*, Oostend, chapter 11, p.35-41.
- 9 **M. Hlavacek**, Break-up of oil-in-water emulsions induced by permeation through a microfiltration membrane, 1995, *Journal of Membrane Science*, vol.102, p.1-7.
- 10 **U. Daiminger, W. Nitsch, P. Plucinski and S. Hoffmann**, Novel techniques for oil/water separation, 1995, *Journal of Membrane Science*, vol.99, p.197-203.
- 11 **H. Unno, H. Saka and T. Akehata**, Oil separation from oil-water mixture by a porous poly(tetrafluoroethylene) membrane, 1986, *Journal of Chemical Engineering of Japan*, vol.19, no.4, p.281-286.
- 12 **K. Ueyama, K. Fukuura and S. Furusaki**, Oil-phase permeation behavior of O/W emulsion through a porous polytetrafluoroethylene membrane, 1987, *Journal of Chemical Engineering of Japan*, vol.20, no.6, p.618-622.
- 13 **M.J. Semmens and P. Magdich**, Breaking oil water emulsions with microporous membranes, 1990, *Proceedings of the 1990 International Congress on Membranes and Membrane Processes*, p.61-62.
- 14 **V.B. Hughes and A.W. Foulds**, Coalescence of oil-in-water emulsions: Development of a novel fibrous bed coalescer using surface treated polypropylene fibers, 1986, *Proceedings of the World Filtration Congress*, Oostende, Belgium, 21-24 April.

- 15 **Y.P. Sedlukho**, Application of new coalescence method for treatment of emulsified petroleum products waste water, 1991, *Water Science and Technology*, vol.24, no.7, p.261-269.
- 16 **G. Akay and R.J. Wakeman**, Ultrafiltration and microfiltration of surfactant dispersions: an evaluation of published research, 1993, *TransIChemE*, vol.75-A, p.411.
- 17 **C.G. Vinson and S.W. Churchill**, Removal of drops from liquid-liquid dispersions upon flow through screens, 1970, *The Chemical Engineering Journal*, vol.1, p.110-119.
- 18 **F.N.M. Knops, H. Futselaar, T. Reith and I.G. Rácz**, Efficiëntere microfiltratie met transversaal aangestroomde module, 1991, *Procestechnologie*, vol.11, p.21-27.
- 19 **H.B. Winzeler and H. Zindel**, Enhanced Ultrafiltration with Secondary and Pulsed Flow, 1993, *Abstracts of the International Congress on Membranes and Membrane Processes*, Heidelberg, Germany, p.4.23.
- 20 **D.F. Sherony, R.C. Kintner and D.T. Wasan**, Coalescence of Secondary Emulsions in Fibrous Beds, 1978, *Surface and Colloid Science* vol.10, p.99-161.
- 21 **J.T.F. Keurentjes, M.A. Cohen Stuart, D. Brinkman, C.G.P.H. Schroën and K. van 't Riet**, Surfactant-induced Wetting Transitions; Role of Surface Hydrophobicity and Effect on Oil Permeability of Ultrafiltration Membranes, 1990, *Colloids and Surfaces*, vol.51, p.189-195.
- 22 **S.S. Sareen, P.M. Rose, R.C. Gudesen and R.C. Kintner**, Coalescence in fibrous beds, 1966, *AIChE Journal*, vol.12, no.6, p.1045-1050.
- 23 **S. Basu**, A study on effect of wetting on mechanism of coalescence in a model coalescer, 1993, *Journal of Colloid and Interface Science*, vol.159, p.68-76.
- 24 **J. Chieu, E.F. Gloyna and R.S. Schechter**, Device for Evaluating Coalescence of Oil Emulsions, 1977, *Journal of the Environmental Engineering Division*, vol.4. p.163-175.
- 25 **D.G. Austin and G.V. Jeffreys**, Coalescence phenomena in liquid-liquid systems, 1981, *Journal of Chemical Technology and Biotechnology*, vol.31, p.475-488.
- 26 **E.J. Clayfield, A.G. Dixon, A.W. Foulds and R.J.L. Miller**, The coalescence of secondary dispersions, 1985, *Journal of Colloid and Interface Science*, vol.104, no.2, p.500-519.
- 27 **G.A. Davies and G.V. Jeffreys**, Coalescence of droplets in Packings; Factors affecting the Separation of Droplets Dispersions, 1969, *Filtration and Separation*, July/August, p.349-354.
- 28 **F. Penacorada, A. Angelova, H. Kamusewitz, J. Reiche and L. Brehmer**, Scanning Force Microscopy and wetting studies of the surface modification of a polypropylene membrane by means of a Langmuir-Blodgett film deposition, 1995, *Langmuir*, vol.11, no.2, p.612-617.
- 29 **E. Dickinson, B.S. Murray and G. Stainsby**, Direct automated observation of emulsion droplet coalescence, 1986, *Food Emulsions and Foams; Proceedings of an International Symposium organized by the Food Chemistry Group of the Royal Society of Chemistry at Leeds*, p.286-288.

- 30 J.C. Dijt, Kinetics of polymer adsorption, desorption and exchange, 1993, Ph.D. thesis at the Agricultural University of Wageningen, The Netherlands.
- 31 K. Schroën, Physical Chemistry and process engineering of an emulsion/membrane bioreactor, 1995, Ph.D. thesis at the Agricultural University of Wageningen, The Netherlands.
- 32 S.Y. Shulepov and G. Frens, Surface roughness and the particle size effect on the rate of slow, perikinetic coagulation, 1995, *Journal of Colloid and Interface Science*, vol.170, p.44-49.
- 33 M.A. Hubbe, Detachment of colloidal particles from flat surfaces exposed to flow; Mechanism of release, 1985, *Colloids and Surfaces*, vol.16, p.249-270.
- 34 G. Tchobanoglous and F.L. Burton, *Waste Water Engineering Treatment, Disposal and Reuse*, 1991, New York, McGraw-Hill, 1334 p's.
- 35 K. Boode, Partial coalescence in oil-in-water emulsions, 1992, Ph.D. thesis at the Agricultural University of Wageningen, The Netherlands.
- 36 P.A. Buining, C. Pathmamanoharan, A.P. Philipse and H.N. Lekkerkerker, Preparation of (non-)aqueous dispersions of colloidal boehmite needles, 1993, *Chemical Engineering Science*, vol.48, no.2, p.411-417.
- 37 P.A. Buining and H.N.W. Lekkerkerker, Isotropic-Nematic Phase Separation of a Dispersions of Organophilic Boehmite Rods, 1993, *The Journal of Physical Chemistry*, vol.97, no.44, p.11510-11516.

Summary

The reuse or discharge of industrial waste waters, containing small fractions of dispersed oil, requires a purification treatment for which membranes can be used. If only little oil is present, removal of the dispersed phase might be preferable to the more commonly applied removal of the continuous phase. For this purpose dispersed phase separators can be applied, which combine the features of conventional coalescers and membrane filtration. The membrane surface promotes coalescence (similar to a coalescer) but in the mean time the coalesced phase is separated and transferred in a continuous oil permeate phase.

In the present thesis the possibility to use sheets of polypropylene membrane (with a pore diameter of $0.1\text{ }\mu\text{m}$) as dispersed phase separators for treatment of secondary (bromo-) hexadecane-in-water emulsions stabilized by Tween-40 is investigated. The weight fraction of the dispersed phase is always lower than 0.06 and the volume to surface averaged diameter of the oil droplets is generally smaller than $10\text{ }\mu\text{m}$. The research focuses on understanding the mechanisms controlling the permeation behavior of the oil droplets. The process can be described in two stages: firstly the droplets have to be transported from the bulk of the emulsion towards the membrane and secondly they have to coalesce and permeate.

In chapter 2 and 3 the transport mechanisms are determined both experimentally and theoretically. It is shown that the theories developed for collectors of solid particles, based on the convective diffusion equation, can be used to describe the transport behavior of the oil droplets in membrane modules. The main transport mechanisms are diffusion, gravity and interception. The latter occurs if the location of the stream lines and the droplet size results in contact between droplet and membrane. The influence of several parameters, such as droplet size, density of the dispersed phase, flow rate and module design can be explained using the convective diffusion theory, assuming the membrane to be a perfect sink. This means that as soon as a droplet reaches the membrane it coalesces and permeates. Since theory and experimental results agree qualitatively, it can be concluded that the system is transport limited in most cases.

In chapter 4, the coalescence mechanism is discussed. Only if the contact time between droplet and membrane becomes smaller than the time needed for coalescence, the system will be coalescence limited. The coalescence time, t_c [s], is determined by the drainage of the aqueous film between droplet and membrane. Calculations show that t_c for the small droplets under investigation against a liquid interface is smaller than 1 second while in case of the presence of a membrane t_c will be even smaller. As the contact times are at least a few seconds, coalescence will occur which is in agreement with the perfect sink assumption. Only in case of a dead end module at high flow velocities the system becomes coalescence limited because of short contact times. Finally, at high surfactant concentrations coalescence is not detected.

As oil droplets are slightly negatively charged, the transport can be enhanced by electrophoresis. Therefore, in chapter 5 possibilities to apply an electric field over the emulsion are investigated. If the anode is placed at the feed side of the membrane the transport velocity is increased significantly. However, not all droplets permeate and a cream layer is formed in front of the membrane. If the anode is placed at the permeate side of the membrane, problems are encountered because of the large resistance of the continuous oil permeate phase. The electric field is situated mainly over this phase, at the

cost of the electric field over the emulsion. The resistance of the permeate phase can be successfully decreased by addition of an apolar electrolyte (TBAI). Also, it is possible to circulate an aqueous phase at the permeate side. In this case, oil droplets with a diameter of several millimeters are detected in the permeate. Here, the membrane acts as a conventional coalescer. All systems show indeed an enhanced extraction in the presence of an electric field. However, we think that only the first and the last are scaleable.

Finally, in the general discussion the dispersed phase separator is compared to conventional emulsion separation methods. The dispersed phase separator becomes advantageous at low oil concentrations. Feasibility will increase if the remaining oil fraction in the retentate can be decreased further. Ideas for optimization in case of transport limitation are introduced, such as adjusting the flow profile to increase the interception mechanism. Problems are encountered in practice because of the presence of all kinds of impurities in industrial waste waters which will hinder the coalescence. In that case, research should focus on coalescence enhancing parameters of the membrane material such as surface potential and surface roughness. Preliminary experiments using a reflectometer indicate the importance of surface roughness, which is explained theoretically.

Samenvatting

Voordat industrieel afvalwater kan worden hergebruikt of geloosd, moeten de aanwezige verontreinigingen, waaronder olie, verwijderd worden. Hiervoor kunnen membranen worden toegepast. Meestal wordt de continue fase door het membraan getransporteerd, terwijl de verontreinigingen in het retentaat achterblijven. Indien er slechts een kleine hoeveelheid olie als disperse fase aanwezig is, kan het echter gunstig zijn om deze disperse fase te verwijderen in plaats van de continue water fase. In dit geval wordt een disperse-fase-afscheider gebruikt. Deze combineert de coalescentie-bevorderende eigenschappen van een conventioneel coalescentiefilter met de scheidende eigenschappen van een membraan, zodat het permeaat bestaat uit een continue oliefase.

In dit proefschrift wordt de mogelijkheid onderzocht om polypropyleen membranen (met een gemiddelde poriediameter van $0.1\text{ }\mu\text{m}$) als disperse-fase-afscheiders te gebruiken om secundaire (bromo-)hexadecaan-in-water emulsies, gestabiliseerd met Tween-40, te destabiliseren. De gewichtsfractie van de disperse fase is altijd lager dan 0.06 en de volume-opervlakte gemiddelde diameter van de oliedruppels is kleiner dan $10\text{ }\mu\text{m}$. De mechanismes die het permeatiegedrag van de oliedruppels bepalen, zijn onderzocht. Het proces kan worden opgesplitst in 2 deelprocessen. In de eerste plaats moeten de druppels vanuit de bulk naar het membraan oppervlak getransporteerd worden. Vervolgens moeten

zij met het membraanoppervlak coalesceren en zich door het membraan naar de permeaatzijde verplaatsen.

In hoofdstuk 2 en 3 worden de transportmechanismen zowel experimenteel als theoretisch onderzocht. Theorieën gebaseerd op de convectieve diffusie vergelijking kunnen worden gebruikt om het transport gedrag te beschrijven. De belangrijkste mechanismen zijn diffusie, oproming en interceptie. Deze laatste vindt plaats wanneer de combinatie van de locatie van de stroomlijnen en de druppelgrootte resulteren in contact tussen druppel en membraan. De invloed van diverse parameters, zoals druppelgrootte, dichtheid van de oliephase, stroomsnelheid en module-ontwerp, kunnen met deze theorie worden verklaard indien aangenomen wordt dat het membraan zich gedraagt als een bodemloze put; zodra een oliedruppel het membraan bereikt, coalesceert hij en verdwijnt uit de emulsie. Aangezien theorie en experiment kwalitatief overeenstemmen, kan geconcludeerd worden dat het systeem transport-gelimiteerd is.

Het coalescentie-mechanisme wordt besproken in hoofdstuk 4. Coalescentie-limitatie zal alleen optreden wanneer de contacttijd tussen druppel en membraan kleiner is dan de tijd nodig voor coalescentie. Deze laatste wordt bepaald door de drainagetijd van de waterige film tussen druppel en membraan. Berekeningen tonen aan dat de coalescentietijd van de secundaire oliedruppels, zoals gebruikt in dit onderzoek, tegen een vloeibaar, vlak oppervlak kleiner is dan 1 seconde. Indien een membraan aanwezig is in het oppervlak zal deze tijd nog kleiner worden. Aangezien de contacttijden over het algemeen minstens een paar seconden zijn, wordt voldaan aan de voorwaarde van de bodemloze put. Alleen in het geval van een dead-end module bij hoge snelheden kan de coalescentie limiterend worden, evenals bij hoge surfactant-concentraties.

Aangezien oliedruppels negatief geladen zijn, kan elektroforesis gebruikt worden om het transport te bevorderen. Dit wordt onderzocht in hoofdstuk 5. Wanneer de anode aan de voedingszijde van het membraan geplaatst wordt, wordt de transportsnelheid significant verhoogd. Echter, een roomlaag van oliedruppels wordt gevormd voor het membraan

omdat niet alle druppels naar de permeaatzijde verplaatst worden. Wanneer de anode aan de permeaatzijde van het membraan wordt geplaatst, ontstaan problemen vanwege de hoge weerstand van de continue oliefase. Het elektrisch veld is voornamelijk gesitueerd over deze fase, ten koste van het veld over de emulsie. De weerstand van de oliefase kan worden gereduceerd door een apolair electrolyt (TBAI) toe te voegen. Tevens is het mogelijk om een waterige fase aan de permeaatzijde te circuleren. In dit geval gedraagt het membraan zich als een conventioneel coalescentiefilter; oliedruppels met een diameter van enkele millimeters worden waargenomen in de permeaاتفase. Hoewel alle onderzochte systemen de olie-extractie bevorderen, zullen alleen de eerste en de laatste opgeschaald kunnen worden.

Tot slot wordt in hoofdstuk 6 de disperse-fase-afscheider vergeleken met conventionele scheidingsmethoden. Bij lage oliefracties wordt de disperse-fase-afscheider voordelig. De toepasbaarheid van het systeem zal verhoogd worden wanneer de oliefractie in het achterblijvende retentaat verder verlaagd kan worden. Mogelijkheden tot optimalisatie in geval van transportlimitatie worden besproken, zoals aanpassing van het stromingsprofiel om interceptie te bevorderen. In de praktijk zal echter de aanwezigheid van allerlei verontreinigingen in het afvalwater de coalescentie bemoeilijken, waardoor coalescentielimitatie zal optreden. In dat geval is het interessant om onderzoek te doen naar coalescentiebevorderende eigenschappen van het membraanmateriaal, zoals oppervlaktepotentiaal en -ruwheid. Inleidende experimenten met een reflectometer wijzen op het belang van oppervlakteruwheid.

Nawoord

Op deze plaats wil ik een woord van dank richten aan iedereen die op de een of andere manier een steentje heeft bijgedragen aan de totstandkoming van dit proefschrift en aan de prettige werksfeer waarin dit kon geschieden. De directe begeleiding was in handen van Klaas van 't Riet en Albert van der Padt, terwijl ook Martien Cohen Stuart en Bert Bijsterbosch me van adviezen voorzagen tijdens de werkbesprekingen. Bedankt daarvoor.

Een aantal studenten heeft in het kader van een afstudeervak of stage werk voor mij verricht waarvan de resultaten in dit boekje zijn belandt. Henk Donkers, Rudolf Bakker, Peter Vermeiden, Gerhard Kolenbrander, Johan Vente, Marianne Renkema, Munasri Hadini, Corine Hassink, Karlo Hering, Ed van der Ent en Vesna Rafajlovska; dank voor jullie bijdrage, inclusief het genereren van de vele data. Tevens gaat mijn dank uit naar de mensen van de werkplaats, die heel wat perspex membraanmodules hebben gefabriceerd, de bibliotheek en de fotolokatie. De collega's bij de vakgroep Fysische en Kolloïdchemie waren altijd zeer behulpzaam (o.a bij de lichtverstrooiings- en AFM-metingen), evenals die bij de vakgroep Levensmiddelen natuurkunde (bedankt voor de talloze malen dat ik de homogenisator kon gebruiken). De prettige werksfeer werd verzorgd door de ex-collega's van de sectie Proceskunde.

Mijn ouders mag ik op deze plek natuurlijk niet vergeten. Zij hebben me alle mogelijkheden geboden. En last but not least: Abco, die al mijn 'geneuzel' heeft moeten ondergaan. Bedankt dat je er voor me bent!

Curriculum Vitae

Ageeth Lefferts werd op 1 juli 1967 geboren te Enschede. In 1985 behaalde zij het diploma Gymnasium β aan het St. Jacobus College in haar geboorteplaats. In dat zelfde jaar startte zij de studie Levensmiddelentechnologie aan de Landbouwniversiteit te Wageningen. Afstudeervakken werden afgelegd in de richtingen Levensmiddelen Procestechnologie en Bestuurlijke Informatiekunde. Haar stage periode bracht zij door aan de 'Chemical Department of the Rensselaer Polytechnic Institute' te Troy, New York, Verenigde Staten, bij professor G. Belfort.

Na haar afstuderen in augustus 1991 begon zij met haar promotie onderzoek aan de sectie Proceskunde van de Landbouwniversiteit Wageningen, waarvan dit proefschrift het resultaat is. Momenteel is zij werkzaam bij de Process Development Department van de Industrial Pharmaceutical Products Division van Gist-Brocades te Delft.